Performance Analysis for Cognitive Radio Networks

Ping, Shuyu

Awarding institution:
King's College London

Performance Analysis for Cognitive Radio Networks

by
Shuyu Ping

A Thesis Submitted for the Degree of
Doctor of Philosophy
at King's College London

May 2016

To my family, best friends and Hamid

Acknowledgements

This thesis would not have been possible without the guidance and the support of several individuals.

First of all, I owe my deepest gratitude to Prof. Hamid Aghvami for his continuous support, relentless and insightful guidance. Without your help, I will never be what I am. Thank you, sir. Your motivation, knowledge and long lasting experience are irreplaceable assets for me.

I am deeply indebted to Dr. Adnan Aijaz for his helpful advice and useful guidance related to my research. Never in my life have I seen a person as committed to his work as Adnan. I will never forget the moment you helped me to overcome the difficulties of my research and life. You never hesitate to share great ideas and experience to me, which are invaluable to me.

I would like to thank Dr.Oliver Holland for allowing me to work with him on the SOLDER Project and on the collaborative project with Sapienza University of Rome. The great experience added an extra dimension to my work and helped me network with professionals across Europe. I would also like to thank Dr. Yansha Deng for her kindly help during the last moment of my PhD life.

I am particularly grateful to all my current and erstwhile colleagues at CTR, including Stan, Yaqub, Paul, Alex, Wataru, Jing, Mati, Menglan, Hong, Ehsan (the prick), Omar, Fahad, Bright, Christoforos, Giorgos, Zhenzhuang, Gao, Jinwei, Xi, Xun, Fei and the visiting researchers Zhutian, Jie and Jian. Thank you guys for all the support and cooperation you have extended to me and for making my stay at CTR as the most memorable time of my life.

I would like to thank Dr. Maged Elkashlan and Dr. Keivan Navaie for healthy criticism and invaluable suggestions that led to significant improvements in this thesis.

Last, but not the least, I wish to thank my parents, who have always stood by me through thick and thin. It is to them that I owe all the success in life.

Abstract

Cognitive Radio (CR) networks provide a novel approach to address the spectrum scarcity and spectrum inefficiency issues in wireless networks. The main objective of this research is to investigate the challenges, provide solutions, and evaluate the performance of four different types of CR Networks; Cognitive Radio Ad-Hoc Networks (CRAHNs), Cognitive Radio enabled Sensor Networks (CSNs), Cognitive Radio enabled AMI (CR-AMI) Networks, and Cognitive Femtocell Networks. My research is focusing on developing novel solutions, algorithms, and protocol enhancements for different layers of the protocol stack for CR networks.

For CRAHNs, a Spectrum Aggregation-based Cooperative Routing Protocol (SACRP) is proposed. The primary objective of SACRP is to provide higher energy efficiency, improve throughput, and reduce network delay for CRAHNs. In this regard, two different classes of routing protocols are proposed as; *Class A* for achieving higher energy efficiency and throughput, and *Class B* for reducing end-to-end latency. Based on stochastic geometry approach, A comprehensive analytical model is built for the proposed protocol. Besides, the proposed protocol is also compared with the state of the art cooperative and non-cooperative routing algorithms with spectrum aggregation.

On the other hand, CR is expected to play a vital role in smart grid networks. Cognitive Sensor Networks (CSNs) can effectively address the unique challenges of WSNs in smart grid. Against this background, an energy efficient and reliable Medium Access Control (MAC) protocol is designed for CSNs. The proposed MAC protocol, termed as CRB-MAC, can provide high energy efficiency and reliability. In addition, CRB-MAC explicitly accounts for the peculiarities of a CR environment, which provides a viable solution for CSNs.

As an integral component of the smart grid ecosystem, Advanced Metering Infrastructure (AMI) networks are practically deployed as a static multi-hop wireless mesh network. It is expected that the use of cognitive radio (CR) technology for AMI networks will be indispensable in near future. In this respect, a new RPL-based

routing protocol is proposed for cognitive radio enabled AMI (CR-AMI) networks. This protocol utilizes a global optimization algorithm to select the best route from the whole network. In addition, the proposed routing protocol explicitly protects primary (licensed) users while meeting the utility requirements of the secondary network. The proposed protocol enhances the quality of service (QoS) of the existing RPL-based routing protocols for CR-enabled AMI networks.

In heterogeneous networks (HetNets), Cognitive femtocells provide low-power, low-cost, and short-range wireless broadband access, which achieve higher network capacity and spectrum efficiency. Based on a stochastic geometry approach, the rate coverage of two-tier HetNets with cognitive femtocells is analysed. The closed-form expressions for downlink rate coverage of both networks are derived. Moreover, the impact of frequency reuse on the rate coverage in HetNets is evaluated.

At last, according to the overall picture of the research conducted, the main conclusions together with some directions for the future work are presented.

Table of Contents

List of Tables

List of Figures

List of Acronyms

AASA Aggregation Aware Spectrum Assignment.

ACK Acknowledgement.

AMC Adaptive Modulation and Coding.

AMI Advanced Metering Infrastructure.

AODV Ad hoc On-Demand Distance Vector.

BER bit error rate.

CCA clear channel assessment.

CCASA Channel Characteristic Aware Spectrum Aggregation.

CCC common control channel.

CDF Cumulative Distribution Function.

CI checking interval.

CO Coordination Overhead.

CORPL Cognitive and Opportunistic RPL.

CR Cognitive Radio.

CR-AMI cognitive radio enabled AMI.

CRAHN Cognitive Radio Ad-Hoc Network.

CRB-MAC Cognitive Receiver-Based MAC.

CRF Collision Risk Factor.

CRTF Cognitive Radio Transmission Factor.

CSB-MAC Cognitive Sender-Based MAC.

CSNs Cognitive Radio Sensor Networks.

CST Channel Status Table.

CTS Clear-To-Send.

DAGs Directed Acyclic Graphs.

DE delay estimation.

DIO DAG Information Object.

DMACO Directional Mutation Ant Colony Optimization.

DMM directional mutation mechanism.

DOFDM Discontiguous Orthogonal Frequency Division Multiplexing.

DSA Dynamic Spectrum Access.

DSR Dynamic Source Routing.

DVP deadline violation probability.

ETX expected transmission count.

FA-OFDM Frequency-aware OFDM.

FBSs femtocell base stations.

FCC Federal Communications Commission.

FW Fenton-Wilkinson.

HetNet heterogeneous network.

IETF Internet Engineering Task Force.

IR Interference Ratio.

ISM industrial, scientific and medical.

LSP link success probability.

LTE Long Term Evolution.

M2M Machine-to-Machine.

MAC Media access control.

MACO Mutated Ant Colony Optimization.

MBSs macrocell base stations.

MDMS Meter Data Management System.

MSA Maximum Satisfaction Algorithm.

PDF probability density function.

PDR Packet Delivery Ratio.

PHY Physical.

PMF Probability Mass Function.

PPP Poisson Point Process.

PU primary user.

QoS Quality of Service.

RAT Radio Access Technology.

RES Reservation.

RPL Routing Protocol for Low Power and Lossy Netwoks.

RREP route reply.

RREQ route request.

RTS Ready-To-Send.

SACRP Spectrum Aggregation-based Cooperative Routing Protocol.

SDR Software Defined Radio.

SIFT Signal Interpretation before Fourier Transform.

SNR signal-to-noise ratio.

SSR spectrum sensing region.

UHF Ultra high frequency.

UMTS Universal Mobile Telecommunications System.

VHF Very high frequency.

Wi-Fi Wireless-Fidelity.

WRAN wirelss regional area networks.

WSNs Wireless Sensor Networks.

Chapter 1

Introduction

The wireless communications have seen an explosive growth over the past decades in terms of the number of users and the amount of carried traffic. A large number of wireless devices such as laptops, tablets, and smart phones compose a variety of networks, which results in a huge portion of the spectrum usage. As spectrum is a naturally limited resource, the spectrum scarcity and spectrum inefficiency issue have become the bottleneck of future wireless networks. Spectrum efficient utilization plays an important role in wireless networks. However, the existing wireless technologies such as Wireless-Fidelity (Wi-Fi), Universal Mobile Telecommunications System (UMTS), and Long Term Evolution (LTE) cannot guarantee the efficient utilization of spectrum. In this regard, Cognitive Radio (CR) [2] technology is envisaged to solve such problems in wireless communications.

CR technology aims to enhance the spectrum utilization in the licensed spectrum without introducing interference to the transmission of licensed (primary) users. Dynamic Spectrum Access (DSA) technique, as shown in Fig. 1.1, is involved to obtain and access the best available spectrum through its cognitive capability and reconfigurability[1]. It enables the unlicensed (CR) users opportunistically use the unused licensed bands/spectrum, which is referred to as *spectrum hole* or *white space*. Whenever a licensed user is detected, the CR users will either move to another spectrum hole or stay in the same band by altering its transmission power/ modulation scheme to avoid the interference to licensed user [2].

In this regard, the spectrum regulators (e.g., Federal Communications Commission (FCC) and Ofcom) have proposed the regulatory rules and technical

[1]Cognitive capability and reconfigurability are two main characteristics of CR [2–5], which will be fully discussed in Chapter 2

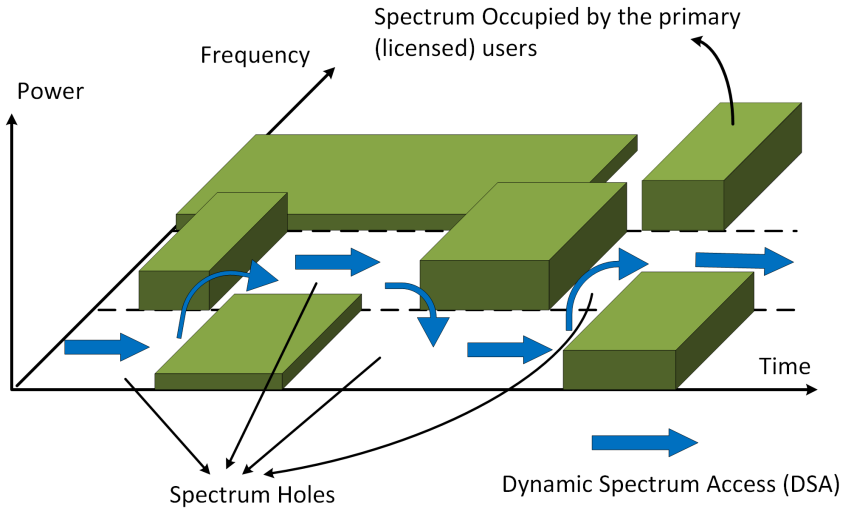

Figure 1.1: Spectrum hole concept and Dynamic Spectrum Access technique [2].

principles to conduct the applications of CR technology. the FCC in the United States issued a report which permits cognitive use of TV white space spectrum[2], wherein the Very high frequency (VHF) and Ultra high frequency (UHF) spectrum provide superior propagation and building penetration compared to other unlicensed spectrum in other bands, e.g., 2.4 and 2.5 GHz [8]. The Ofcom also issued a statement approving of TV white space usage in the UK by license-exempt devices operating under the developing geolocation database-based framework [9]. IEEE 802.22 [10] as the first worldwide standard with respect to CR technology is still in the process of standardization. It specifies the air-interface standard based on the techniques such as spectrum sensing, spectrum sharing and spectrum management for the wirelss regional area networks (WRAN) in the utilization of specific TV spectrum. The new regulatory rules outline a number of requirements to operate CR technology in TV white space, including spectrum management and protection for the licensed users. Therefore, it not only provides an opportunity for the development of wireless networks, but also imposes technical challenges regarding new wireless Physical (PHY) and Media access control (MAC) layer designs for CR characteristics.

[2]TV white spaces exist between 54 MHz and 806 MHz [6] for digital terrestrial TV broadcasting in the U.S, but exist between 470 MHz and 790 MHz [7] in the UK.

1.1 Scope of the Work

CR technology provides a novel approach to address the spectrum scarcity and spectrum inefficiency issues in wireless networks. The recent developments in spectrum policy and regulatory domains have allowed the CR technology to support a variety of applications [11], e.g., broadband cellular, Ad-Hoc networks, smart grid [12], and heterogeneous network (HetNet). Although it improves spectrum utilization and exploits alternate spectrum opportunities through DSA capabilities, it creates various challenges for existing communication networks, due to the high fluctuation in the available spectrum as well as diverse Quality of Service (QoS) requirements [3]. In addition, some key distinguishing factors of CR networks such as the distributed multi-hop architecture, the dynamic network topology, and the time and location varying spectrum availability make it incompatible with the current wireless platforms or protocols.

Against this background, a large volume of research has been conducted in the CR area in the last decade [13]. However, most of them have only paid attention to the lower layers. For example, *spectrum sensing* as the front line functionality of PHY layer has been considered in many literatures, as it needs to be completed in an efficient and accurate manner to enable an opportunistic CR network architecture. The research of the upper layer design such as MAC and network layers, has not been considered well. Novel solutions related to upper layers are needed to meet the key requirements of CR networks in terms of scalability, energy efficiency, reliability, and diversity of QoS. On the other hand, the emerging applications of CR technology within different types of networks are proliferating rapidly [14], which open up new research areas for future wireless communications.

The primary objective of this research is to investigate different challenges of CR networks. It not only focuses on developing novel solutions, algorithms, and protocol enhancements for different layers of the protocol stack, e.g., MAC, and Network layers, but also emphasises on the application of CR in different wireless environments, e.g., Cognitive Radio Ad-Hoc Network (CRAHN), smart grid, and

HetNet. For CRAHNs, A distributed routing protocol with indispensable cross-layer design is proposed with emphasis on energy efficiency, network throughput and end-to-end delay. Novel protocols for smart grid, which is one of the largest and most rapidly growing application area for CR communications, are designed with special emphasis on Cognitive Radio Sensor Networks (CSNs) and CR-AMI networks, respectively. On the other hand, A modeling analysis related to the HetNets with cognitive femtocells is conducted as well.

1.2 Thesis Contributions

1.2.1 Key Outcomes

The contributions of this thesis cover the performance analysis of four different types of CR networks, in terms of CRAHNs, CSNs, CR-AMI Networks and Cognitive Femtocell networks. The key outcomes of this work in the form novel solutions, algorithms, protocol design, and analysis are summarised as follows.

1. Although the routing protocol design and spectrum aggregation for CRAHNs have been considered in a number of studies, there is still no routing protocol with spectrum aggregation exists in literature. Moreover, compared with the non-cooperative approach, the cooperative approach provides an opportunity of enhancing the performance in terms of different metrics, e.g., energy efficiency, throughput, and end-to-end reliability. In this regard, a Spectrum Aggregation-based Cooperative Routing Protocol, termed as SACRP, for CRAHNs is presented in Chapter 3. Initially, this chapter highlights the motivation of combining cooperative routing and spectrum aggregation in CRAHNs. Then, the spectrum aggregation framework for CRAHNs is discussed, which includes the design of PHY and MAC layer. Three spectrum aggregation algorithms are proposed, which allow a CR user to transmit data over aggregated channels/bands simultaneously with three different objectives, e.g., energy efficiency, throughput maximization, and end-to-end

latency minimization. Based on the spectrum aggregation algorithms, two different classes of cooperative routing protocol is proposed with special emphasis on energy efficiency, network throughput, and end-to-end delay. Furthermore, The proposed protocol is evaluated through analytical modelling and simulation studies. Performance evaluation demonstrates the effectiveness of SACRP in terms of energy efficiency, throughput, and end-to-end delay.

2. A Cognitive Receiver-Based MAC (CRB-MAC) protocol is presented in Chapter 4. The proposed MAC protocol is designed with special emphasis on energy efficiency, end-to-end delay, and reliability requirements of CSNs operating in smart grid environments. In order to achieve high energy efficiency, the protocol uses preamble sampling [15] approach to minimize idle listening and supporting sleep/wakeup modes without synchronization overheads. In addition, it exploits the broadcast nature of wireless medium and adopts an opportunistic forwarding technique with multiple receivers to provide low end-to-end delay and high reliability. Analytical models and simulation studies are used for evaluating the performance of proposed protocol. The simulation results confirm that CRB-MAC generates less retransmissions and therefore, enhances the overall energy, end-to-end delay and reliability performance in lossy cognitive wireless environments.

3. Advanced Metering Infrastructure (AMI) networks, which are an integral component of the smart grid ecosystem, are practically deployed as a static multi-hop wireless mesh network. Recently, routing solutions for AMI networks have attracted a lot of attention in literature. On the other hand, it is expected that the use of CR technology for AMI networks will be indispensable in near future. Chapter 5 investigates a global optimization-based routing protocol for enhancing QoS in CR-AMI networks. In accordance with practical requirements of smart grid applications, a new RPL-based routing protocol, termed as DMACO-RPL, is proposed for CR-AMI networks. This protocol utilizes a global optimization algorithm to select the best route from the whole

network. In addition, DMACO-RPL explicitly protects primary (licensed) users while meeting the utility requirements of the secondary network. System-level simulations demonstrate that the proposed protocol enhances the performance of existing RPL-based routing protocols for CR-enabled AMI networks.

4. Cognitive femtocells provide low-power, low-cost, and short-range wireless broadband access in two-tier HetNet, achieving higher network capacity and spectrum efficiency. In Chapter 6, the rate coverage analysis of two-tier HetNets with cognitive femtocells is studied. Based on a stochastic geometry approach, the Poisson Point Process (PPP) is adopted to model the locations of the macrocell base stations (MBSs) and the femtocell base stations (FBSs). The concept of "guard-zone" is exploited into the analysis of cognitive femtocells and therefore, the closed-form expressions for downlink rate coverage of both networks are derived, respectively. In addition, the impact of frequency reuse on the rate coverage is also evaluated in two-tier HetNet. Numerical and simulation results demonstrate that cognitive femtocells significantly enhance the rate coverage of the whole HetNet.

1.2.2 List of Publications

The publications related to the main contributions of this thesis are stated as follows. The chapter relevance of different publications is given in Table 1.1.

Journals

(1). **S. Ping**, A. Aijaz, O. Holland, and A.H. Aghvami, "SACRP: A Spectrum Aggregation-based Cooperative Routing Protocol for Cognitive Radio Ad-Hoc Networks," *IEEE Transactions on Communications*, vol.63, no.6, pp.2015-2030, June 2015.

(2). A. Aijaz, **S. Ping**, M.R. Akhavan, and A.H. Aghvami, "CRB-MAC: A Receiver-based MAC Protocol for Cognitive Radio Equipped Smart Grid

Table 1.1: Publications Related to Individual Chapters.

Chapter	Journals	Conferences	Book Chapter
Chapter 2	-	(3), (4)	(1)
Chapter 3	(1)	(1), (2), (3), (4)	(1)
Chapter 4	(2), (4)	(5)	-
Chapter 5	(3), (4)	(6)	-
Chapter 6	(5)	-	-

Sensor Networks," *IEEE Sensors Journal*, vol.14, no.12, pp.4325-4333, Dec. 2014.

(3). Z. Yang, **S. Ping**, A. Aijaz, and A.H. Aghvami, "A Global Optimization-based Routing Protocol for Cognitive Radio Enabled Smart Grid AMI Networks," accepted by *IEEE Systems Journal*, Nov. 2015.

(4). Z. Yang, **S. Ping**, H. Sun, and A.H. Aghvami, "CRB-RPL: A Received-based Routing Protocol for Cognitive Enabled AMI Networks in Smart Grid," accepted by *IEEE Transactions on Vehicular Technology*, Nov. 2015.

(5). **S. Ping**, A. Aijaz, and A.H. Aghvami, "On the Rate Coverage Analysis of Two-Tier Heterogeneous Networks with Cognitive Femtocells," submitted to *IEEE Communications Letters*, Nov. 2015.

Peer-Reviewed Conferences

(1). **S. Ping**, A. Aijaz, O. Holland, and A.H. Aghvami, "Spectrum aggregation-based cooperative routing in Cognitive Radio Ad-Hoc Networks," in proc. *IEEE International Conference on Communications (ICC) Workshop*, vol., no., pp.514-519, 8-12 June 2015.

(2). **S. Ping**, A. Aijaz, O. Holland, and A.H. Aghvami, "Energy and interference aware cooperative routing in cognitive radio ad-hoc networks," in proc. *IEEE Wireless Communications and Networking Conference (WCNC)*, vol., no., pp.87-92, 6-9 April 2014.

(3). O. Holland, **S. Ping**, A. Aijaz, J.M. Chareau, P. Chawdhry, Y. Gao, Z. Qin and H. Kokkinen, "To White Space Or Not To White Space: That Is The Trial Within The Ofcom TV White Spaces Pilot," in proc. *IEEE International Conference on Dynamic Spectrum Access Networks (DySPAN)*, Sweden, 2015.

(4). O. Holland, A. Aijaz, **S. Ping**, S. Wong, J. Mack, L. Lam, and A. Fuente, "Aggregation in TV White Space and Assessment of an Aggregation-Capable Wi-Fi White Space Device," accepted by *IEEE International Conference on Communications (ICC)*, 2016.

(5). Z. Yang, **S. Ping**, A. Nallanathan, and L. Zhang, "ECR-MAC: An Energy-efficent Receiver-based MAC Protocol for Cognitive Sensor Networks in Smart Grid," accepted by *IEEE International Conference on Communications (ICC) workshop*, 2016.

(6). Z. Yang, **S. Ping**, A. Nallanathan, and L. Zhang, "A Receiver-based Routing Protocol for Cognitive Radio Enabled AMI Networks," accepted by *IEEE Vehicular Technology Conference (VTC) workshop*, 2016.

Book Chapter

(1). F. Kaltenberger, T.A. Tsiftsis, F. Foukalas, **S. Ping** and O. Holland, "Aggregation of Spectrum Opportunities," published in "Opportunistic Spectrum Sharing and White Space Access: The Practical Reality," *John Wiley & Sons*, 22 April 2015.

1.3 Outline of the Thesis

The rest of the thesis is organized as follows. Chapter 2 provides the preliminaries on the required technical background for understanding the research area addressed in this thesis. In addition, this chapter presents the related work on different aspects of CR networks.

1.3 Outline of the Thesis

The main contributions of the thesis, which are related to the applications of four distinct areas; CRAHNs, CSNs, CR-AMI Networks and Cognitive Femtocell networks, are discussed in Chapters 3, 4, 5, and 6. Since each contribution chapter addresses a unique research problem, concluding remarks are presented therein. Based on the overall picture of the research conducted in the thesis, the main conclusions together with some directions for future work are presented in Chapter 7.

Chapter 2

Preliminaries and Related Work

This chapter provides a detailed overview of the existing research works on CR networks. CR networks not only provide a dynamic spectrum utilization, but also introduce new specific characteristics and functionalities, which are incompatible with the traditional wireless systems. Therefore, a large volume of research with respect to novel architectures, protocols and solutions for CR networks has been done in order to address the incompatibilities or improve the performance. At the beginning of this chapter, the basic concepts regarding the definition, motivations, functions and characteristics of CR networks are introduced to give readers a global view of CR networks. Then, the background studies about two famous research areas (e.g,. smart grid and HetNet) where CR technologies applied are presented, respectively. At last but not least, the related work of the specific cognitive networks on which this thesis focused is conducted. It includes the existing research achievements and challenges in these specific CR areas, which is an emphasis on the contribution of this thesis.

2.1 Cognitive Wireless Communications

Cognitive Radio can formally be defined as "*a radio that can change its transmitter parameters based on interaction with the environment in which it operates.*" [2,3,16], which includes two main characteristics: 1. Cognitive capability, which refers to the ability of radio technology to capture or sense the information from the environment. It includes sophisticated techniques such as spectrum sensing, spectrum analysis and spectrum decision in order to capture the temporal and spatial variations in the radio environment, select the best spectrum with appropriate

parameters and avoid interference to PUs; and 2. Reconfigurability, which enables the cognitive radio to adapt easily to the dynamic radio environment only by adjusting operating parameters for the transmission without any modifications on the hardware components. As mentioned in the previous chapter, it allows the unlicensed users (secondary users or CR users) dynamically access the frequency bands/channels whenever the licensed users (primary users or PUs) are absent and need to vacate the bands/channels whenever the licensed users are detected.

There are several motivations for using CR technology in the wireless communications as described below.

- Spectrum Scarcity: This is one of the primary bottlenecks for the development of the future wireless communications systems. It has been a tremendous growth over the last few years in terms of the number of users and the amount of carried traffic. As expected by Ericsson, there will be more than 50 billion connected users by 2020. Meanwhile, FCC has reported that there is a large portion of the assigned spectrum used sporadically, which leads to inefficient spectrum utilization. Those problems create a major challenge for existing wireless networks in terms of spectrum congestion and spectrum inefficiency. With CR technology, the existing spectrum can be utilized more efficiently in order to avoid the potential scarcity of spectrum and support large-scale data transmission.

- Interference: With a tremendous of wireless users (devices) operating in the unlicensed spectrum, significant interference issues will arise between self-existing and co-existing users. It will severely deteriorate the performance of the network. CR network enables wireless users to access alternate spectrum such as TV white spaces, which provide significant bandwidth availability and superior propagation characteristics. Furthermore, its DSA capability and dynamic transmit power allocation allow more users to share the spectrum and decrease the interference. These features significantly reduce the interference issues and improve the performance of network.

- Green Communications: There has been a growing trend towards energy efficient or green communications in the wireless communication world. This is primarily due to the factors such as the rising fuel prices worldwide, the awareness of harmful effects of CO_2 emissions on environment, the depletion of non-renewable energy sources etc. On the other hand, energy savings enhance the battery life of wireless devices which will also imporve the network performance. The use of CR technology has been demonstrated to be green or energy efficient as the users can adaptively adjust their transmit power levels based on operating environment [17].

- Network Heterogeneity: The future wireless networks will become more diverse in terms of applications and services, which will also cause diversity in network protocols and data formats. CR provides a more efficient and flexible way to deal with the heterogeneity. The reconfigurability of CR technology guarantees the users to be compatible with heterogeneous wireless architectures and to satisfy the diverse QoS requirements of applications.

- Coverage Issue: One of critical issues in wireless networks is the mobility and the huge uncertainty of user locations. For example, some users might be deployed in the areas where wireless connectivity is not always guaranteed (e.g., A big building blocks the wireless signal or a user stands on the edge of a network). CR technology enables users to overcome this issue through dynamic spectrum access of alternate spectrum bands such as TV white spaces.

Apart from addressing the technical challenges, CR technology also introduces a diversity of new applications [11].

2.1.1 Cognitive Radio Architecture

CR networks can be classified into two broad domains: *Infrastructure-based CR networks* and *non-infrastructure-based CR networks* (cognitive radio ad-hoc networks or CRAHNs) [3]. In infrastructure-based CR networks, there is a central network entity such as a base station in cellular networks or an access point

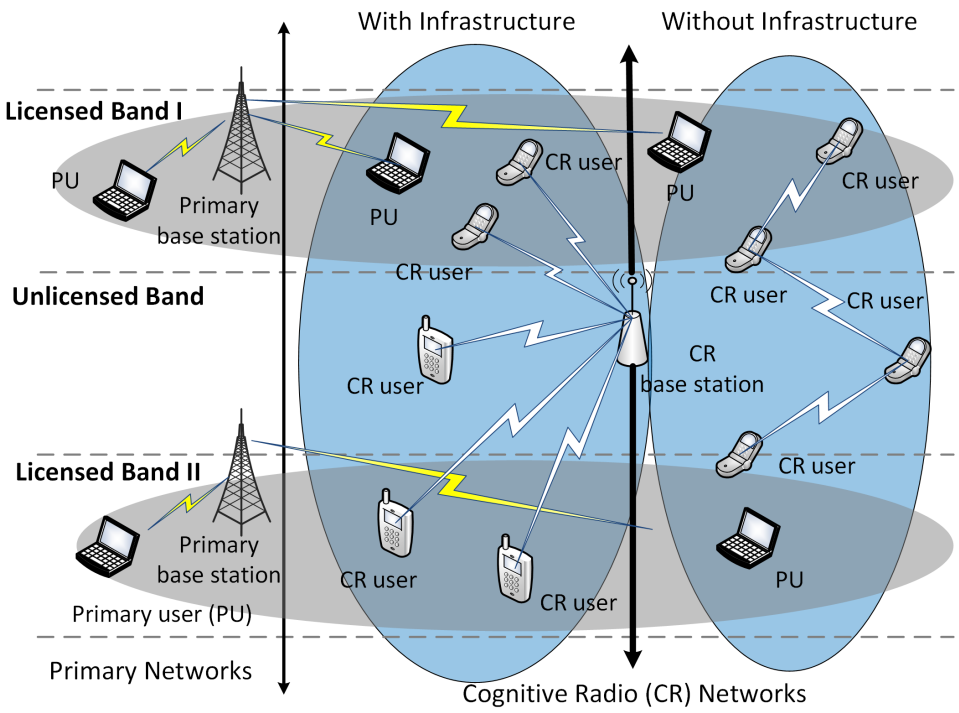

Figure 2.1: Cognitive Radio Network architecture [2].

in wireless local area networks (LANs). The central network entity provides functionalities such as spectrum sharing and spectrum management based on the information sensed and analysed by each CR user, so that it can make decisions on how to allocate the spectrum resources to CR users without introducing interference to primary networks. On the other hand, there is no any infrastructure backbone in CRAHNs. Hence, CR users can communicate with each other through ad-hoc connections on both licensed and unlincensed spectrum. Each user needs to have all CR capabilities and is responsible for determining its actions based on the local information it observed.

The main components of the CR network architecture including both infrastructure-based and non-infrastructure-based networks are illustrated in Fig. 2.1. The components can be classified into two groups: the primary network and the secondary (CR) network. The basic elements and functions of the primary and the CR networks are described as follows [2].

- Primary network: An existing network infrastructure which has an exclusive

right to a certain spectrum band (licensed band). Current primary network includes the TV broadcast networks and the common cellular networks. Two components of the primary network are as follows.

  - Primary user: The user who has the right to operate in a certain licensed spectrum band. This operating right is only controlled by the primary base-station. Actually, primary users do not need any modifications or additional functions for co-existence with CR networks as their operations should not be influenced by any other CR users.
  - Primary base station: The primary base station is a fixed infrastructure network component which owns a spectrum license. For example, the base station transceiver system in a cellular networks or the TV transmitter in TV white space systems. It does not have any CR capabilities for sharing spectrum with CR users, but may be required to have both legacy and CR protocols in order to allows CR users to be able to access the primary spectrum bands.

- CR network: The network (either infrastructure-based or ad-hoc network) which does not have right to operate in a licensed band. Unlike the primary network, the CR network can operate in both licensed and unlicensed spectrum bands, as shown in Fig. 2.1. Therefore, the spectrum access is only allowed in an opportunistic manner. The components of a CR network are defined as below.

  - CR user: CR (unlicensed) users do not have spectrum license, so that additional techniques and functionalities such as spectrum sensing, spectrum sharing, and spectrum management, are required to allow CR users sharing the licensed spectrum band without introducing interference to the primary network. In CRAHNs, the CR users have all functionalities and capabilities to ensure the access of the licensed spectrum band in an opportunistic manner.

- CR base station: The CR base station only exists in the infrastructure-based networks, which is a fixed infrastructure component with CR capabilities and functionalities providing single hop connection to CR users without spectrum access license.
- Spectrum broker: It is a spectrum information manager that shares the spectrum resources among different CR networks. A spectrum broker enables coexistence of multiple CR networks but only exists in the infrastructure-based networks.

As mentioned earlier, the specific network architecture and unique characteristics of CR network require a various of functionalities to support the operations of CR network in the mixed spectrum environment. Therefore, the overview of the specific functionalities of CR networks is outlined in the next section.

2.1.2 Features of Cognitive Radio Networks

In a general sense, a CR network can be perceived as an intelligent overlay network which contains multiple coexisting networks where CR users can communicate with each other [18]. specific system designs (e.g., PHY, MAC, network layer and etc.) are required to adapt CR functionalities and capabilities in the dynamic spectrum environment.

Spectrum sensing as one of the basic functionalities in PHY layer, allows CR users to monitor the licensed spectrum bands and identify the available spectrum holes. This functionality is required to find available spectrum holes over a wide frequency band and to monitor the present of primary networks for avoiding interference. Typically, it can be classified as *non-cooperative spectrum sensing* and *cooperative spectrum sensing*, which are outlined as follows.

- Non-cooperative sensing: It is based on the detection of the received signal from the primary user or base-station through the local observations of CR users. Three detection techniques are usually used in non-cooperative sensing as *matched filter detection*, *energy detection* and *feature detection* [19]. The

matched filter detection provides a coherent detection, which uses a linear optimal filter to maximize the received signal-to-noise ratio (SNR). It provides a fast spectrum sensing but requires a priori knowledge of the primary signal such as the modulation type, the pulse shape and the packet format. The energy detection only measures the energy of the received signal then compares with a threshold to decide whether a primary user is present or not. If the energy of the received signal is larger than or equal to the threshold, it means the primary user is detected, otherwise, it is not detected. This type of detection is easy to be implemented but sometimes not accurate as the energy detector cannot differentiate signal types. At last, feature detection determines the presence of primary signals by extracting their specific features such as pilot signals, cyclic prefixes, symbol rate or modulation types from its observation. It provides a robust sensing result as it can distinguish the signals from different networks. The disadvantage of feature detection is that it is computationally complex and requires significantly long sensing time.

- Cooperative sensing: Cooperative sensing provides more accurate sensing results compared with non-cooperative sensing. This is because cooperative sensing gathers all the sensing information from CR users to detect the presence of the PU. Cooperative sensing can operate either in a centralized or in a distributed way. In the centralized way [20, 21], the CR network contains a fusion centre which plays the role to gather the all the sensing information from the CR users and makes the sensing decision. The distributed method is usually used in CRAHNs where the sensing information is exchanged among the CR users.

At the PHY layer, signal processing techniques and specific hardware implementations provide the main functions of spectrum sensing. However, the frame structure consists of a sensing slot and a transmission slot which provide the periodical spectrum sensing and data transmission, respectively, at the MAC layer. Therefore, lots of attentions have been drawn on the techniques of improving the

performance (e.g., throughput) by reducing the spectrum sensing time.

Spectrum sharing provides the capability of maintaining the QoS of CR users without introducing interference to the PUs. It includes many functionalities such as spectrum access and resource allocation, which coordinate the multiple access of CR users as well as allocate radio resources adaptively to the changes of the environment. Therefore, based on the spectrum sensing results, CR users select the proper channels and adjust the transmission power to achieve the QoS requirements and resource fairness. In multiple user scenario, the spectrum access enables multiple CR users to share the spectrum resource by determining which channel to be accessed or when to access the channel. At the PHY layer, the specific designs are needed in order to allocate the channels to CR users and adjust the transmission power to avoid the interference. Unlike spectrum sensing, spectrum sharing includes MAC functionalities as well. For example, the MAC layer may require a common control channel (CCC) which facilitates many spectrum sharing functions such as communication with a central entity, exchange with sensing information and transmitter receiver handshake.

Spectrum management includes the functions as spectrum analysis and spectrum decision, which decides on the best spectrum band to meet the QoS requirements based on spectrum sensing results. Spectrum analysis investigates the characteristics of different spectrum bands such as interference, path loss, wireless link errors and delays, which can be exploited to select the spectrum band appropriate to the user requirements. Channel capacity and SNR are usually considered as two main factors for the spectrum analysis, which have already been applied in many research area. After analyzing spectrum characteristics, the best spectrum band is select to the CR user based on the user requirements.

At the network layer, the routing protocol design becomes a important topic in CRAHNs. Currently, two different types of routing protocols have been investigated: cooperative routing and non-cooperative routing protocols. Compared with non-cooperative routing protocols, the cooperative approach provides an opportunity of enhancing the performance in terms of different metrics such as

capacity gain or transmit power gain. The related work regarding routing protocols in CRAHNs will be fully discussed in section 2.4.1.

It is noted that, as one of the main objectives of this thesis emphasises on the upper layer (e.g., MAC and network layer) designs, the design of PHY layer for CR networks is beyond the scope of the thesis.

2.2 Smart Grid

The legacy electric power grid, which has lasted for years, is energy inefficient, insecure, and prone to frequent transmission failures and congestion [22]. The term *smart grid* refers to the next generation of electric grid, where power distribution and management is upgraded by incorporating advanced bi-directional communications, automated control, and distributed computing capabilities for improved agility, efficiency, reliability, and security [12]. It allows electricity providers, distributors, and consumers to maintain a real time awareness of operating requirements and capabilities. An integrated high performance, reliable, scalable, robust, and secure communication network is critical for the successful operation of smart grid in order to gather remote and timely information from different areas of grid equipment as well as to support different applications such as smart metering, automated demand response and micro grid management [23].

The smart grid communication infrastructure consists of a multi-tier network extending across different grid operation areas including generation, transmission distribution and consumer premises [24]. Basically, the smart grid network can be divided into three main networks [25]: a home area network (HAN), which creates a communication path between home appliances, in-home displays, energy management systems and energy dashboards; a neighborhood area network (NAN), which collects the metering and service information from multiple HANs and transmits them to a local access point; and a wide area networks (WAN) that provides a broadband communication between smart grid substations, NANs, distributed grid devices and the electric utilities.

2.2 Smart Grid

Smart grid represents one of the largest and most rapidly growing application areas of wireless communications. It provides a modernization of generation, transmission and distribution of a power system with the integration of advanced information and communication technologies (ICTs) infrastructure [25]. So far, two different types of wireless networks are widely applied in the smart grid communications as: Advanced Metering Infrastructure (AMI) networks and Wireless Sensor Networks (WSNs).

In AMI networks, multiple smart meters communicate with a local access point (located at customer premises) which is further connected to a control centre for storage, processing and management of meter data. Through the AMI network, utility providers can manage on demand power requirements and regulate electricity usage. Recently, Routing protocol for Low Power and Lossy Networks (RPL) has been standardized to specifically meet the requirements of AMI applications. RPL is based on the idea of maintaining a directed acyclic graph (DAG) structure for the network, wherein each node maintains its position by using a rank property to determine its relations with other nodes in the DAG [26].

WSNs have been identified as a connected and intelligent monitoring system platform for smart grid, wherein the low-cost wireless sensor nodes can be distributed over wild field [27]. The information gathered from those sensor nodes is not only used for real time default detection but also for supporting different applications, such as automatic metering reading, remote system monitoring and automatic demand response.

Furthermore, the application of CR technology in smart grid communications has drawn much attention. This is not only because its excellent capability to improve the spectrum usage, but also it can alleviate the burden of purchasing licensed spectrum for utility providers [28]. The research based on the applications of CR technology in AMI networks and in WSNs will be discussed in section 2.4, respectively.

2.3 Heterogeneous Networks

It has been reported that the global mobile data traffic grew by 81 percent in 2013, and the monthly mobile traffic is predicted to surpass 15 exabytes by 2018, almost 10 times more than in 2013 [29]. The impressive growth of the demand for capacity urges the revolution of wireless communications. One of the efficient ways is to deploy base stations with hierarchical cell structures [30]. HetNet comprises a conventional cellular network overlaid with a diverse set of lower-power base stations such as picocells, femtocells, and perhaps relay base stations [31]. It is expected to an essential mean for providing higher end-user throughput and expanded indoor and cell-edge coverage.

In [32], the authors proposed novel analytical models for the multi-cell signal-to-interference-plus-noise ratio (SINR) by using stochastic geometry. The Poisson point process (PPP) is used to model the location of the base stations. The closed-form expressions of downlink coverage probability, average rate and the coverage gain from static frequency reuse of cellular networks (not HetNets) were derived, which not only gave more tractable results than the traditional grid-based models, but also provided an efficient approach to analyse the HetNets.

Therefore, in [33], the authors developed a tractable framework for SINR analysis in downlink HetNets with flexible cell association policies. The HetNet is a multi-tier cellular network where each tier's base stations are randomly located with PPP and have a particular transmit power, path loss exponent, spatial density and bias towards admitting mobile users. In that paper, the outage probability of a typical user in the whole network or a certain tier was given. The average ergodic rate of the typical user and the minimum average user throughput were also derived. The results shown that neither the number of base stations or tiers changes the outage probability or average ergodic rate in an interference-limited full-loaded HetNets with unbiased cell association. Similarly, the model of coverage probability for a downlink HetNet was derived in [34]. The downlink rate coverage with tier association probability for HetNets was also considered in [35, 36].

However, in HetNets, different network tiers, which may differ in terms of data rate, channel access protocol, transmit power, and coverage, co-exist in the same vicinity and operate simultaneously. The intra-tier and inter-tier interference may significantly degrade the network performance. Hence, the CR technology was introduced into the HetNet to avoid the interference and improve the performance, wherein the spectrum sensing technique is used to sense the spectrum and avoid using the same frequency channel/band that are simultaneously used by major interference sources. The detailed work regarding the cognitive based HetNets is summarized in the next section.

2.4 Related Work

In this section, a survey of the state of the art in CR networks is presented. The related work on different aspects of CR networks is summarized as follows.

2.4.1 Cognitive Radio Ad-Hoc Networks

In literature, the specific properties and research challenges of the CRAHNs were investigated in [3]. The novel spectrum functionalities such as spectrum sensing, spectrum sharing and spectrum decision were introduced from the viewpoint of a network requiring distributed coordination. Moreover, the influence of these functionalities on the performance of the upper layer protocols such as the network layer and the transport layer protocols were investigated. Finally, a new research direction for CRAHNs was proposed.

After that, the authors in [37] provided an extensive overview of the research in the field of routing for CRAHNs, where the routing problems for CRAHNs are differentiated into two main categories: approaches based on a full spectrum knowledge and approaches only based on the local spectrum knowledge. The proposed design methodologies, routing metrics and practical implementation issues were explained for each category. At last, the authors also proposed several directions for the future research.

In [38], a distributed CR routing protocol (CRP) for ad-hoc networks was proposed to evaluate the performance trade-off between primary network and CR network. The key novelty of CRP is the mapping of spectrum selection metrics and local PU interference observations to a packet forwarding delay over the control channel, where the route information are exchanged among all the intermediate nodes, thereby reducing the computational overhead at the destination. The CRP allows two classes of routes: *class I*: provides better CR network performance; *class II*: achieves a higher measure of protection of the PUs. The results demonstrated that the trade-off incurs in the CR performance to reduce the interference to PU receivers.

The authors in [39] proposed an optimal routing metric for CRAHNs, as referred to OPERA. It was designed to achieve the optimality when combined with both Dijkstra and Bellman-Ford based routing protocols, and the accuracy as OPERA exploits the route diversity provided by the intermediate nodes to measure the actual end-to-end delay. An analytical model of the proposed routing metric was derived for both static and mobile networks. Performance evaluation confirmed the benefits of OPERA for CRAHNs.

A spectrum aware on-demand routing for CRAHNs has been proposed in [40]. The authors proposed an approach to reactively initiate route computing and frequency band selection. A novel multi-flow multi-frequency scheduling scheme was proposed for single node to relief the multi-flow interference and frequent switching delay. The simulation results shown that the proposed routing protocol provides better adaptability to the dynamic spectrum and multi-flow environment. Moreover, the authors in [41] proposed an opportunistic cognitive routing (OCR) protocol which allows users to exploit the geographic location information and discover the local spectrum access opportunities to improve the transmitting performance for each hop. In addition, a novel metric as referred to cognitive transport throughput (CTT) was introduced to capture the unique properties of CRAHNs. A heuristic algorithm was proposed to reduce the searching complexity of the optimal selection of channel and the next hop. The results shown that OCR well adapts the spectrum

dynamics and outperforms existing routing protocols in CRAHNs.

In [42], the authors investigated the applications of cooperative transmission in CRAHNs. Several types of cooperative transmission as well as a new resource allocation problem regarding the joint relay selection and the channel allocation are described, respectively. Therefore, a heuristic algorithm based solution was also proposed to solve this problem. In [43], the authors provided a geometric approach to analyse the cooperative communication in CR networks. An analytical model for two different types of routing strategies were derived, termed as "the nearest-neighbor routing (NNR)" and " the farthest-neighbor routing (FNR)". Numerical results have shown the out-performance by using the cooperative transmission.

The authors in [44] proposed a cooperative routing protocol for CRAHNs to achieve higher channel capacity gain and less end-to-end delay. Due to spectrum heterogeneity characteristics, the channel which provides maximum capacity is selected for transmission in each direct link, and the node that can provide the maximum capacity gain is selected as the relay node for cooperative routing. An on-demand routing protocol was used to find an end-to-end minimum cost path between a pair of source and destination. The simulation results demonstrated that the proposed cooperative routing protocol not only obtains higher end-to-end throughput, but also reduces the end-to-end delay compared with the previous work.

2.4.2 Cognitive Radio Sensor Networks

Currently, the research for CSNs is still in infancy, but is growing rapidly. The authors in [45] classified the existing literature for this fast emerging application area, highlighted the key research that has already been undertaken, and discussed the future research directions. Besides that, the authors in [46] have introduced the main principles, potential application areas and network architectures of cognitive radio sensor networks.

In [47], the authors implemented CSNs in smart grid communications in Pakistan. The experiment results have shown that the CSN provides an efficient and low-cost communication in smart grid so that can improve the electricity distribution

network.

In [48], a novel energy-efficient and spectrum aware multi-channel MAC protocol for cognitive radio sensor network was proposed. The authors have designed a spectrum aware asynchronous duty cycle approach which caters to the requirements of both WSNs and CR networks. Performance of the proposed MAC protocol was evaluated through both simulations and analytical methods, where the proposed approach outperforms the multi-channel scheme for WSNs.

A decentralized MAC protocol for CSNs has been proposed in [49], which allows the CR users (sensor nodes) to recognize spectrum opportunities and transmits data based on the PUs arrival prediction without using a dedicated common control channel. Due to energy efficiency, it estimates the number of active CR users and adjusts their sleep cycles. The authors evaluated the performance of the proposed protocol in terms of delay, energy consumption and throughput through simulations. The results shown that the proposed MAC protocol achieves higher energy efficiency with a small cost of delay and a good throughput performance.

The authors in [50] has developed a multi-constrained QoS aware MAC protocol, termed as MQ-MAC, for a cluster based CSN. In MQ-MAC, a data channel and a backup channel are assigned to a secondary user by using dynamic channel priorities. CR users of a cluster are also prioritized with respect to the urgency of their generated data packets. The features of MQ-MAC include prioritized medium access, dynamic channel allocation, intelligent fusion operation for the channel sensing results, and a dynamic switching mechanism between the data and backup channels. The simulation has been done in NS-3, which proves the efficiency of the proposed protocol.

2.4.3 Cognitive Radio enabled AMI Networks

The authors in [51] provided a comprehensive survey on the CR communication paradigm in smart grid, which also demonstrates how CR can be used in AMI networks. A Packet Reservation Multiple Access (PRMA)-based MAC protocol was investigated in [52] to develop a scheduling algorithm for smart meters. The

authors specifically presented a case study for application of the proposed protocol in cognitive radio enabled AMI networks. In that case, smart meters are placed on power users, served by a single bus (whereby a bus is a common structure connecting multiple electrical devices in a power system). An access point capable of performing spectrum sensing provides wireless connectivity to all the smart meters within the range of the bus. The channel availability and power pricing information is conveyed by the preamble. The multi-frame is periodically scheduled and divided into a fixed number of time slots according to the requirements of utility provider and the power system dynamics. A two state Markov chain models the power load variations. A scheduling algorithm was developed to balance the supply and demand by modifying the backoff procedure such that the smart meter with the highest power load variation is given higher scheduling priority than other meters with lower power load variations.

In [53], the authors provided an enhanced RPL for cognitive radio enabled AMI networks, termed as CORPL. The proposed routing protocol provides novel modifications to RPL in order to address the routing challenges in Cognitive radio environment along with the protection for the primary users as well as meeting the utility requirements of CR networks. Results shown that CORPL improves the reliability of the network while reducing harmful interference to PUs by up to 50% as well as reducing the deadline violation probability for delay sensitive traffic. The detailed overview of CORPL is represented in chapter 5.

2.4.4 Cognitive Femtocell Networks

Recently, femtocells have emerged as a promising solution to provide wireless broad band access coverage in cellular dead zones and indoor environments [54]. Combined with CR technology, CR enabled femtocells achieve higher network capacity and spectrum efficiency and less interference in two-tier HetNets. Stochastic geometry provides an elegant tool to model HetNets with random topology. In [55], the authors presented a comprehensive survey on the stochastic geometry models for cognitive enabled HetNets. The models of HetNets provide

useful insights to the network design and have been adapted to optimize the deployment of base stations, transmission rate and outage probability. At last, the research challenges and future research directions were discussed.

In [56], the authors used stochastic geometry to model and analysed the performance of two-tier HetNets with cognitive femtocells, in terms of outage probability, in a Rayleigh fading environment. The proposed model explicitly accounts for the spatial distribution of macro base stations (MBSs), Femtocell base stations (FBSs) and users in a multichannel environment. The results have shown that the cogntion is an important feature that can boost up the overall network performance. The spectrum sensing threshold is a critical parameter for femotcells, the correct choice of which can decrease the outage probability by 60 percent for the femtocell users. In addition, there is a quite misleading to look into the overall outage performance of the HetNets as it does not convey the performance of the femtocell users.

The authors in [57] used stochastic geometry tools to develop a paradigm that captures the effect of two channel assignment techniques (e.g., random channel assignment and sequential channel assignment) at the macro tier on both the macro users coverage probability and the opportunistic spectrum access performance of cognitive small cells. The results shown that although the coverage probability of the macro users is always better under random channel assignment at the macro tier, the sequential channel assignment can enhance the spectrum access performance of the small cells.

In [58], the authors proposed efficient solutions to mitigate the cross-tier interference for two-tier HetNets with cognitive femtocells. The theoretical results were derived on the donwlink capacity of two-tier networks by using stochastic geometry, while meeting a per-tier outage constraint under different CR capabilities and interference-aware allocation approaches at femtocells. The numerical results shown that the more information is cognized at femtocells, the more spatial reuse gain can be found.

In [59], the authors analysed the trade-off between the traffic offloading from the

macrocell and the energy consumption of the small cells. The uplink capacity were derived for the cognitive small cells located in the Voronoi cell of a macrocell base station. The model accounts for channel fading, aggregated network interference, network topology and load. Numerical results revealed that the knowledge of the interference environment can lead to a substantial reduction of energy consumption for cognitive small cells.

Chapter 3

Spectrum Aggregation-based Cooperative Routing Protocol in Cognitive Radio Ad-Hoc networks

3.1 Introduction

As mentioned in Chapter 1, spectrum scarcity is one of the primary bottlenecks for the development of future wireless communication systems. Under current spectrum allocation policies, the spectrum utilization efficiency in licensed spectrum at a particular time and location is very low [60]. The FCC estimates the usage of assigned spectrum to be between 15% and 85% [2]. In order to address such inefficiency given limited spectrum availability, the FCC has approved solutions such as opportunistic usage of licensed spectrum such as TV white spaces [61]. Such solutions will be eventually realized through the adoption of CR [2, 3] technology, which is envisaged to increase spectrum utilization through DSA technique, wherein unlicensed (CR) users opportunistically use licensed bands when not occupied [62]. Consequently, the utilization of spectrum can be greatly enhanced by opportunistic communication on licensed spectrum.

3.1.1 Motivation and Related Work

The traditional wireless techniques can only support the utilization of continuous spectrum resources. However, wide continuous spectrum bands are rarely available under the current situation of spectrum resources and the policy of stable licensed spectrum utilization. In this regard, *spectrum aggregation* [63] technique has been proposed to satisfy the increasing bandwidth demands. Recently, a number of studies (e.g., see [60, 64–68]) have focused on different spectrum aggregation algorithms for CR networks for increasing spectrum efficiency and throughputs.

Such studies are generally based on an advanced wireless technique: Discontiguous Orthogonal Frequency Division Multiplexing (DOFDM) [69], which can switch off the sub-carriers occupied by primary user(PU) and thus, enables a single CR user to access several spectrum fragments simultaneously on the PHY layer with only one Radio Front (radio transceiver). In [67], Aggregation Aware Spectrum Assignment (AASA) Algorithm is proposed based on a greedy algorithm, which aggregates spectrum fragments from low frequency to high frequency to satisfy the bandwidth requirements. AASA optimizes the spectrum assignment and maximizes the number of supported users. However, it assumes all the nodes have the same bandwidth requirements which is not practical. The authors in [65] provide a Maximum Satisfaction Algorithm (MSA) to allocate the spectrum bands under different bandwidth requirements for CR users. This algorithm always assigns the spectrum bands for the user with higher bandwidth requirement first, and can accommodate more users than AASA when the bandwidth requirements are different. A Channel Characteristic Aware Spectrum Aggregation (CCASA) algorithm has been proposed in [68], which combines Adaptive Modulation and Coding (AMC) [1] and spectrum aggregation to increase the network throughput under hardware constraints.

On the other hand, CRAHN has attracted much attention in the research community in recent years. Unlike either traditional CR networks or ad-hoc networks, CRAHNs provide a non-infrastructure support and spectrum heterogeneity based wireless network which raises unique issues and challenges. In [3], the authors summarize the unique features of CRAHNs and outline the relevant research issues. An important issue is the design of routing protocols for CRAHNs. The authors of [70] review several adaptations of different kinds of on-demand routing protocols: Ad hoc On-Demand Distance Vector (AODV), Dynamic Source Routing (DSR), and hybrid on-demand protocols for CRAHNs. They also investigate the challenges and issues of each routing protocol in CRAHNs. Recently, a number of studies (e.g., see [38, 41, 44, 71–74]) have investigated routing protocols for CRAHNs. So far, two distinct types of routing protocols have been investigated: cooperative routing and non-cooperative routing protocols. A distributed CR

routing protocol is proposed in [38] to specifically address the problems of PU receiver protection, service differentiation in CR routes, and joint spectrum-route selection. In [44], a cooperative routing protocol has been considered for achieving higher channel capacity gain. Due to spectrum heterogeneity characteristics, the channel which provides maximum capacity is selected for transmission in each direct link, and the node that can provide the maximum capacity gain is selected as the relay node for cooperative routing. Furthermore, the authors in [42] propose a heuristic algorithm for cooperative routing to solve the resource allocation problem, which is based on the metric of utility-spectrum ratio of transmission groups. The results demonstrate the improvement of the cooperative transmission over the direct transmission.

3.1.2 Contributions and Outline

Against this background, our objective in this chapter is to design a spectrum aggregation-based routing protocol for CRAHNs. To the best of authors' knowledge, no routing protocol with spectrum aggregation exists in literature for CRAHNs. Our focus is specifically on the design of cooperative routing protocol as the cooperative approach provides an opportunity of enhancing the performance in terms of different metrics, compared to the non-cooperative approach. The proposed protocol is termed as SACRP (Spectrum Aggregation-based Cooperative Routing Protocol) for CRAHNs. The main contributions of the chapter can be summarized as follows.

- We begin our discussion with the spectrum aggregation framework for CRAHNs. This includes the design of PHY and MAC layer needed to aggregate different spectrum bands/channels. After this, we propose three different spectrum aggregation algorithms that allow a CR user to transmit data over aggregated bands/channels simultaneously with different objectives related to the utility of the CR network. The first algorithm minimizes the transmit power for CR users based on a rate demand. The second algorithm maximizes the aggregate channel capacity for a CR user. Finally, the third

algorithm minimizes the end-to-end latency for the CR network.

- Based on the spectrum aggregation algorithms, we design a cooperative routing protocol, termed as SACRP. The proposed protocol uses two different routing classes with special emphasis on energy efficiency, network throughput, and end-to-end delay.

- A comprehensive analytical model for the proposed protocol is built using tools from stochastic geometry. We adopt Poisson Point Process (PPP) for modeling the location of CR nodes in our network and derive analytical expressions capturing different aspects of the proposed routing protocol including MAC layer collisions, average number of hops, end-to-end power, throughput and latency.

- In order to validate the analytical modeling, we conduct a comprehensive simulation-based performance evaluation. We also compare the performance of the proposed protocol with state of the art cooperative and non-cooperative routing protocols for CRAHNs with spectrum aggregation.

The rest of the chapter is organized as follows. In Section 3.2, we provide the network architecture and system model. Section 3.3 focuses on the design of PHY and MAC layers needed for spectrum aggregation and the proposed spectrum aggregation algorithms. This is followed by the framework for the proposed spectrum aggregation-based cooperative routing protocol in Section 3.4. In Section 3.5, analytical modeling of the proposed protocol has been carried out. A comprehensive performance evaluation has been conducted in Section 3.6. Finally, Section 3.7 concludes the chapter.

3.2 Network Architecture and System Model

We consider a CRAHN where nodes are randomly distributed within a specified region. Each node (CR user) is equipped with a single radio transceiver that can be tuned to any channel in the licensed/unlicensed spectrum. The radio transceiver uses

Table 3.1: Frequently Used Notations and Symbols for SACRP.

Notation	Description
$\mathbb{P}_d$	Probability of detection
$\mathbb{P}_f$	Probability of false alarm
$\mathbb{P}_{acc}^{j}$	Probability of accessing the j^{th} cognitive channel
P_{max}	Maximum total transmit power for the CR node
$\mathcal{P}^a$	Maximum allowed transmit power of the channel
$P_{x,y}$	Transmit power for CR node x transmitting to CR node y
$\mathcal{P}_{i,j}$	Transmit power of the j^{th} channel of the i^{th} spectrum
R_d	Rate demand
$\mathcal{R}$	Transmission range
$C_{x,y}$	Channel capacity of link (x, y)
$\mathcal{C}_{i,j}$	Channel capacity of the j^{th} channel of the i^{th} spectrum
Θ	Throughput
Φ	Delay
T_s	Spectrum sensing duration
T	Transmission duration
T_e	Effective transmit time
χ	Channel status
ϵ	Maximum number of aggregated channels
$\mathcal{E}$	The expected transmission count
ρ	Probability of transmitting data through cooperative link
N_a	The number of available channels
N_A	The number of aggregated channels
N	Average number of hops of the routing protocol

Frequency-aware OFDM (FA-OFDM) [1] and Signal Interpretation before Fourier Transform (SIFT) techniques[1] to avoid cross-channel interference and aggregate channels of different spectrum bands, respectively. This allows the CR user to access multiple bands simultaneously with different transmit powers [76]. We assume that all CR users share one dedicated CCC for exchanging control information. Further, we assume N stationary PU transmitters (and hence N available spectrum bands) with known locations and maximum coverage ranges. Each spectrum band contains M channels. Thus, the total number of channels are represented as: $\mathbf{F} = [[f_{1,1}, \ldots, f_{1,M}], [f_{2,1}, \ldots, f_{2,M}], \ldots, [f_{N,1}, \ldots, f_{N,M}]]^T$.

The PU activity model for the j^{th} channel is given by a two state independent and identically distributed (i.i.d.) random process such that the duration of busy and idle periods is exponentially distributed with a mean of $\frac{1}{\mu^j_{ON}}$ and $\frac{1}{\mu^j_{OFF}}$, respectively. Let S^j_b denote the state that the j^{th} channel is busy (PU is active) with probability $\mathbb{P}^j_b = \frac{\mu^j_{OFF}}{\mu^j_{ON}+\mu^j_{OFF}}$, and S^j_i the state that the j^{th} channel is idle with probability $\mathbb{P}^j_i$, such that $\mathbb{P}^j_i + \mathbb{P}^j_b = 1$. We assume that a node employs energy detection technique [77] for primary signal detection wherein it compares the received energy (E) with a predefined threshold (σ) to decide whether the j^{th} channel is occupied or not i.e.,

$$Sensing\ Decision = \begin{cases} S^j_b & \text{if} \quad E \geq \sigma \\ S^j_i & \text{if} \quad E < \sigma \end{cases}, \ j \in \mathbf{F}. \tag{3.1}$$

The two principle metrics in spectrum sensing are the detection probability ($\mathbb{P}_d$), and the false alarm probability ($\mathbb{P}_f$). A higher detection probability ensures better protection to incumbents, whereas a lower false alarm probability ensures efficient utilization of the channel. As per [78], false alarm and detection probabilities for the j^{th} channel can be expressed as follows.

$$\mathbb{P}^j_f = \Pr\left\{E \geq \sigma \mid S^j_i\right\} = \frac{1}{2}\text{Erfc}\left(\frac{1}{\sqrt{2}}\frac{\sigma - 2n_j}{\sqrt{4n_j}}\right), \tag{3.2}$$

[1]SIFT technique is proposed in [75], which performs an efficient time-domain analysis of the raw signal to detect the presence of PU activity and determine its bandwidth.

$$\mathbb{P}_d^j = \Pr\left\{E \geq \sigma \mid S_b^j\right\} = \frac{1}{2}\text{Erfc}\left(\frac{1}{\sqrt{2}}\frac{\sigma - 2n_j\left(\gamma_j + 1\right)}{\sqrt{4n_j\left(2\gamma_j + 1\right)}}\right), \tag{3.3}$$

where Erfc$(\cdot)$ is the complementary error function, and γ_j and n_j denote the SNR of the primary signal and the bandwidth-time product for the j^{th} channel, respectively.

We are interested in probability of accessing the cognitive channel. The CR users can only use the licensed channel in the absence of PU activity. However, in practice, there can be an element of inaccuracy in spectrum sensing. Let $\mathbb{P}_{acc}^j$ denote the probability of accessing the j^{th} cognitive channel which can be evaluated considering the following cases: (i) when S_b^j and the node misses to detect it; (ii) when S_i^j and no false alarm is generated. Hence $\mathbb{P}_{acc}^j$ is given by

$$\mathbb{P}_{acc}^j = \mathbb{P}_b^j\left(1 - \mathbb{P}_d^j\right) + \mathbb{P}_i^j\left(1 - \mathbb{P}_f^j\right). \;\; j \in \mathbf{F}. \tag{3.4}$$

It can be easily verified that under perfect spectrum sensing conditions i.e., $\mathbb{P}_d^j = 100\%$ and $\mathbb{P}_f^j = 0\%$, (3.4) reduces to $\mathbb{P}_i^j$, which is intuitive.

3.3 Spectrum Aggregation for CRAHNs

In this section, we design the PHY and MAC layer for spectrum aggregation for CRAHNs. This is followed by the proposed spectrum aggregation algorithms.

3.3.1 PHY layer for Spectrum Aggregation

In order to aggregate multiple channels from different spectrum bands, each CR node has to perform a multiple-channel spectrum sensing operation for the licensed spectrum bands. We assume that the CR user has this capability of sensing multiple channels periodically. It is assumed that each CR node maintains a Channel Status Table (CST), $\mathbf{X}$, which represents the status of the licensed spectrum bands based on the spectrum sensing results such that

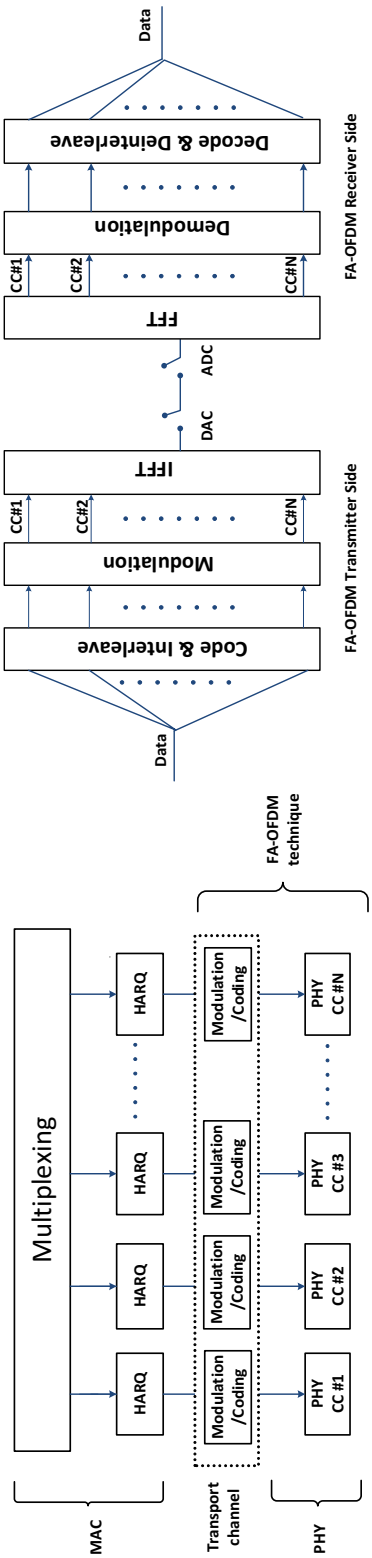

Figure 3.1: (a) MAC and PHY layer structures for spectrum aggregation (HARQ refers to Hybrid Automatic Repeat Request), (b) PHY layer design based on FA-OFDM technique (adapted from [1]).

$$\mathbf{X} = \begin{bmatrix} \chi_{11} & \chi_{12} & \cdots & \chi_{1M} \\ \chi_{21} & \chi_{22} & \cdots & \chi_{2M} \\ \vdots & \ddots & \vdots & \\ \chi_{N1} & \chi_{N2} & \cdots & \chi_{NM} \end{bmatrix}_{N \times M}, \quad \chi_{i,j} \in \{0, 1\}, \tag{3.5}$$

where $\chi_{i,j}$ denotes the channel status on the j^{th} channel of the i^{th} spectrum. If $\chi_{i,j} = 1$, the channel is available for CR nodes, otherwise, it is not. The CST will be updated periodically with spectrum sensing.

In general, the spectrum for CR users is fragmented due to fixed allocation of PUs in different bands. The size of each fragment can vary among different bands/channels. We assume that nodes in our CR network employ the SIFT technique for detecting available bands/channels with different bandwidths.

On the PHY layer, the selected channels are aggregated and the split data packets (as discussed in the next Section on MAC layer design) are carried by different carriers with different transmit powers or transmit rates. To achieve this, FA-OFDM technique is used on both transmitter and receiver sides. As shown in Fig. 3.1b, unlike traditional OFDM, FA-OFDM uses independent modulation and coding schemes for each OFDM channel based on its individual received SNR. Therefore, different transmit rates and different transmit powers can be used on different channels.

3.3.2 MAC Layer Design for Spectrum Aggregation

The MAC frame structure in a CR network consists of a sensing slot (T_s) and a transmission slot (T). In periodic spectrum sensing scenarios, there is a possibility of causing harmful interference to PUs due to imperfect spectrum sensing in practice. This interference is quantified in terms of Interference Ratio (IR), defined as the expected fraction of ON duration of PU transmission interrupted by the transmission of secondary users and is given for the j^{th} channel as follows [79].

$$IR_j = \left(1 - \mathbb{P}_d^j\right) \mathbb{P}_b^j + \mathbb{P}_i^j \left(1 - \mathbb{P}_f^j\right) + e^{-\mu T} \left(\mathbb{P}_f^j - \mathbb{P}_d^j\right), \tag{3.6}$$

where $\mu = \max(\mu^j_{ON}, \mu^j_{OFF})$. We assume that the nodes in our network employ optimal transmission time that maximizes the throughput of the secondary network subject to an interference constraint i.e., $IR_j \leq IR^j_{max}$, where IR^j_{max} denotes the maximum tolerable interference ratio on the j^{th} channel. This transmission time is given for the j^{th} channel as follows.

$$T_j = \mu^{-1}\left[\ln \mathbb{P}^j_i - \ln\left(\mathbb{P}^j_i \mathbb{P}^{'}_d + \mathbb{P}^j_b(1-\mathbb{P}^{'}_d) - IR^j_{max}\right) + \ln(2\mathbb{P}^{'}_d - 1)\right], \tag{3.7}$$

where $\mathbb{P}^{'}_d$ is the detection probability threshold, defined as the detection probability at SNR level as low as γ_{min}, where γ_{min} is specified by the regulator. We propose spectrum aggregation algorithms for SACRP in which the data packets are split on the MAC layer before being transmitted on the PHY layer, as shown in Fig. 3.1a. The transport channel provides modulation and coding operation on data packets, connecting MAC and PHY layers. Before that, each pair of nodes[2] completes exchanging control packets, which include *Ready-To-Send (RTS)*, *Clear-To-Send (CTS)*, and *Reservation (RES)*. After exchanging control information, the set of aggregated channels from multiple spectrum bands and the transmission power of each channel can be determined. Thus the transmission involving spectrum aggregation can be set up between the source and destination node pair. The MAC layer transmission process is described as follows:

- *RTS Packet:* According to the multiple-channel spectrum sensing result, the *RTS* packet is sent from the source to the destination over all available channels.

- *CTS Packet:* For each available channel, the destination node calculates the received SNR[3] after the *RTS* packet received. The destination node performs the spectrum selection operation to select the best set of channels from multiple

[2]The source and destination nodes in this case refer to the sending and receiving nodes within 1-hop vicinity.

[3]The SNR is the ratio of the signal power to the noise power which is given by [1] : $SNR_{i,j} = \frac{\mathcal{P}^{rx}_{i,j}}{N_0} - 1$, where $\mathcal{P}^{rx}_{i,j}$ is the received power over the j^{th} channel of spectrum i and N_0 is the noise power.

spectrum bands based on their received SNRs. After that, a *CTS* packet will be sent back to the source node over the CCC. It contains the information about the selected channels $\mathcal{F} = \{f_1^s, f_2^s \dots f_{N_A}^s\}$ as well as the required transmit power $\mathcal{P}_{tx}$ and transmission rate R_{tx} (discussed in the next section).

- *RES Packet:* If the source node receives the *CTS* packet, it will send a *RES* packet to confirm the successful reception of the *CTS* packet and to notify its neighbor nodes about the transmission. The *RES* contains the same information as the *CTS* packet.

- *Data packets transmission:* After exchanging control information, the source and destination nodes switch to the selected channels and start transmitting data packets. The data packets are split over the aggregated channels (e.g., if there are L_{data} data packets and N_A number of aggregated channels, the data packets per channel would be $\lceil \frac{L_{data}}{N_A} \rceil$). The data packets are transmitted simultaneously on different carriers with different transmit powers or rates. After receiving data packets, the destination node sends an *Acknowledgement (ACK)* packet to the source node to confirm the reception of data packets.

It should be noted that a collision for control packets may occur owing to simultaneous transmission from multiple nodes in a multi-user scenario. We assume that a CR node takes a random back-off after a collision. The back-off taken by a CR node, in terms of back-off time slots, after the i^{th} collision is randomly distributed in the interval $[1, 2, ..., \kappa]$, where $\kappa = 2^i - 1$ denotes the upper bound on the back-off time slots. A detailed analysis of the collision scenario has been conducted in Section 3.5.

Last, but not the least, the MAC and PHY layer design has been summarized as Algorithm 1.

3.3.3 Proposed Spectrum Aggregation Algorithms

In this section, we propose three different spectrum aggregation algorithms in order to meet the energy efficiency, throughput and end-to-end delay requirements

Algorithm 1: PHY AND MAC LAYER DESIGN FOR SPECTRUM AGGREGATION

The source node S performs multiple-channel spectrum sensing for all **F** channels in sensing slot T_s, and updates the CST **X**
for $i = 1 : N$ **do**
  for $j = 1 : M$ **do**
    if $\chi_{i,j} \neq 0$ **then**
      S sends a *RTS* packet to node D over this channel;
      Node D calculates $SNR_{i,j} = \frac{\mathcal{P}_{i,j}^{rx}}{N_0} - 1$
    end
  end
end
Node D sends back a *CTS* packet containing $\{f_1^s, f_2^s \dots f_{N_A}^s\}$ over the CCC;
Node S sends the *RES* packet before data transmission.
for *j=1:* N_A **do**
  FA-OFDM provides different modulation and coding based on the SNR of each channel, and $\lceil \frac{L_{data}}{N_A} \rceil$ of data is transmitted simultaneously by node S.
  if *data packet received (by node D)* **then**
    return ACK
    else
      Node S re-transmits the packet
    end
  end
end

of the secondary network, respectively.

Algorithm I

We aim to calculate the minimum transmission power for each CR user based on a rate demand. This is achieved by adapting the channel capacity given by Shannons Theorem. The capacity of the link between CR users x and y over the k^{th} channel is given by

$$C_{x,y}^{k} = W_{x,y}^{k} \log_2 (1 + SNR_k^y), \tag{3.8}$$

where $W_{x,y}^{k}$ is the potential bandwidth of the k^{th} channel, SNR_k^y is received SNR at node y, which is given by $SNR_k^y = \frac{P_{x,y}^{k}|h_{x,y}|^2}{\delta^2}$ such that $P_{x,y}^{k}$ is the transmit power of x^{th} node to the y^{th} node over the k^{th} channel, δ^2 is the noise power and $h_{x,y} = F_{x,y}^{k}\sqrt{1/L_{x,y}}$ is the channel coefficient, where $F_{x,y}^{k}$ is the fading coefficient of the channel while $L_{x,y}$ is the pathloss.

For each CR user, we assume a minimum requested rate demand R_d. Thus the channel capacity should satisfy the following condition.

$$C_{x,y}^{k} = W_{x,y}^{k} \log_2 (1 + SNR_k^y) \geq R_d. \tag{3.9}$$

Using the expression for SNR and solving for transmit power P, we obtain

$$P_{x,y}^{k} \geq \frac{\left(2^{\frac{R_d}{W_{x,y}^{k}}} - 1\right)\delta^2}{|h_{x,y}|^2}. \tag{3.10}$$

The potential bandwidth of the k^{th} channel for transmission between CR users x and y is obtained as follows.

$$W_{x,y}^{k} = \mathbb{P}_{acc}^{k} B_k, \tag{3.11}$$

where B_k is the bandwidth of the k^{th} channel. Note that the potential bandwidth actually provides the usable bandwidth since CR users access a channel with certain

probability given by (3.4).

Thus, the minimum required transmit power from the CR node x to the node y over the k^{th} channel is given by

$$P_{x,y}^{min,k} = \frac{\left(2^{\frac{R_d}{\mathbb{P}_{acc}^k B_k}} - 1\right)\delta^2}{|h_{x,y}|^2}. \tag{3.12}$$

Similarly, the minimum transmit power for all $\mathbf{F}$ channels can be calculated and represented as a matrix: $\mathbf{P} = [[\mathcal{P}_{1,1}, \ldots, \mathcal{P}_{1,M}], [\mathcal{P}_{2,1}, \ldots, \mathcal{P}_{2,M}], \ldots, [\mathcal{P}_{N,1}, \ldots, \mathcal{P}_{N,M}]]^T$. The spectrum aggregation algorithm is represented as an optimization problem, given as follows.

$$\begin{aligned}
P_1: \quad & \min \quad \sum_{i=1}^{N}\sum_{j=1}^{M} \mathcal{P}_{i,j}\chi_{i,j} \\
s.t \quad & (a) \quad \mathcal{P}_{i,j} \leq \mathcal{P}_{i,j}^a, \quad \forall\, i \in N, \forall\, j \in M \\
& (b) \quad \sum_{i=1}^{N}\sum_{j=1}^{M} \mathcal{C}_{i,j}\chi_{i,j} \geq R_d \\
& (c) \quad \sum_{i=1}^{N}\sum_{j=1}^{M} \chi_{i,j} \leq \epsilon \\
& (d) \quad \sum_{i=1}^{N}\sum_{j=1}^{M} \mathcal{P}_{i,j}\chi_{i,j} \leq P_{max} \\
& (e) \quad \chi_{i,j} \in \mathbf{X}, \quad \forall\, i \in N, \forall\, j \in M,
\end{aligned} \tag{3.13}$$

where $\mathcal{P}_{i,j}^a$ is the maximum allowed transmit power of the j^{th} channel of the i^{th} spectrum, P_{max} is the maximum total transmit power for a CR node, ϵ is the maximum number of channels that can be aggregated by the CR node due to the hardware constraints. The constraint (13a) ensures that the transmit power of each aggregated channel is limited by $\mathcal{P}_{i,j}^a$ in order to avoid interference to PUs. The constraint (13b) ensures that the total capacity of the aggregated channels must satisfy the minimum rate demand R_d. Lastly, the constraint (13d) ensures that the

maximum transmit power constraint for a CR node is met. It is noted that the optimization problem provided in this chapter is used for the best set of channels selection. As the main contribution of this chapter is proposing and modelling the routing protocol in CRAHNs. We do not solve the optimization problem here.

Algorithm II

The aim of this algorithm is to maximize the aggregated channel capacity for a CR node. Using (4.4), the channel capacity of all $\mathbf{F}$ channels is represented as a matrix: $\mathbf{C} = [[\mathcal{C}_{1,1}, \ldots, \mathcal{C}_{1,M}], [\mathcal{C}_{2,1}, \ldots, \mathcal{C}_{2,M}], \ldots, [\mathcal{C}_{N,1}, \ldots, \mathcal{C}_{N,M}]]^T$. The spectrum aggregation algorithm is represented as the following optimization problem.

$$
\begin{aligned}
P_2: \quad & \max \quad \sum_{i=1}^{N}\sum_{j=1}^{M} \mathcal{C}_{i,j}\chi_{i,j} && (3.14)\\
s.t. \quad & (a) \quad \mathcal{P}_{i,j} \leq \mathcal{P}^a_{i,j}, \quad \forall\, i \in N, \forall\, j \in M \\
& (b) \quad \sum_{i=1}^{N}\sum_{j=1}^{M} \mathcal{P}_{i,j}\chi_{i,j} \leq P_{max} \\
& (c) \quad \sum_{i=1}^{N}\sum_{j=1}^{M} \chi_{i,j} \leq \epsilon \\
& (d) \quad \sum_{i=1}^{N}\sum_{j=1}^{M} \mathcal{C}_{i,j}\chi_{i,j} \geq R_d \\
& (e) \quad \chi_{i,j} \in \mathbf{X}, \quad \forall\, i \in N, \forall\, j \in M.
\end{aligned}
$$

Note that the constraints have similar meaning and significance as in the optimization problem (3.13).

Algorithm III

The aim of this algorithm is to minimize the end-to-end latency for the CR network. In CR networks, the CR users perform spectrum sensing (with the duration of T_s) at periodic intervals to update the spectrum occupancy information on CSTs. For energy detection based spectrum sensing, the adjacent CR users must be silenced

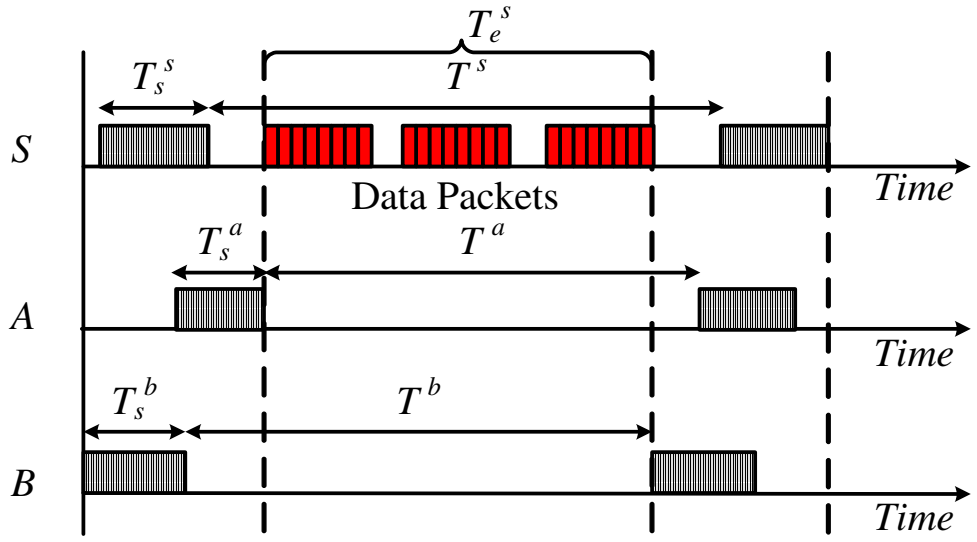

Figure 3.2: The effective transmission time T_e^s for the CR node S with its two neighbors A and B

during the sensing period. Hence, a delay arises when CR users have to stop their transmissions due to the enforcement of silence period. The effective transmit duration [38] for which the transmission is allowed at a candidate forwarding node, over a given channel, is an important criterion for the end-to-end delay of the CR network. Fig. 3.2 depicts the effective transmit time (T_e^S) for the node S. It is clear that the T_e^S is reduced due to the enforcement of silence period arising from the periodic spectrum sensing by neighboring nodes A and B.

Using Fig. 3.2 the effective transmit time of node S is calculated as follows.

$$T_e^S = \max\{T_s^i + T^i\} - \bigcup\{T_s^i\}, \tag{3.15}$$

where $\max\{T_s^i + T^i\}$ represents the maximum duration of the sensing and transmission time among all the neighbors of S and $\bigcup\{T_s^i\}$ is the cumulative duration of silence period. Note that T^i (for the i^{th} neighbor) is given by (3.7).

Recall that (3.4) provides the probability of accessing a cognitive channel. Hence, the total effective transmit time of node S on the k^{th} channel is given by

$$T_{E_k}^S = \mathbb{P}_{acc}^k T_e^S. \tag{3.16}$$

In order to reduce the end-to-end latency, the channels which provide the maximum effective time must be aggregated by the CR node S. Therefore, the spectrum aggregation algorithm can be represented as the following optimization problem.

$$P_3: \quad \max \quad \sum_{i=1}^{N}\sum_{j=1}^{M} T_{E_{(i,j)}}\chi_{i,j} \tag{3.17}$$

$$\begin{aligned} s.t. \quad (a) \quad & \mathcal{P}_{i,j} \leq \mathcal{P}^{a}_{i,j}, \quad \forall\ i \in N, \forall\ j \in M \\ (b) \quad & \sum_{i=1}^{N}\sum_{j=1}^{M} \mathcal{P}_{i,j}\chi_{i,j} \leq P_{max} \\ (c) \quad & \sum_{i=1}^{N}\sum_{j=1}^{M} \mathcal{C}_{i,j}\chi_{i,j} \geq R_d \\ (d) \quad & \sum_{i=1}^{N}\sum_{j=1}^{M} \chi_{i,j} \leq \epsilon \\ (e) \quad & \chi_{i,j} \in \mathbf{X}, \quad \forall\ i \in N, \forall_{\mathrm{J}} \in M. \end{aligned}$$

Note that the constraints have similar meaning and significance as in the optimization problem (3.13).

3.4 SACRP Framework

In this section, we provide the framework for our proposed protocol, termed as SACRP. Our route selection algorithm is based on the shortest path selection. Initially, the source node sends a route request (RREQ) packet to the destination over the CCC. Each node along the packet forwarding path updates three fields in the RREQ. The first is the $< spect >$ field which contains the aggregated channels of each hop, the second is the $< hop >$ field which calculates the hop count of the path, and the third is the $< relay >$ field which contains the relay node of each hop. When receiving the first RREQ packet, the destination node sets up a timer $\triangle t$ to wait for receiving the same RREQ packets from other paths. From all

received RREQ packets, the destination node selects the best path which has the minimum hop count as the direct path. For each hop of the direct path, the relay node is selected. SACRP considers two classes of routing protocols based on relay node selection: *Class A* for energy efficiency and throughput maximization, and the *Class B* for minimizing the end-to-end delay. After that the destination node sends a route reply (RREP) packet along the selected path over the CCC.

3.4.1 Cooperative Routing Protocol for Class A

As mentioned above, the minimum required transmit powers for the aggregated channels are determined by (3.13). We assume that the required data rate R_d is fixed for each hop from the source to the destination. Considering a cooperative transmission as shown in Fig. 3.3, we propose to use the relay node r if and only if the cumulative minimum transmission power of the cooperative links (s, r) and (r, d) is less than that of the direct link (s, d). This condition is given by

$$\text{if and only if,} \quad P_{s,d} > P_{s,r} + P_{r,d}, \tag{3.18}$$

where $P_{s,d}$ is the minimum transmission power of the direct link (s, d), $P_{s,r}$ is the minimum transmission power of the cooperative link (s, r), and $P_{r,d}$ is the minimum transmission power of the cooperative link (r, d). If there are multiple relay nodes satisfying the condition (3.18), SACRP will select the one which provides the maximum cooperative gain. Note that the condition (3.18) may increase the interference to other CR users, therefore, decrease the performance of CR networks. However, as we do not consider the interference among CR users in SACRP, we just ignore this influence. The author encourages the interest readers to investigate the interference influence in SACRP and to provide better solutions.

The same process continues from the source to the destination. The selected path from the source node S to the destination node D is denoted as $Path = \{S, node1, node2, , D\}$. The total transmit power of link (i, j) by involving

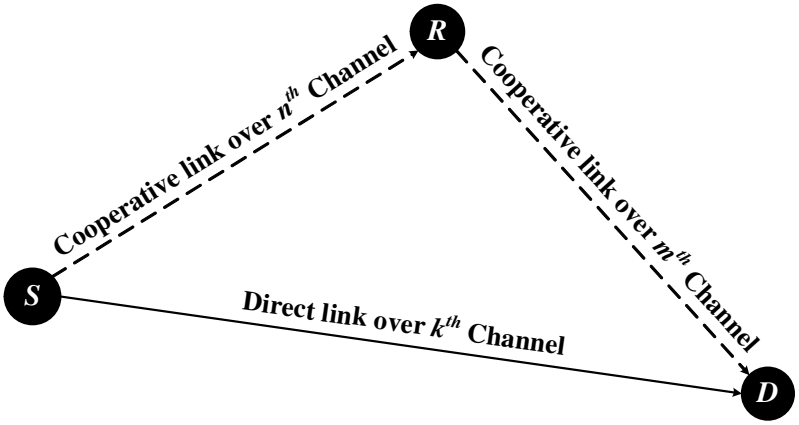

Figure 3.3: Cooperative transmission in CRAHNs

cooperative routing is given by

$$P_{i,j}^{tx} = (1-\rho)\, P_{i,j} + \rho\, (P_{i,r} + P_{r,j})\,, \tag{3.19}$$

where ρ is the probability of transmitting data over cooperative links. The total transmission power from S to D can be obtained by

$$P_{S,D}^{tx} = \sum_{i=S,\ldots,(D-1)}^{j=i+1} \left\{ P_{i,j}^{tx} \right\}. \tag{3.20}$$

Similarly a relay node is selected, if it provides higher channel capacity than the direct link. The capacity of a cooperative link over a given channel has been evaluated in [44, 71]. However, these studies assume that both direct link and cooperation links are using the same channel, which is rather unrealistic for CRAHNs. In CRAHNs, the relay node may use different channel from the direct link (as shown in Fig. 3.3). Thus, the capacity of the cooperative link over different channels is given by

$$C_{s,r,d} = \min\{W_{s,r}^{n} \log_2 \left(1 + SNR_{s,r}^{n}\right), \quad W_{r,d}^{m} \log_2 \left(1 + SNR_{r,d}^{m}\right)\}. \tag{3.21}$$

The relay node selection condition is given by

$$\text{if and only if,} \quad C_{s,r,d} > C_{s,d}. \tag{3.22}$$

Hence, the total capacity of link (i, j) is represented by

$$C_{i,j}^{t} = (1 - \rho)\, C_{i,j} + \rho\, C_{i,r,j}. \tag{3.23}$$

For multi-hop network, the total capacity from the S to D of the selected path is given by

$$\sum_{i=S,\ldots,(D-1)}^{j=i+1} \left\{ C_{i,j}^{t} \right\}. \tag{3.24}$$

3.4.2 Cooperative Routing Protocol for Class B

The end-to-end delay in a multi-hop network depends on the hop count and the number of retransmissions at each hop. We use expected transmission count (ETX) [80] as the default metric for relay node selection. The ETX of link from node s to node d is given by $\mathcal{E}_{s,d} = 1/p_{s,d}^{ss}$, where $p_{s,d}^{ss}$ is the probability of node d successfully receiving a transmission from node s. The ETX of a link will be measured and updated continuously, once the link starts to carry data traffic. For a direct link (s, d), if there is a node r providing smaller ETX than that of the direct link, it will be selected as the relay node. This condition is given as follows.

$$\text{if and only if,} \quad \mathcal{E}_{s,d} > \mathcal{E}_{s,r} + \mathcal{E}_{r,d}, \tag{3.25}$$

where $\mathcal{E}_{s,d}$ is the ETX of the direct link (s, d), $\mathcal{E}_{s,r}$ is the ETX of the cooperative link (s, r) and $\mathcal{E}_{r,d}$ is the ETX of the cooperative link (r, d).

The total delay of a link (s, d) with the relay node r is given as follows.

$$\Phi_{s,r,d} = (1 - \rho)\, \mathcal{E}_{s,d}\, \Phi_{s,d} + \rho\, (\mathcal{E}_{s,r}\, \Phi_{s,r} + \mathcal{E}_{r,d}\, \Phi_{r,d}), \tag{3.26}$$

where $\Phi_{s,d}$ is the delay of direct link (s, d) for single transmission, $\Phi_{s,r}$ is the delay of cooperative link (s, r) and $\Phi_{r,d}$ is the delay of cooperative link (r, d). Similarly, the delay for multi-hop network is given by

$$\sum_{i=S,\ldots,(D-1)}^{j=i+1} \{\Phi_{i,j}\}\,. \tag{3.27}$$

It should be noted that there is a possibility that a relay node is selected by multiple CR users. However, at any time instant, only one pair of CR users (sender and receiver nodes) can use the relay node for transmission. This is due to the fact that the proposed MAC layer design ensures that only one sender-receiver pair is active at any time instant.

Algorithm 2: PROPOSED SACRP FRAMEWORK

Input: *Source*: S, *Destination*: D, R_d, $\mathcal{P}^a$, P_{Max}, ϵ
Output: *Route*: $Path$
while $S \longrightarrow D$ **do**
  Node S sends the RREQ packet over the CCC;
end
if *Node D receives the first RREQ packet* **then**
  set a timer $\triangle t$
  if $t \leq \triangle t$ **then**
    Node D continues receiving RREQ packets
  end
  if $t > \triangle t$ **then**
    Node D stops receiving RREQ packets
  end
end
Node D compares the received RREQ packets and selects the route $Path$ which has the minimum number of hops;
for *each hop* $(i, j) \in Path$ **do**
  if *class A* **then**
    if *for energy efficiency* **then**
      the best channels are selected by (3.13), the relay node is selected by (3.18).
    end
    if *for throughput* **then**
      the best channels are selected by (3.14), the relay node is selected by (3.22).
    end
  end
  if *class B* **then**
    the channels are selected by (3.17), the relay node is selected by (3.25).
  end
end
return *RREP packet with Path*

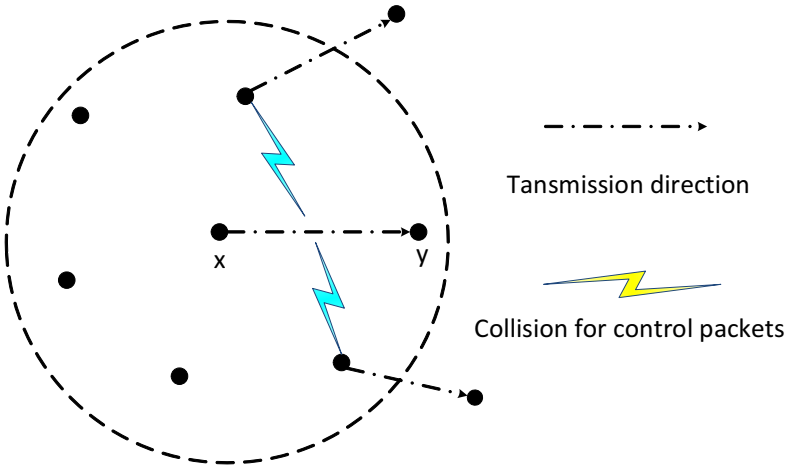

Figure 3.4: The collision scenario for the control packets.

3.5 Analytical Model for SACRP

In this section, we provide an analytical model for our proposed cooperative routing protocol. We adopt tools from stochastic geometry to develop the analytical model. In practice, nodes in an ad-hoc network are randomly distributed. Therefore, for the sake of developing a realistic model, we adopt the PPP for modeling the location of CR nodes in our network[4]. We assume that nodes are distributed according the PPP in an Euclidean plane with intensity λ.

3.5.1 Analysis of the Collision Scenario for Control Packet Transmission

In this section, we analyse the collision scenario for the transmission of control packets on the MAC layer. As shown in Fig. 3.4, a collision may happen when multiple CR nodes transmit control packets over the same channel at the same time. We need to calculate the probabilities of a series of collisions, including *RTS*, *CTS*, and *RES* packets collisions.

[4]Recently, a number of studies have employed the PPP for modeling random ad-hoc networks [55, 81, 82]

Collision of RTS Packets

As the *RTS* packets are transmitted over all available channels, the collision may occur on one or more channels when one of the neighbors (interfering nodes) of the sender start transmission at the same time. The probability of *RTS* collision, denoted by $\mathbb{P}_{RTS}$, is given by

$$\mathbb{P}_{RTS} = 1 - (1-\tau)^{N_a\left(\lambda\pi\mathcal{R}^2-1\right)}, \tag{3.28}$$

where τ denotes the probability that the collision occurs on a single channel, λ is the CR node density, $\mathcal{R}$ is the transmission range of CR nodes, and N_a denotes the number of available channels based on the multi-channel spectrum sensing results in (3.5). Note that $\lambda\pi\mathcal{R}^2 - 1$ denotes the number of neigbors of a sender node.

Since N_a is a random variable, we need to find its expected value. The probability density function (PDF) of N_a is given by

$$f_{N_a}(n) = \begin{pmatrix} NM \\ n \end{pmatrix} \left(\mathbb{P}^j_{acc}\right)^n \left(1 - \mathbb{P}^j_{acc}\right)^{NM-n}, \tag{3.29}$$

where $\mathbb{P}^j_{acc}$ is given by (3.4) and NM is the total number of channels. Hence, the expected value of N_a can be calculated as

$$\mathbb{E}\left[N_a\right] = \sum_{N_a=1}^{NM} \begin{pmatrix} NM \\ N_a \end{pmatrix} \left(\mathbb{P}^j_{acc}\right)^{N_a} \left(1 - \mathbb{P}^j_{acc}\right)^{NM-N_a}. \tag{3.30}$$

Collision of CTS Packets

Since the *CTS* packet is sent by the receiving node over the CCC, a collision may occur when the nodes located in the transmission range of the receiving node start their transmissions at the same time. The probability of *CTS* collision is given by

$$\mathbb{P}_{CTS} = 1 - (1-\tau)^{\lambda\pi\mathcal{R}^2-1}. \tag{3.31}$$

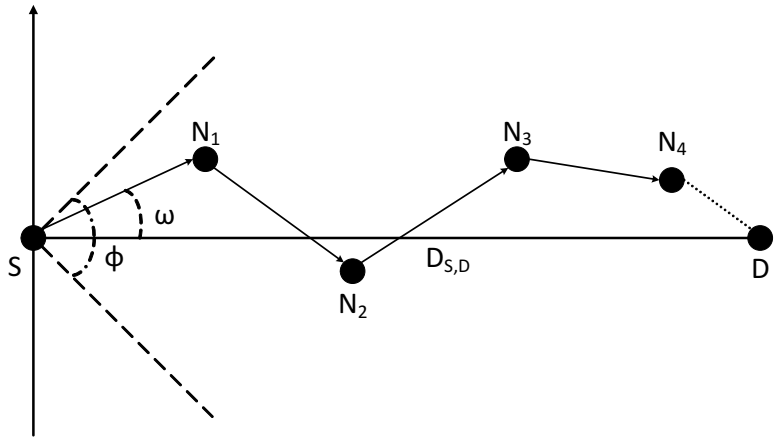

Figure 3.5: The routing model with the source node at the origin and the x-axis pointing in the direction towards the destination node within a sector ϕ. ω is the angle between the x-axis and the path between nodes S and N_1.

Collision of RES Packets

Similarly, the collision for the *RES* packet occurs when the interference nodes initiate their transmissions during the *RES* packet transmission process on the CCC. The probability of *RES* collision is given by

$$\mathbb{P}_{RES} = 1 - (1 - \tau)^{\lambda\pi\mathcal{R}^2 - 1}. \tag{3.32}$$

3.5.2 Analysis of the Routing Protocol

As our model is based on stochastic geometry approach for routing in random networks, we refer the interested reader to [43] for preliminaries. For analysis, we only consider Rayleigh fading channel. The fading coefficient of the k^{th} channel from a CR node x to a CR node y is denoted by $F^k_{x,y}$ such that $\mid F^k_{x,y} \mid^2$ is Exponentially distributed with mean $1/\mu$.

In SACRP, the objective is to find the path which has the minimum number of hops to destination. For each hop of the route, a relay node may be selected with different requirements. The model of the route selection can be considered as the farthest neighbor (within the transmission range) routing in the direction of the destination, as shown in Fig. 3.5.

Firstly, we determine the average number of hops towards destination. For this purpose, let $D_{S,D}$ denote the distance between the source and the destination node. The PDF of the distance to the farthest neighbor from a sender node with the transmission range $\mathcal{R}$ in a sector ϕ, given that there is at least one neighbor in the sector, is given by [81]

$$f_{\mathcal{R}}(\mathrm{r}) = \frac{\lambda\phi \mathrm{r} e^{\frac{\lambda\phi \mathrm{r}^2}{2}}}{e^{\lambda A} - 1}, \qquad \text{for } \; 0 \leq \mathrm{r} \leq \mathcal{R}, \tag{3.33}$$

where $A = \frac{\phi\mathcal{R}^2}{2}$ is the area of the sector. In a PPP network with density λ, all the node distances of the route follow the same PDF. Thus, the mean hop length $\mathbb{E}[d]$ is given by

$$\mathbb{E}[d] = \frac{\mathcal{R}e^{\lambda A} - \sqrt{\frac{\pi}{2\lambda\phi}}\mathrm{erfi}\left(\mathcal{R}\sqrt{\lambda\phi/2}\right)}{e^{\lambda A} - 1}, \tag{3.34}$$

where $\mathrm{erfi}\,(y) = \frac{2}{\sqrt{\pi}} \int_0^y e^{t^2}\, dt$ is the inverse error function. The proof is given in [81].

Further, the angle ω_k from the origin to the k^{th} node follows a Gaussian distribution with variance $V\,(\phi, k) \approx \phi^2/12k$ [82]. Thus, the path efficiency[5] of the selected nodes in farthest neighbor routing scheme is given by [43]

$$\overline{\eta\,(\omega)} \approx \left(1 - \frac{\phi^2}{24\lambda A}\right)\left(1 - e^{-\lambda A}\right) + \frac{\phi^2}{24} e^{-\lambda A}. \tag{3.35}$$

Therefore, the average number of hops N of the routing protocol is given by

$$N = \frac{D_{S,D}}{\mathbb{E}[d]\overline{\eta\,(\omega)}}. \tag{3.36}$$

Next, we determine the average distance between any pair of sender/receiver nodes and the relay node. For each hop of the route, the relay node may be selected by the condition (3.18), (3.22) or (3.25). The relay node and the receiver node must be located in transmission range of the sender node. The pdf of the distance between the relay node and the receiver node within the transmission range of the

[5]The path efficiency is the ratio of the Euclidean distance between the end nodes and the actual distance travelled.

sender node is given by [83]

$$f_d(\mathrm{r}) = \frac{2\mathrm{r}}{\mathcal{R}^2}\left(\frac{2}{\pi}\cos^{-1}\left(\frac{\mathrm{r}}{2\mathcal{R}}\right) - \frac{\mathrm{r}}{\pi\mathcal{R}}\sqrt{1-\frac{\mathrm{r}^2}{4\mathcal{R}^2}}\right), \quad \text{for} \;\; 0 \leq \mathrm{r} \leq \mathcal{R}. \tag{3.37}$$

Similarly, the PDF of the distance between the sender node and the relay node is given by (3.37). Hence, the average distance between the relay node and the sender/receiver node is given by

$$\mathbb{E}[\mathrm{r}] = \int_0^{\mathcal{R}} \frac{4\mathrm{r}^2}{\pi\mathcal{R}^2}\cos^{-1}\left(\frac{\mathrm{r}}{2\mathcal{R}}\right) - \frac{2\mathrm{r}^3}{\pi\mathcal{R}^3}\sqrt{1-\frac{\mathrm{r}^2}{4\mathcal{R}^2}}\; d\mathrm{r}. \tag{3.38}$$

Power and Throughput Model for Class A

In Rayleigh fading channel, the single hop minimum power consumption for a node x transmitting to a node y, subject to a rate demand, over all the aggregated channels is given by

$$P_{x,y}^{min} = \sum_{k=1}^{N_A}\int_0^{\infty} 1 - \exp\left[\frac{-\mu\left(2^{\frac{R_d^k}{\mathbb{P}_{acc}^k B_k}} - 1\right)\delta^2 L_{x,y}}{t}\right] dt, \tag{3.39}$$

where N_A is the number of aggregated channels, R_d^k is the rate demand of the k^{th} aggregated channel, and $L_{x,y}$ is the path loss which can be calculated using (3.34) or (3.38) for the direct or relay transmission scenario respectively, with the selected path loss model. Note that $\sum_{k=1}^{N_A} R_d^k \geq R_d$ which means the total capacity of all aggregated channels must be larger than or equal to the rate demand.

The derivation of (3.39) is given in Appendix A.

The total capacity of all aggregated channels in Rayleigh fading environment is given by

$$C_{x,y} = \sum_{k=1}^{N_A}\int_0^{\infty} \exp\left[\frac{-\mu\left(2^{\frac{t}{\mathbb{P}_{acc}^k B_k}} - 1\right)\delta^2 L_{x,y}}{\mathcal{P}_k^a}\right] dt, \tag{3.40}$$

where $\mathcal{P}_k^a$ is the maximum allowed transmit power of the k^{th} channel.

The derivation of (3.40) can be obtained in a similar way as described in Appendix A.

In order to evaluate the probability of transmitting data over the cooperative link, ρ, we need to evaluate the probability of a successful transmission, which is given by

$$\begin{aligned} p^{ss} &= \mathbb{P}\left[SNR \geq \gamma\right] \\ &= \mathbb{P}\left[|F_{x,y}|^2 \geq \frac{\gamma \delta^2 L_{x,y}}{P_{x,y}}\right] \\ &= \exp\left(\frac{-\mu\gamma\delta^2 L_{x,y}}{P_{x,y}}\right), \end{aligned} \tag{3.41}$$

where γ is the threshold SNR for successful data transmission. Therefore, we have

$$P_{x,y} = \frac{\mu\gamma\delta^2 L_{x,y}}{-\ln p^{ss}}. \tag{3.42}$$

Using (3.42), $C_{x,y}$ can be expressed as

$$C_{x,y} = \sum_{k=1}^{N_A} W_{x,y}^k \log_2\left(1 + \frac{\mu\gamma|F_{x,y}^k|^2}{-\ln p^{ss}}\right), \tag{3.43}$$

where $W_{x,y}^k$ is obtained from (3.11).

As the power consumption and capacity are calculated according to Shannon's Theorem, the node which provides the maximum capacity must provide the minimum transmit power. According to (3.22) and (3.43), the probability of transmitting data over the cooperative link, ρ_A, for *Class A* is given by (3.44).

Using (3.19) and (3.44), the transmit power of link (x, y) by involving a relay node r is given by (3.45).

Subsequently, the end-to-end power consumption from the source node to the destination node is given by

$$P_{S,D}^{tx} = N P_{x,y}^{tx}, \tag{3.46}$$

$$\begin{aligned}\rho_A =& \mathbb{P}\left[C_{x,r,y} > C_{x,y}\right] = \mathbb{P}\left[C_{x,r} > C_{x,y}\right]\mathbb{P}\left[C_{r,y} > C_{x,y}\right] \\ &= \mathbb{P}\left[|F_{x,r}|^2 > \frac{\left(2^{\frac{C_{x,y}}{W_{x,r}}} - 1\right)\left(-\ln p_{x,r}^{ss}\right)}{\gamma\mu}\right]\mathbb{P}\left[|F_{r,y}|^2 > \frac{\left(2^{\frac{C_{x,y}}{W_{r,y}}} - 1\right)\left(-\ln p_{r,y}^{ss}\right)}{\gamma\mu}\right] \\ &= \exp\left[\frac{\left(2^{\frac{C_{x,y}}{W_{x,r}}} - 1\right)\left(-\ln p_{x,r}^{ss}\right) + \left(2^{\frac{C_{x,y}}{W_{r,y}}} - 1\right)\left(-\ln p_{r,y}^{ss}\right)}{\gamma}\right].\end{aligned} \tag{3.44}$$

where N is given by (3.36).

Next, using (3.23), the end-to-end throughput from the source node to the destination node is given by (3.47), where $C_{x,y}$ is the capacity of link (x, y) which is given by (3.40), and $C_{x,r,y}$ is the capacity of the cooperative link which is equal to $\min\left[C_{x,r}, C_{r,y}\right]$ according to (3.21).

$$\begin{aligned}\Theta =& \left((1-\rho)(1-\mathbb{P}_{RTS})(1-\mathbb{P}_{CTS})(1-\mathbb{P}_{RES})p_{x,y}^{ss}\right)^N C_{x,y} \\ &+ \left((\rho(1-\mathbb{P}_{RTS})(1-\mathbb{P}_{CTS})(1-\mathbb{P}_{RES}))^2 p_{x,r}^{ss} p_{r,y}^{ss}\right)^N C_{x,r,y}.\end{aligned} \tag{3.47}$$

Delay Model for Class B

We use ETX as a default metric for relay node selection in *Class B*. Recall that ETX is defined as $\mathcal{E} = 1/p^{ss}$, where p^{ss} is given by (3.41). Therefore, the ETX between node x and node y can be expressed as

$$\mathcal{E}_{x,y} = \exp\left[\alpha L_{x,y}\right], \tag{3.48}$$

where $\alpha = \mu\gamma\delta^2/P_{x,y}$. According to the condition (3.25), the probability of transmitting data over cooperative link for *Class B*, ρ_B can be expressed as

$$\rho_B = \frac{1}{2} + \frac{1}{2}\mathrm{erf}\left[\frac{\ln \mathcal{E}_{x,y} - \mu_{etx}^{'}}{\sqrt{2}\sigma'}\right], \tag{3.49}$$

$$
\begin{aligned}
P_{x,y}^{tx} = \sum_{k=1}^{N_A} \Bigg(& 1 - \exp\left[\frac{\left(2^{\frac{C_{x,y}}{W_{x,r}}} - 1\right)\left(-\ln p_{x,r}^{ss}\right) + \left(2^{\frac{C_{x,y}}{W_{r,y}}} - 1\right)\left(-\ln p_{r,y}^{ss}\right)}{\gamma} \right] \Bigg) \int_0^{\infty} 1 - \exp\left[-\mu \frac{\left(2^{\frac{R_d^k}{\mathbb{P}_{acc}^k B_k}} - 1\right)\delta^2 L_{x,y}}{t} \right] dt \\
& + \left(\sum_{n=1}^{N_A'} \int_0^{\infty} 1 - \exp\left[-\mu \frac{\left(2^{\frac{R_d^n}{\mathbb{P}_{acc}^n B_n}} - 1\right)\delta^2 L_{x,r}}{t} \right] dt + \sum_{m=1}^{N_A''} \int_0^{\infty} 1 - \exp\left[-\mu \frac{\left(2^{\frac{R_d^m}{\mathbb{P}_{acc}^m B_m}} - 1\right)\delta^2 L_{r,y}}{t} \right] dt \right) \times \\
& \exp\left[\frac{\left(2^{\frac{C_{x,y}}{W_{x,r}}} - 1\right)\left(-\ln p_{x,r}^{ss}\right) + \left(2^{\frac{C_{x,y}}{W_{r,y}}} - 1\right)\left(-\ln p_{r,y}^{ss}\right)}{\gamma} \right].
\end{aligned}
\tag{3.45}
$$

where $\text{erf}(y) = \frac{2}{\sqrt{\pi}} \int_0^y e^{-t^2}\ dt$ is the error function, $\sigma'^2 = \ln\left(\frac{\exp(\alpha^2)-1}{2} + 1\right)$ and $\mu'_{etx} = \ln 2 + \frac{1}{2}\left(\alpha^2 - \sigma'^2\right)$.

Proof The proof of (3.49) is given in Appendix B.

Considering the collisions for control packets, the single hop delay without re-transmissions is given by

$$\Phi = \left[\frac{1 - \min(\mathbb{P}^j_{acc})}{\min(\mathbb{P}^j_{acc})} + \left\lceil \frac{N_{data} L_{data}}{T R_d} \right\rceil - 1\right] T_s + \frac{N_{data} L_{data}}{R_d} + T_b, \tag{3.50}$$

where $\mathbb{P}^j_{acc}$ is given by (3.4) such that $j \in \mathcal{F}$, N_{data} is the number of data packets, L_{data} is the data packet size, T is the transmission time, R_d is the rate demand, and T_b is the average back-off time for control packets until successful transmission which is given by (3.51),

$$T_b = T_{slot} \times \left(\frac{1}{(1-\mathbb{P}_{RTS})(1-\mathbb{P}_{CTS})(1-\mathbb{P}_{RES}) \left[1 - [(1-\mathbb{P}_{RTS})(1-\mathbb{P}_{CTS})(1-\mathbb{P}_{RES})]^{\frac{1}{\lambda\pi\mathcal{R}^2-1}}\right]} - 1 \right), \tag{3.51}$$

where T_{slot} is the back-off slot duration, and $\lambda\pi\mathcal{R}^2 - 1$ denotes the number of neigbors of a sender node.

Proof The proof of (3.50) and (3.51) is given in Appendix C.

Using (3.26) and (3.27), the end-to-end delay from the source node to the destination node is given by

$$\Phi_{S,D} = N\left((1-\rho)\,\mathcal{E}_{x,y}\Phi_{x,y} + \rho\left(\mathcal{E}_{x,r}\Phi_{x,r} + \mathcal{E}_{r,y}\Phi_{r,y}\right)\right), \tag{3.52}$$

where N is given by (3.36), ρ_B is given by (3.49), and Φ is given by (3.50).

3.6 Performance Evaluation

In this section, we analyse the performance of our proposed cooperative routing protocol. For the sake of validating the analytical results, we also perform a

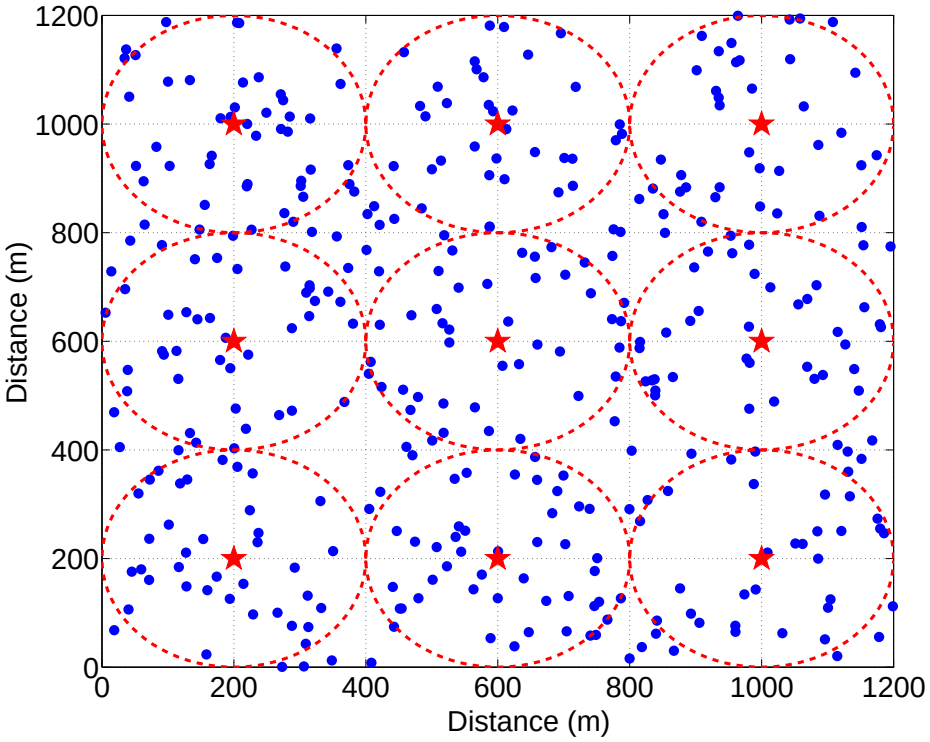

Figure 3.6: Simulated network topology. The stars and dotted circles represent the location and coverage area of PU transmitters, respectively. The dots represent the location of CR users.

simulation study. We implement SACRP in MATLAB with the network topology as shown in Fig. 3.6. Other simulation parameters are given in Table 3.2. A square region of side 1200m is assumed with 9 PU transmitters. Each PU transmitter has 5 channels. Similar to the analytical model, we assume that the CR users are Poisson distributed in the whole region with a density $\lambda = 200$ nodes/km. The parameters characterizing the *ON* and *OFF* times of PU transmitters are randomly set in the interval $[0, 1]$. We consider a frequency selective Rayleigh fading channel between any two nodes, where the channel gain accounts for Rayleigh fading and path loss.

Firstly, we validate the analytical results. Fig. 3.7 shows the end-to-end power consumption against the network density. As shown, the transmission power decreases when the network density increases. This is because the probability of finding a relay node increases with the network density. Moreover, the end-to-end

Table 3.2: Simulation Parameters for SACRP.

Parameter	**Value**
Range of Frequency Bands	3 bands each in 900 MHz, 1800 MHz and 2100 MHz
Detection probability threshold ($\mathbb{P}_d^{'}$)	0.9
Probability of false alarm ($\mathbb{P}_f$)	0.1
Channel bandwidth	2 MHz
Maximum Interference Ratio (IR_{max})	0.25
Spectrum sensing duration (T_s)	20 ms
Back-off slot duration(T_{slot})	20 μs
Transmission time of a data packet (T)	60 ms
Maximum transmit power ($\mathcal{P}_{max}$)	30 dBm
Maximum allowed transmit power ($\mathcal{P}^a$)	20 dBm
PU transmission range ($\mathcal{R}_{PU}$)	200 m
CR node transmission range ($\mathcal{R}_{CR}$)	150 m
Antenna height	15 m
Transmission rate demand (R_d)	512 kbps
Number of data packets (N_{data})	100
Data Packet size (L_{data})	1000 bytes
Path loss model	Okumura model [84] applicable for 150-3000 MHz

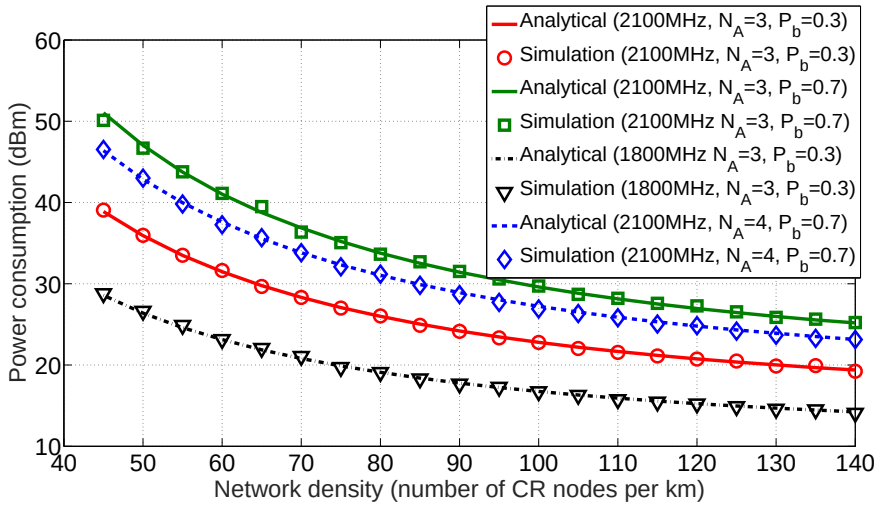

Figure 3.7: End-to-end power consumption against network density in SACRP, which can be obtained by (3.36). N_A is the number of aggregated channels, and P_b is the PU activity.

power consumption in high frequency band is larger than that of the low frequency band, as the high frequency band suffers more path loss. In addition, for a given probability of PU being active, P_b, the power consumption is reduced when the number of aggregated channels increases due to the infamous bandwidth-power inverse relationship. The power consumption increases as P_b increases due to the fact that a higher PU activity will reduce the potentially available bandwidth. Note that the simulation results closely follow the analytical results and hence validate the analytical modeling.

The analytical and simulation results for the end-to-end throughput are given in Fig. 3.8. It is noted that the throughput initially increases and then decreases with the network density. This is because the probability of finding a relay node, which provides higher capacity, increases with the network density. On the other hand, the probability of control packet collision also increases with the network density; as a result of which the throughput degrades. Besides, the low frequency band provides higher throughput than the high frequency band due to the fact that the latter suffers more path loss. As expected, for a given P_b, the end-to-end throughput increases with the number of aggregated channels. Furthermore, the end-to-end

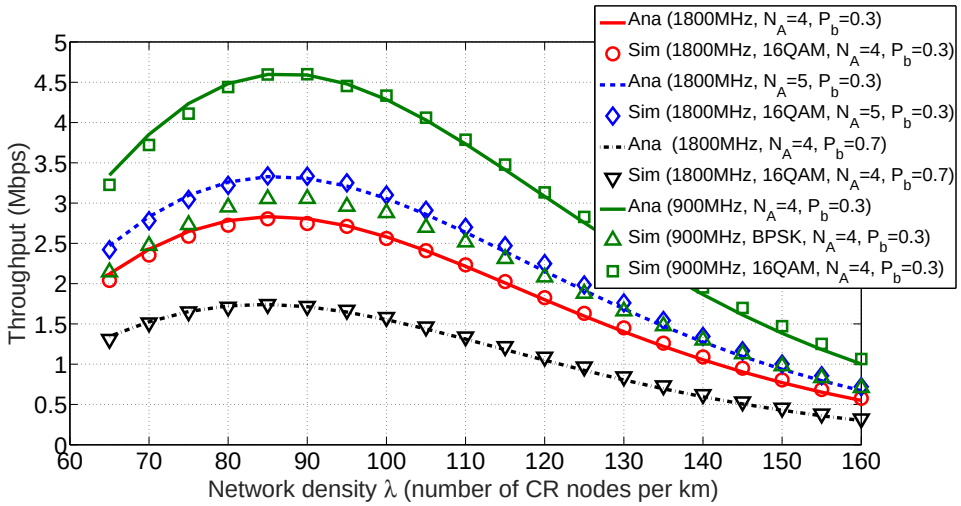

Figure 3.8: End-to-End throughput against network density in SACRP, which can be obtained by (3.47). N_A is the number of aggregated channels, and P_b is the PU activity.

throughput decreases with higher PU activity. We also note that increasing the order of modulation in simulations achieves higher throughput, which is intuitive. Moreover, higher order modulation performs close to the analytical results.

Fig. 3.9 depicts the end-to-end delay against the network density. We vary the ETX of the cooperative link and note that the relay node provides lower end-to-end delay in good channel conditions (i.e., low ETX). Moreover, the end-to-end delay initially decreases and then increases as the network density increases. This is because the probability of finding a relay node, providing lower ETX, increases with the network density. However, the probability of control packet collision also increases with the network density, which increases the number of re-transmissions. In addition, the end-to-end delay increases with higher PU activity as the effective transmission time for a CR node is reduced. As before, the simulation results closely follow the analytical results and hence validate the analytical modeling.

The analytical and simulation results for the cumulative probability of collision (for all types of control packets) against the number of source-destination pairs are shown in Fig. 3.10. It can be seen that the probability of collision increases with the the number of source-destination pairs. For a given network density, the probability

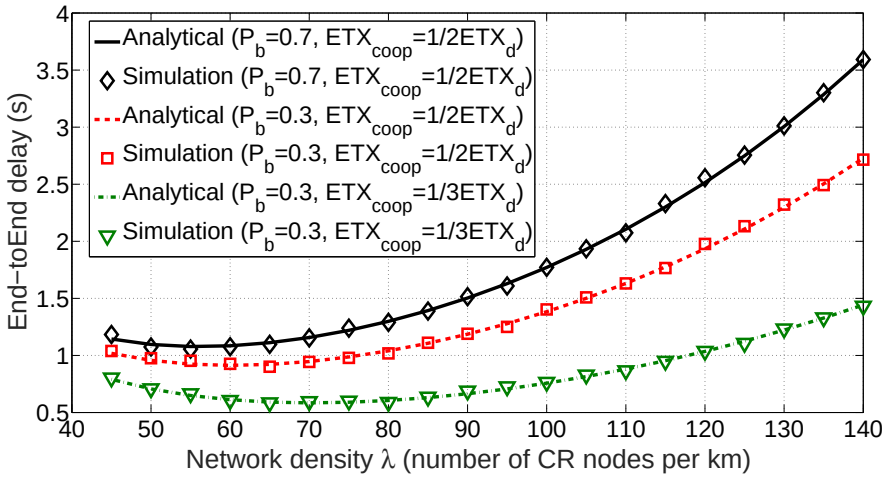

Figure 3.9: End-to-End delay against network density in SACRP, which can be obtained by (3.52). P_b is the PU activity.

of collision increases with higher PU activity. This is due to the reduction in effective resources (shared by all CR nodes) for the transmission of CR nodes. Besides, for a given P_b, a higher network density will result in higher probability of collision. As before, the simulation results closely follow the analytical results and hence validate the analytical modeling.

After validating the analytical results with simulations, we conduct a simulation-based performance evaluation and a performance comparison of the proposed routing protocol.

Firstly, we evaluate the performance of transmit power consumption in our proposed *Class A* protocol. Fig. 3.11 depicts the transmit power as a function of the rate demand between the source and the destination. As the rate demand increases, the power consumption also increases. As shown, our proposed *Class A* can reduce the transmit power significantly. The transmit power is further reduced as more channels are aggregated. However, as the number of aggregated channels increases, the transmit power gain is decreased. As shown in Fig. 3.11, the maximum gain is achieved with two aggregated channels. This is because the CR node has to overcome more attenuation (path loss and fading) of the aggregated channels when the number of aggregated channels increases.

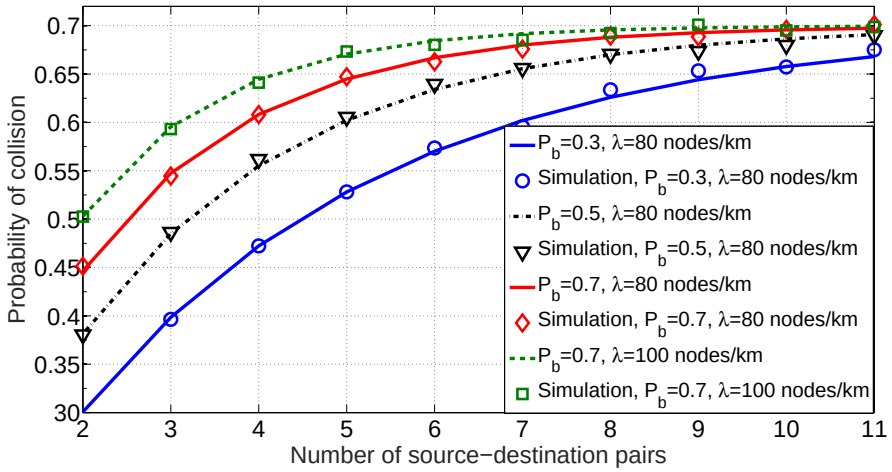

Figure 3.10: The probability of collision against the number of source and destination pairs. The collision models are given in subsection 3.5.1. λ is the network density, P_b is the PU activity.

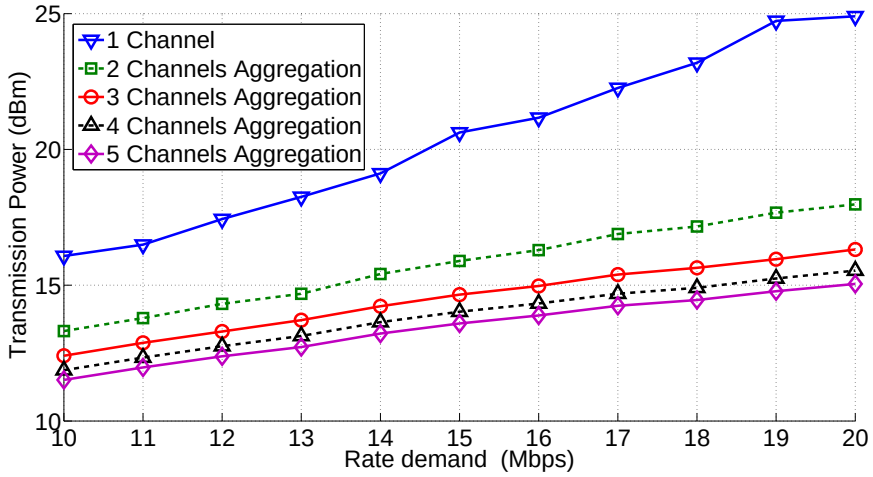

Figure 3.11: Transmission power consumption against the rate demand in SACRP *Class A*.

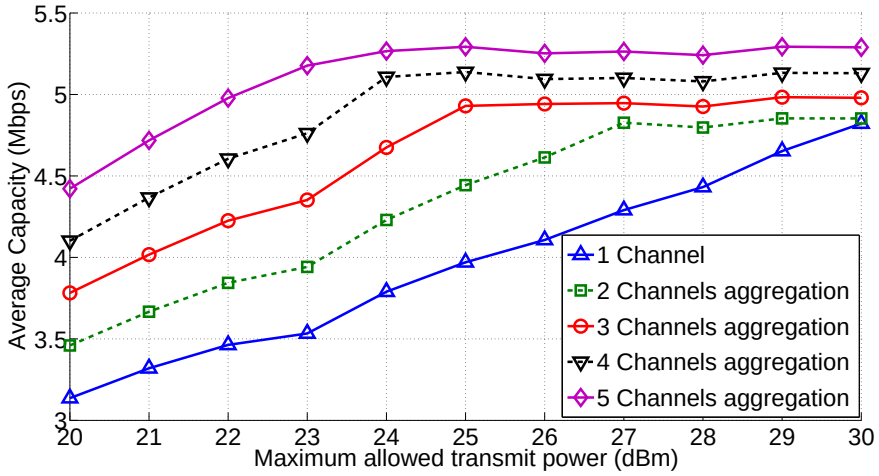

Figure 3.12: Average capacity performance against the maximum allowed transmit power of each channel ($\mathcal{P}^a$) in SACRP *Class A*.

The average capacity performance against the maximum allowed transmit power of each channel ($\mathcal{P}^a$) is shown in Fig. 3.12. In this case, we assume that the $\mathcal{P}^a$ of each channel is fixed and increases from 20 dBm to 30 dBm. The maximum power constraint P_{max} of each CR node is set as 30 dBm. With the increase in $\mathcal{P}^a$, the capacity performance increases. The capacity performance reaches a saturation point as soon as the total transmission power reaches the constraint P_{max}.

Next, we compare our proposed SACRP with other protocols with spectrum aggregation in the same simulation configurations. We assume that the MSA spectrum aggregation algorithm [65] is combined with non-cooperative Routing Protocol: CRP-*Class I* [38] and cooperative routing protocol: COOP [44], respectively.

Fig. 3.13 presents the transmit power performance as a function of the distance between the source and the destination. We observe that the transmit power grows with the distance. Our proposed *Class A* costs the minimum transmit power compared with other three protocols. Both *Class A* and *Class B* have better performance than other protocols. This is because *Class A* always aggregates the channels which can provide the minimum transmit power. For different channel quality, it is able to adjust the transmit power in order to reduce the overall power

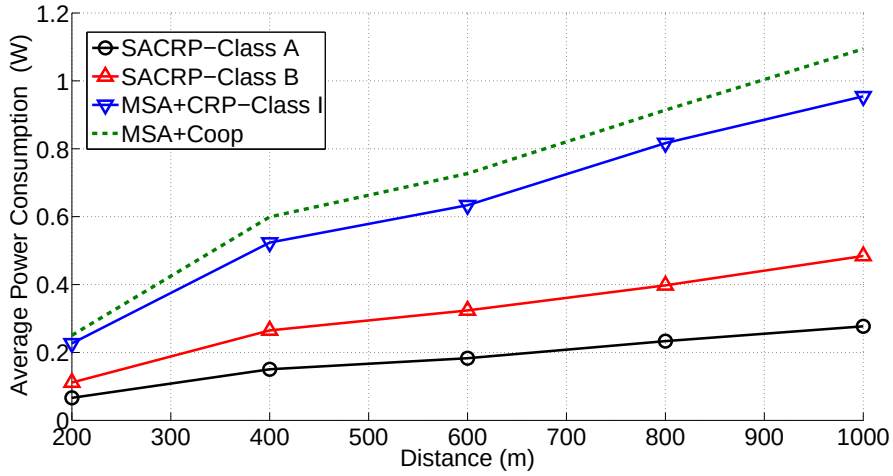

Figure 3.13: Transmit power consumption against the distance between the source and destination.

consumption. Moreover, *Class B* aggregates channels that provide more effective transmission time, which increases the potential capacity and therefore reduces the transmit power.

From Fig. 3.14, it can be seen that the *Class A* protocol achieves the maximum throughput performance. In this case, *Class A* aggregates the spectrum channels which have the maximum capacity and adjusts the transmit power under the power constraints to achieve high throughput. However, MSA algorithm only aggregates the channels which satisfy the bandwidth requirements. It does not consider the channel quality and power control. Notice that, the throughput performance of *Class B* is better than that of the MSA with CRP-*Class I*. This is due to higher effective transmission time and cooperative link selection with better ETX.

Last, but not least, we also evaluate the delay performance of our proposed protocol. In Fig. 3.15, we consider the hop count performance. It is clear that our proposed SACRP incurs less hop count than COOP, but has a larger hop count compared to CRP-*Class I*. This is because SACRP selects the route which has the minimum hop count; however, the cooperative link will increase the number of hops. As shown in Fig. 3.16, SACRP *Class B* results in the minimum end-to-end delay. Even though it's hop count is larger than CRP-*Class I*, more effective transmit

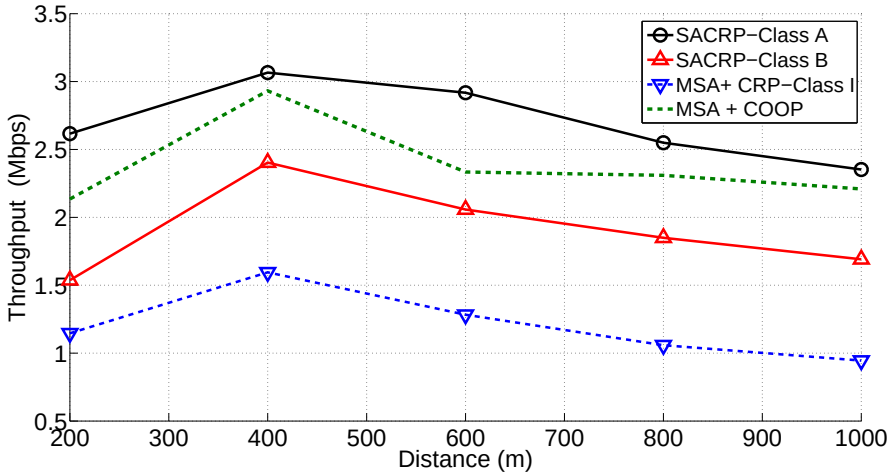

Figure 3.14: Throughput against the distance between the source and destination.

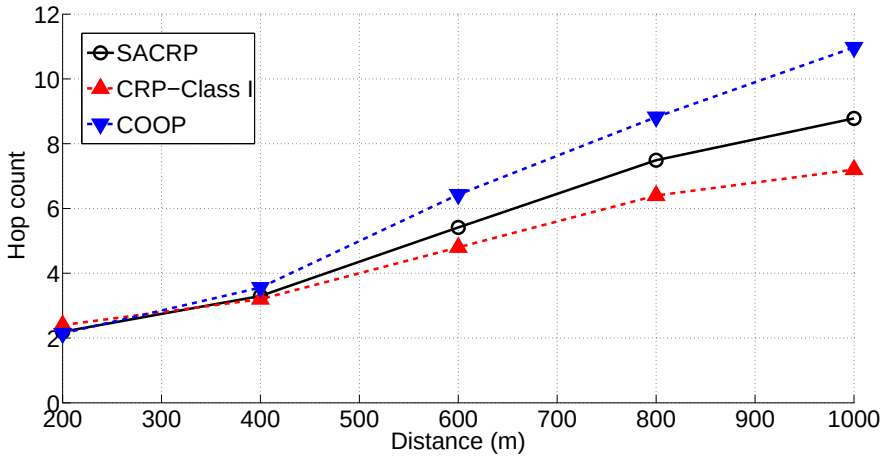

Figure 3.15: Hop count against the distance between the source and destination.

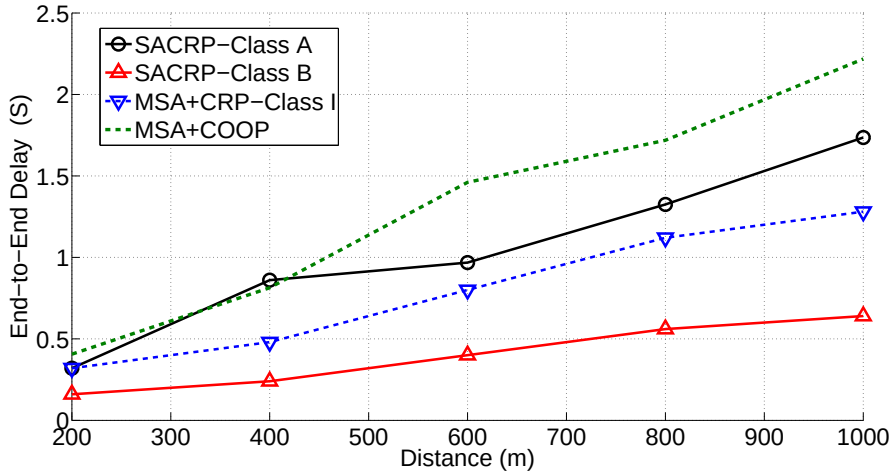

Figure 3.16: The end-to-end delay against the distance between the source and destination.

time provided by direct link and less number of retransmissions provided by the cooperative link are able to reduce the end-to-end delay significantly. We note that MSA with COOP shows the worst performance as it cannot guarantee the effective transmit time for aggregated spectrum bands. In addition, COOP generates larger number of hops than SACRP.

3.7 Summary and Conclusion

In this chapter, we have proposed SACRP, which is a spectrum aggregation-based cooperative routing protocol for CRAHNs. SACRP considers two classes of cooperative routing protocols: *Class A* for power minimization or throughput maximization, and *Class B* for reducing the end-to-end delay. A stochastic geometry approach has been used to develop the analytical model for the proposed protocol. Performance evaluation demonstrate that *Class A* aggregates multiple channels and selects suitable relay nodes, and therefore achieves higher power efficiency and throughput. *Class B* reduces the number of re-transmissions by selecting the relay nodes with better channel conditions, and therefore reduces the end-to-end delay. We have also conducted a performance comparison of SACRP with

other relevant protocols in literature. Results shows that SACRP *Class A* reduces the transmit power by up to 70% compared to MSA in cooperative as well well as non-cooperative scenarios. Apart from this it enhances the overall throughput by up to 50% and 20% compared to MSA in non-cooperative and cooperative scenarios, respectively. Besides, SACRP *Class B* reduces the end-to-end delay by up to 38% and 55% compared to MSA in non-cooperative and cooperative scenarios respectively.

As we mentioned previously, Energy efficiency and delay requirements are two important factors to evaluate the performance of CR networks, especially for MAC or routing protocols design. In CRAHNs, the proposed SACRP has demonstrated the outstanding performance in energy efficiency and end-to-end delay. However, as the CR technique has been used in different types of wireless networks, the question still remains: What about the energy and delay performance in other types of CR based networks and how to design a MAC or routing protocol to achieve such objective in other types of CR based networks. In order to further analyse the performance and provide solutions for CR based networks, we move the sight line into another famous area: Smart grid. Section 2.2 has provided a brief overview of smart grid. From there we know that two different types of wireless networks are widely applied in smart grid communications as AMI networks and WSNs. Therefore, it would be an interest to investigate the objective in CR enabled WSNs and AMI networks.

Thus, the next two chapters will specially focus on the performance analysis of CR technology operating in two different types of networks: CSNs and CR-AMI networks with emphasis on the energy efficiency, end-to-end delay and reliability.

Chapter 4

Receiver-based MAC Protocol for Cognitive Radio Enabled Sensor Networks

4.1 Introduction

Recently, WSNs [85] are gaining a lot of attention for electric power network [86], [87]. Reliable, efficient, and low cost operation and management of smart grid can be accomplished with the installation of wireless sensor nodes in different parts of grid such as distributed power plants, transmission towers and lines, substations, commercial/residential buildings, etc. Information gathered from these sensors is not only used for real time fault detection but also for supporting different applications such as automated demand response, distributed automation, smart metering, etc. The application of wireless multimedia sensor networks (using acoustic and video sensors) can further enhance the reliability, safety, and security of smart grid [88]. However, wireless links in smart grid are exposed to spatio-temporally varying spectrum characteristics, which arise due to electromagnetic interference, equipment noise, dynamic topology changes, and fading [86]. Therefore, the success of smart grid operation depends on the communication capabilities of sensor nodes in harsh environmental conditions that brings out great challenges for energy efficiency and reliability in WSNs.

On the other hand, there are several motivations for using *cognitive radio* (CR) technology for smart grid communications [89]. Recently, a number of studies (e.g., see [90–94]) have been presented on different smart grid related platforms regarding the application of CR for smart grid communication. More importantly, the use of CR equipped wireless sensor networks (or CSNs) has been proposed to address the unique challenges of WSNs in smart grid environments [95]. With dynamic

spectrum access capabilities, CSNs can overcome the spatio-temporally varying link conditions. CSNs can access both licensed and unlicensed spectrum bands. This is particularly important as the envisioned multitude of connected sensor nodes in smart grid operating in unlicensed bands will result in significant interference issues. Apart from this, higher bandwidth requirements of wireless multimedia sensor networks can be fulfilled. A critical issue in smart grid is the huge variability in sensor node locations. Thus, wireless propagation cannot be guaranteed, especially if operating in the industrial, scientific and medical (ISM) band (worldwide unlicensed band of 2.4 – 2.485 GHz). CSNs can effectively overcome this limitation through dynamic spectrum access of better propagation bands (e.g., TV white spaces [61]). Last, but not the least, CSNs can adapt to varying channel conditions that improves the transmission efficiency, as a result of which power consumption in transmission and reception modes is minimized [96].

Unlike WSNs, CSNs for smart grid is still a relatively unexplored area. Successful operation of CSNs in smart grid requires enhancements and optimizations at different layers of the protocol stack, especially at the Media access control (MAC) layer. A novel MAC protocol is required that provides low overhead spectrum access, jointly considers spectrum sensing and duty cycling for balancing the trade-off between spectral efficiency and energy efficiency, and provides reliable operation in challenging smart grid wireless environments.

Against this background, our objective in this chapter is to design a MAC protocol for CSNs in smart grid. In this regard, we propose a Cognitive receiver-based MAC (CRB-MAC) protocol for CSNs. CRB-MAC is designed with special emphasis on energy efficiency and reliability requirements of CSNs operating in smart grid environments. In order to achieve high energy efficiency, CRB-MAC employs *preamble sampling* [15] approach to tackle *idle listening* and support sleep/wakeup modes without synchronization overheads. CRB-MAC exploits the broadcast nature of wireless medium and adopts an opportunistic forwarding approach with multiple receivers as discussed later in detail. This approach improves the reliability of the network along with reducing the number of retransmissions.

The rest of the chapter is organized as follows. Section 4.2 describes the framework for CRB-MAC including the system model and the protocol description. In Section 4.3, analytical models for different performance metrics are discussed. This is followed by performance evaluation in Section 4.4. Finally, Section 4.5 concludes the chapter.

4.2 CRB-MAC Framework

4.2.1 CRB-MAC Overview

A key aspect of CRB-MAC is *preamble sampling* for achieving high energy efficiency. In preamble sampling approach (also known as asynchronous low power listening), each node selects its sleep/wakeup schedules independently of other nodes. The nodes spend most of their time in sleep mode and wake up for a short duration called *clear channel assessment (CCA)* every *checking interval (CI)* to check whether there is an ongoing transmission on the channel. To avoid deafness, the sender node transmits a long preamble with the same length as CI, followed by the data packet, to ensure that all receivers detect the preamble and obtain the data frame. By tuning CI and CCA, average duty-cycles of below 1% can be achieved without any need for scheduling or synchronization [100].

CRB-MAC is inherently *receiver-based* in nature. Unlike *sender-based*[1] MAC protocol, in receiver-based MAC protocol, a sender node transmits its data without defining a particular node as a receiver. All the neighboring nodes within communication range of the sender node receive the data packet. Based on the information received from the preamble, each individual node decides if it is eligible to participate in forwarding the data. Receivers compete in an *elective* process and the winner forwards the data to the next hop towards gateway/sink.

A key aspect of any CR environment is spectrum sensing. Nodes periodically monitor the current channel for primary user (PU) activity before using it for

[1]In sender-based MAC (such as 1-hopMAC [97] protocol), a node that has data to send, selects a receiver node from its neighbor table, includes the receiver's address in the packet header, and transmits the packet.

transmission. During this interval (sensing time), nodes are not involved in forwarding data packets the network performance is degraded (e.g., in terms of end-to-end throughput, latency, and packet loss ratio). CRB-MAC utilizes a mechanism to improve overall network performance under spectrum sensing state of different nodes. Further, in CRB-MAC, nodes employ optimal transmission time subject to an interference constraint, in order to ensure protection to PUs.

Table 4.1: Frequently used Notations for CRB-MAC.

Notation	Description
P_d	Probability of detection
P_f	Probability of false alarm
p	Bit error probability
m	Size of micro-frame (in bits)
d	Size of data frame (in bits)
r_m	No. of micro-frames in preamble
N	No. of receivers
T_s	Spectrum sensing duration
T_{CI}	Checking interval
T_{pr}	Preamble duration
χ	No. of retransmissions
χ_{ss}	No. of spectrum sensing events

4.2.2 System Model

We consider an ad-hoc network of stationary sensor nodes that are CR enabled. It is important to mention here that the resource constrained nature of sensor nodes creates various challenges at the Physical (PHY) layer of CSNs. Some of the key challenges include low cost Software Defined Radio (SDR) based transceivers for energy efficient reconfigurability operations, lightweight spectrum sensing algorithms with high detection probability, and low cost dynamic spectrum access solutions that require minimum control overhead. However, the design of PHY layer is beyond the scope of this chapter. We assume that each node is equipped with a single radio transceiver that can be tuned to any channel in the licensed spectrum.

We consider J stationary PU transmitters (and hence J available channels) with known locations and maximum coverage ranges. The PU (transmitter) activity model for the j^{th} channel is given by a two state independent and identically distributed (i.i.d.) random process such that the duration of busy and idle periods is exponentially distributed with a mean of $\frac{1}{\mu^j_{ON}}$ and $\frac{1}{\mu^j_{OFF}}$, respectively. Let S^j_b denote the state that the j^{th} channel is busy (PU is active) with probability $P^j_b = \frac{\mu^j_{OFF}}{\mu^j_{ON}+\mu^j_{OFF}}$, and S^j_i the state that the j^{th} channel is idle with probability P^j_i, such that $P^j_i + P^j_b = 1$. We assume that a node employs energy detection[2] technique [77] for primary signal detection wherein it compares the received energy (E) with a predefined threshold (σ) to decide whether the j^{th} channel is occupied or not i.e.,

$$Sensing\ Decision = \begin{cases} S^j_b & \text{if} \quad E \geq \sigma \\ S^j_i & \text{if} \quad E < \sigma \end{cases}. \tag{4.1}$$

The two principle metrics in spectrum sensing are the detection probability (P_d), and the false alarm probability (P_f). A higher detection probability ensures better protection to incumbents, whereas a lower false alarm probability ensures efficient utilization of the channel. As per [78], false alarm and detection probabilities for the j^{th} channel can be expressed as follows.

$$P^j_f = \Pr\left\{E \geq \sigma \mid S^j_i\right\} = \frac{1}{2}\text{Erfc}\left(\frac{1}{\sqrt{2}}\frac{\sigma - 2n_j}{\sqrt{4n_j}}\right), \tag{4.2}$$

$$P^j_d = \Pr\left\{E \geq \sigma \mid S^j_b\right\} = \frac{1}{2}\text{Erfc}\left(\frac{1}{\sqrt{2}}\frac{\sigma - 2n_j\left(\gamma_j + 1\right)}{\sqrt{4n_j\left(2\gamma_j + 1\right)}}\right), \tag{4.3}$$

where Erfc($\cdot$) is the complementary error function, and γ_j and n_j denote the SNR of the primary signal and the bandwidth-time product for the j^{th} channel respectively.

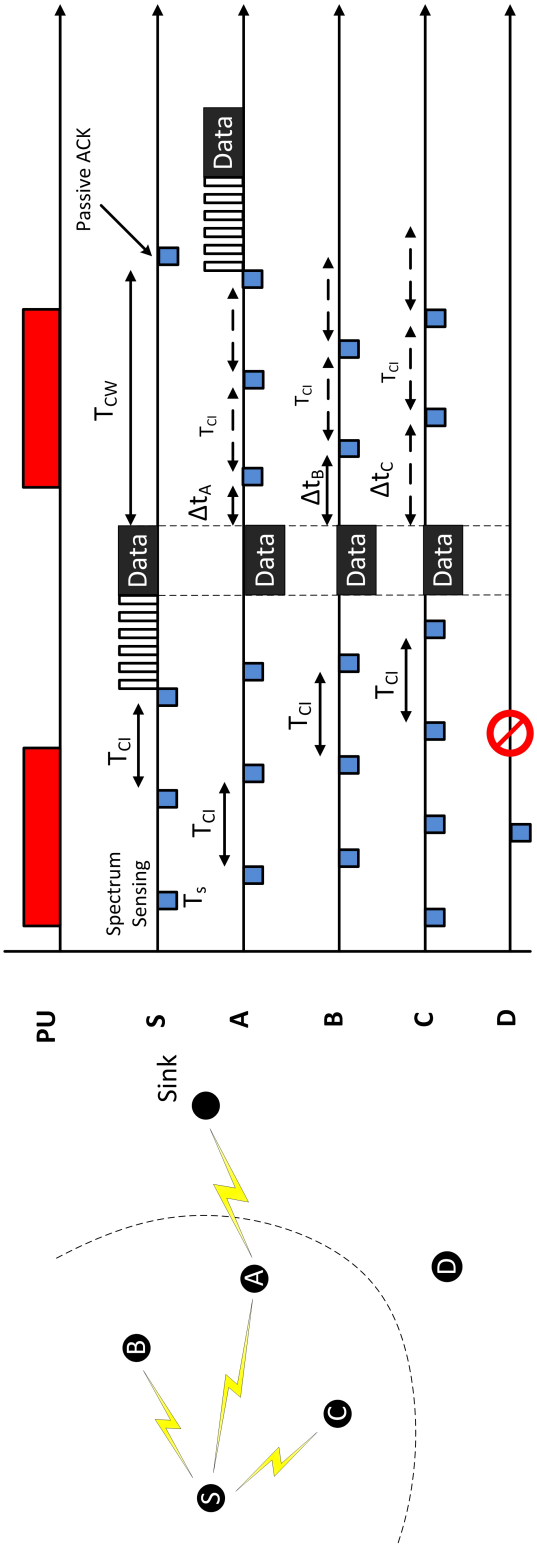

Figure 4.1: Timeline of CRB-MAC protocol with an illustrated scenario of sender and receiver nodes.

4.2.3 Protocol Description

The MAC frame structure in a CR network consists of a sensing slot (T_s) and a transmission slot (T). In periodic spectrum sensing scenarios, there is a possibility of causing harmful interference to PUs due to imperfect spectrum sensing in realistic conditions. This interference is quantified in terms of *Interference Ratio* (IR), defined as the expected fraction of ON duration of PU transmission interrupted by the transmission of secondary users and is given for the j^{th} channel as follows [79].

$$IR_j = \left(1 - P_d^j\right) P_b^j + P_i^j \left(1 - P_f^j\right) + e^{-\mu T} \left(P_f^j - P_d^j\right), \tag{4.4}$$

where $\mu = \max(\mu_{ON}^j, \mu_{OFF}^j)$. We assume that the nodes in our network employ optimal transmission time that maximizes the throughput of the secondary network subject to an interference constraint i.e., $IR_j \leq IR_{max}^j$, where IR_{max}^j denotes the maximum tolerable interference ratio on the j^{th} channel. This transmission time for the j^{th} channel is given as follows.

$$T_j = \mu^{-1} \left[\ln P_i^j - \ln \left(P_i^j P_d^{'} + P_b^j (1 - P_d^{'}) - IR_{max}^j\right) + \ln(2P_d^{'} - 1)\right], \tag{4.5}$$

where $P_d^{'}$ is the detection probability threshold, defined as the detection probability at SNR level as low as γ_{min}, where γ_{min} is specified by the regulator.

Fig. 4.1 illustrates the CRB-MAC protocol operation along with the timeline for different nodes. As shown in the figure, a node S wants to send data to the sink/gateway node by forwarding towards its first hop neighbors (within the transmission range). Firstly, it performs spectrum sensing (with duration given by T_s) to detect any PU activity. If the channel is detected as busy with PU transmission, the sender node goes to sleep mode. The sensing operation is repeated after a duration of checking interval (T_{CI}). If the PU is detected to be absent, the node starts transmitting the preamble followed by the data. The preamble consists of multiple micro-frames (each of duration T_m) and contains identification information for neighboring nodes to distinguish between PU transmission or sensor

[2]Energy detection is particularly attractive for CSNs owing to its simplicity, low signal processing overhead, and minimal computational power requirements.

node transmission. All the nodes within the transmission range of S detect and sample few micro-frames of the preamble to extract necessary information (e.g., sequence number of the data). As shown in Fig. 4.1, only three neigboring nodes of S (i.e., nodes A, B, and C) are eligible to forward the data towards the sink node. They all wake up and receive the data transmitted by node S. If the received data packet is detected to be erroneous, it is simply discarded. The nodes receiving the data packet do not send any *Acknowledgement* (ACK) message. However, they set a timer (Δt) before forwarding the data to the next hop. The timer is set relative to a node's distance[3] from the sink. The node with the shortest timer (closest to the sink) is most likely to forward the data towards the sink. Right after the expiry of the timer, each neighboring node performs the sensing operation. If the channel is occupied by the PU, the node goes back to sleep mode for a duration of T_{CI}. However, if a sensor node transmission is detected, each node compares the sequence number of the transmitted data with its own. If the sequence numbers match, it means that the same data is being transmitted by another node. Therefore, it discards the data packet. Otherwise, a free channel indicates that this node is the winner and can start transmitting the preamble (e.g., in Fig. 4.1, node A is the winner). The sender node S retransmits the data if none of the participating nodes in the contention window is successful to forward the data packet. The sender node can realize this by performing the sensing operation just before ending the contention window (passive ACK). The duration of contention window, T_{CW}, is set according to the transmission radius of sender nodes. In case of multiple hops, the same operation continues until the data is received by the sink.

CRB-MAC uses a technique for mitigating the performance degradation due to spectrum sensing. The key aspect of this technique is to improve the performance by reducing the spectrum sensing time. Reduction of sensing time is possible when a node is situated in region of low PU activity, and hence the number of channel changes that occur over time is small [99]. Initially the sensing time is

[3]The distance is determined by the network layer. For example in case of Routing Protocol for Low Power and Lossy Netwoks(RPL) [98] protocol, each node is assigned a *rank*, based on an *objective function*, that determines a node's virtual position with respect to the sink node.

set to maximum value i.e., $T_s = T_s^{max}$ for a fixed missed detection probability ($P_m^j = 1 - P_d^j$). The sensing time is decreased over time (by tracking the PU activity and establishing the fact that the node is located in region of low PU activity) according to the following relation: $T_s^{new} = T_s - \varphi \cdot \Delta_s$, where Δ_s is the step size, given by $\Delta_s = 0.5 \times T_s$ and φ is a constant which is obtained from the gradient of sensing time versus the missed detection probability curve (see [99] for more details). When successive missed detection events occur, the node increases the sensing time with similar step size.

In general smart grid traffic comprises of two types: low priority monitoring data (that can be considered as best-effort) and high priority delay sensitive alarms that have an associated deadline. In order to successfully handle delay sensitive traffic, we propose an enhancement to CRB-MAC with a deadline aware forwarding process (and hence termed as deadline-aware CRB-MAC) wherein the node that provides the highest delay budget margin forwards the packet. We assume that the time before the deadline expires can be uniformly shared among the nodes in the route. Hence, the delay budget for the transmission of packet P is given by

$$\mathfrak{D}(P) = \frac{1}{h(k)} \cdot [\Theta(P) - t_c] \,, \tag{4.6}$$

where $\Theta(P)$ is the deadline associated with the packet P, t_c is the current time, and $h(k)$ is the hop distance between the k^{th} node and the sink node. We assume that the node is aware of the hop count to sink node through network layer information exchange. When a packet is at node k, the delay before the packet is correctly transmitted to the next hop depends on: (a) the average delay until a vacant channel is found (d_1) and (b) the average delay until the next hop correctly receives the packet (d_2). While d_1 depends on PU activity and can be estimated using (4.16), d_2 is characterized by the MAC layer and can be estimated using link metrics such as ETX (*Expected Transmission Count*[4]) [80].

In order to guarantee that the packet is forwarded to the sink node before the

[4]The ETX of a link between nodes k and l is given by $\text{ETX}_{kl} = 1/p_{kl}$, where p_{kl} is the probability of node l receiving a transmission from node k.

deadline, it is important to give priority to the forwarding node that provides the highest margin for delay budget ($\mathfrak{D}(P) \geq d_1 + d_2$). Therefore, in deadline-aware CRB-MAC, the key difference is that the timer (Δt) is set according to the delay budget i.e., a node which provides a higher delay budget sets a lower timer and vice versa). The deadline information is embedded in the preamble transmission and therefore, available to the neighboring nodes during the checking interval. If the deadline has elapsed after the expiry of timer (Δt) and finding a vacant channel, the receiving node drops the packet.

4.3 Analytical Modeling

4.3.1 Probability of Channel Switching

We are interested in probability of switching transmission to the cognitive channel. The CR users can only use the licensed channel in the absence of PU activity. However, under realistic conditions, there can be an element of inaccuracy in spectrum sensing. Let P_{sw}^{j} denote the probability of switching transmission to the j^{th} cognitive channel which can be evaluated considering the following cases: (i) when S_b^j and the node misses to detect it; (ii) when S_i^j and no false alarm is generated. Hence P_{sw}^{j} is given by

$$P_{sw}^{j} = P_b^j \left(1 - P_d^j\right) + P_i^j \left(1 - P_f^j\right). \tag{4.7}$$

It can be easily verified that under perfect spectrum sensing conditions i.e., $P_d^j = 100\%$ and $P_f^j = 0\%$, (4.7) reduces to P_i^j, which is intuitive.

4.3.2 Energy Consumption and Retransmission Model

In CRB-MAC, failure probability of a single transmission on the j^{th} channel depends on the corruption in preamble or data frame and is given by

$$P_{fail}^{j} = P_{sw}^{j} \left[1 - (1-p)^{m+d}\right], \tag{4.8}$$

where m and d respectively denote the size of micro-frame and data frame in bits, p denotes the bit error probability, and P_{sw}^{j} is given by (4.7).

Let, r_m denote the number of micro-frames in the preamble, given by $r_m = \lceil \frac{T_{pr}}{T_m} \rceil$, where T_{pr} denotes the preamble duration and T_m is the transmission time for one micro-frame. On the transmitter side, the expressions for energy drained in a single successful and failed transmission on the j^{th} channel are given by

$$\mathcal{E}\_T_{succ}^{j} = \mathcal{E}_{ss}^{j} + P_{sw}^{j} \left\{ (1-p)^{m} r_m T_m + (1-p)^{d} T_d \right\} \mathcal{P}_t, \tag{4.9}$$

$$\mathcal{E}\_T_{fail}^{j} = \mathcal{E}_{ss}^{j} + P_{sw}^{j} \left\{ r_m T_m + \left(1 - (1-p)^{d}\right) T_d \right\} \mathcal{P}_t, \tag{4.10}$$

where $\mathcal{P}_t$ denotes the power drained in the transmit mode, T_d is the duration of data frame, and $\mathcal{E}_{ss}^{j}$ denotes the energy drained during spectrum sensing, given by $\mathcal{E}_{ss}^{j} = (\tau + T_s)\mathcal{P}_s$ such that $\mathcal{P}_s$ represents the power required for spectrum sensing operation, and τ is the transition time from sleep mode to active mode.

On the receiver side, the nodes detect the preamble transmission during spectrum sensing if the PU is not active. Hence, the expressions for energy drained in a single successful and failed transmission on the j^{th} channel are given by

$$\mathcal{E}\_R_{succ}^{j} = \mathcal{E}_{ss}^{j} + P_{sw}^{j} \left\{ (1-p)^{m} (\tau + T_s) + (1-p)^{d} (\tau + T_d \right\} \mathcal{P}_r, \tag{4.11}$$

$$\mathcal{E}\_R_{fail}^{j} = \mathcal{E}_{ss}^{j} + P_{sw}^{j} \left\{ (\tau + T_s) + \left(1 - (1-p)^{d}\right) (\tau + T_d) \right\} \mathcal{P}_r, \tag{4.12}$$

where $\mathcal{P}_r$ denotes the power drained in the receive mode. However, in CRB-MAC there are N eligible receivers that can forward the data packet. Therefore, the energy consumed in a single successful transmission in all possible cases where i nodes ($i \leq N$) successfully receive the packet without error is given by

$$\mathcal{E}\_R_{N\_succ}^{j} = \frac{\sum_{i=1}^{N} \binom{N}{i} \left[i\mathcal{E}\_R_{succ}^{j} + (N-i)\mathcal{E}\_R_{fail}^{j} \right]}{\sum_{i=1}^{N} \binom{N}{i}}. \tag{4.13}$$

The energy consumed in a single transmission when all the receiver nodes fail

$$\begin{aligned}\chi =&\mathbb{E}(n_t) = \sum_{a=0}^{Z} a \cdot P_a = \sum_{a=0}^{Z} a \cdot (P_{fail}^j)^{Na}(1-(P_{fail}^j)^N) \\ =&\frac{(P_{fail}^j)^N - (Z+1)(P_{fail}^j)^{N(Z+1)} + Z(P_{fail}^j)^{N(Z+2)}}{(1-(P_{fail}^j)^N)}.\end{aligned} \tag{4.15}$$

to receive the packet without error is given by:

$$\mathcal{E}\_R_{N\_fail}^j = N \cdot \mathcal{E}\_R_{fail}^j. \tag{4.14}$$

In case of a failed transmission, the sender node will retransmit the data. Hence, it is important to have a retransmission model for CRB-MAC. Let P_a denote the probability that a sender node will successfully transmit the packet after a failures. In CRB-MAC the sender node will stop retransmitting if atleast one of the receivers successfully receives the data. Thus, P_a is given by $P_a = (P_{fail}^j)^{Na}(1-(P_{fail}^j)^N)$. Let n_t be the random variable that represents the total number of transmissions until a success transmission. Since P_a is the Probability Mass Function (PMF) of n_t, the average number of retransmissions until success can be calculated as given by (4.15), where Z represents the maximum number of retransmissions.

In CR environments, the retransmissions also depend on channel availability. Hence, it is important to find the expected number of spectrum sensing events to find a vacant channel. Let χ_{ss}^j denote the expected number of sensing events for transmitting over the j^{th} channel, which is given by

$$\chi_{ss}^j = \sum_{i=0}^{\infty} i \cdot (1-P_{sw}^j)^i P_{sw}^j = \frac{1-P_{sw}^j}{P_{sw}^j}. \tag{4.16}$$

Using the retransmission model, the total energy consumption for CRB-MAC (over the j^{th} channel) over a single hop is given by

$$\mathcal{E}_{CRB\_total}^j = \chi(\mathcal{E}\_T_{fail}^j + \mathcal{E}\_R_{N\_fail}^j) + \mathcal{E}\_T_{succ}^j + \mathcal{E}\_R_{N\_succ}^j + \chi_{ss}^j \mathcal{E}_{ss}^j. \tag{4.17}$$

For a multi-hop scenario, the total energy consumption over H hops is given by $\sum_{h=1}^{H} \mathcal{E}_{CRB\_total}^j$.

4.3.3 Delay

Using the retransmission model described in the previous section, the single hop delay for CRB-MAC over the j^{th} channel is given by

$$\mathcal{D}^{j}_{CRB} = \chi \cdot (T_{pr} + T_d + T_{CW}) + \chi^{j}_{ss} \cdot T_s + T_{CI} \cdot (\chi^{j}_{ss} - 1). \tag{4.18}$$

For a multi-hop scenario, the end-to-end delay over H hops is given by $\sum_{h=1}^{H} \mathcal{D}^{j}_{CRB}$.

4.3.4 Reliability

In literature, Packet Delivery Ratio (PDR) is the most commonly used metric to quantify how reliably a protocol can deliver packets to the destination. The PDR is defined as the ratio of number of packets received to the total number of packets sent, and captures the fraction of packets actually delivered to the destination. However, the PDR is generally used in the context of routing protocols and hence implicitly evaluates the performance of underlying MAC protocol.

Analytically, the reliability for CRB-MAC (with N receivers) over the j^{th} channel is given by

$$\mathcal{R}^{j}_{CRB} = 100 \times \left(1 - (P^{j}_{fail})^{N(\chi+1)}\right). \tag{4.19}$$

The multi-hop reliability for CRB-MAC over H hops is given by $\left[\mathcal{R}^{j}_{CRB}\right]^{H}$, which is essentially similar to PDR.

4.4 Performance Evaluation

In this section, we evaluate the single hop and multi-hop performance of CRB-MAC. We perform a MATLAB based simulation (with parameters given in Table 3.1) to validate the analytical models. A square region of side 200 meters is considered that is occupied by 4 PU transmitters. The secondary users are assumed to be Poisson distributed in the whole region with a mean density as shown in Fig.

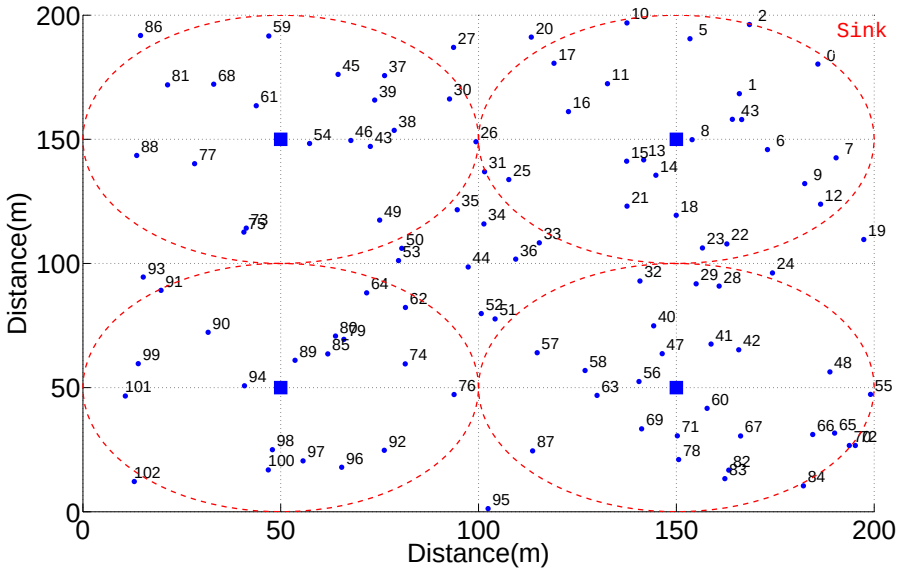

Figure 4.2: Sample simulated topology with Poisson distributed nodes (density = 0.4 nodes per unit area). Node ranks are also displayed. The filled squares and dotted circles represent the location and coverage area of PU transmitters respectively.

4.2. Without loss of generality, we assume that RPL [98] is operating at the Network layer[5]. Each node is assigned a rank (in RPL terminology, the rank represents a node's virtual position in the network with respect to the sink/gateway node (node 0 in our case)). For simplicity, we assume that the node's rank is dependent on its Euclidean distance from the sink node (i.e., the *objective function* is Euclidean distance in our case). The transmission radius of each node is set to 30 meters. Moreover, we assume that each node is equipped with *Texas Instruments* CC2500 Radio Transceiver whose parameters are also given in Table 4.2.

For comparison, we also implement a sender-based MAC protocol (1-hopMAC [97]) in CR environments. The analytical expressions for Cognitive Sender-Based MAC (CSB-MAC) protocol are given in Appendix D.

Fig. 4.3 evaluates the single hop performance of CRB-MAC (based on analytical models) for energy consumption (Fig. 4.3a), delay (Fig. 4.3b), and reliability (Fig. 4.3c) against the bit error rate (BER). Firstly, we discuss the energy performance. In

[5]The RPL protocol needs to be adapted for cognitive radio environments. This has been addressed in authors' previous work in [53].

Table 4.2: Simulation Configuration Parameters for CRB-MAC.

Parameter	**Value**
Detection probability threshold ($P_d^{'}$)	0.9
Probability of false alarm (P_f)	0.1
Channel bandwidth	200 KHz
PU received SNR (γ)	-15 dB
Busy state parameter of PU (μ_{ON})	2
Idle state parameter of PU (μ_{OFF})	3
Maximum Interference Ratio (IR_{max})	0.25
Spectrum sensing duration (T_s)	20 ms
CC2500 RF Transceiver Parameters	
Power drained in transmit mode ($\mathcal{P}_t$)	66.16 mW
Power drained in receive mode ($\mathcal{P}_r$)	70.69 mW
Power drained in spectrum sensing ($\mathcal{P}_s$)	65.83 mW
Checking interval (T_{CI})	144 ms
Preamble length (T_{pr})	144 ms
Transmission time of a data packet (T_d)	4 ms
Transmission time of one micro-frame (T_m)	40 μs
Transition time from sleep mode to active mode (τ)	88.4 μs

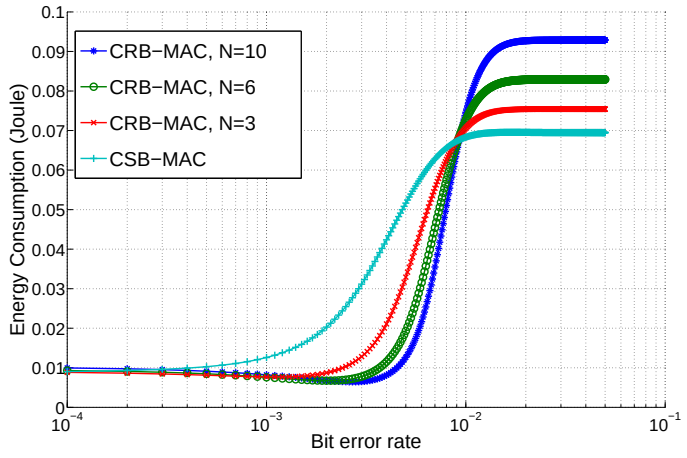

(a)

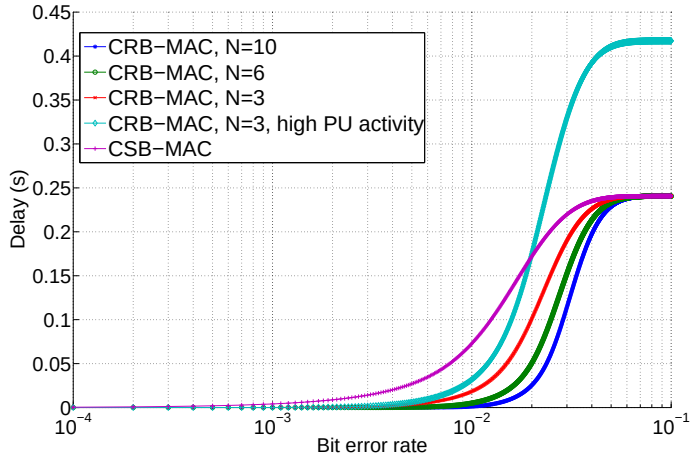

(b)

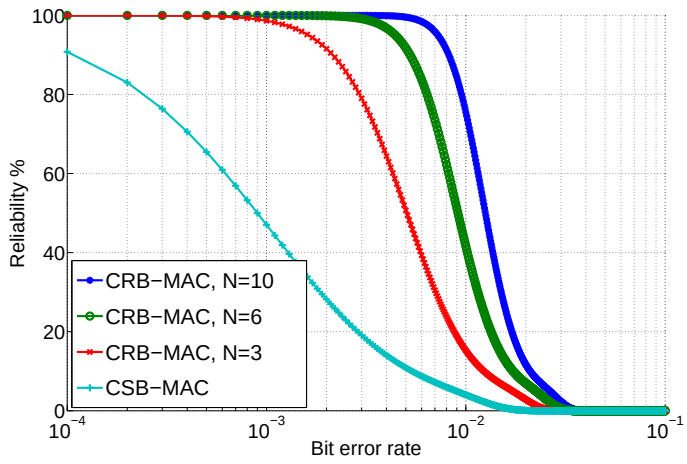

(c)

Figure 4.3: Single hop performance of CRB-MAC, (a) energy consumption, (b) delay, (c) reliability; N represents the number of receivers. Where the energy consumption, delay and reliability can be obtained by (4.17), (4.18) and (4.19), respectively.

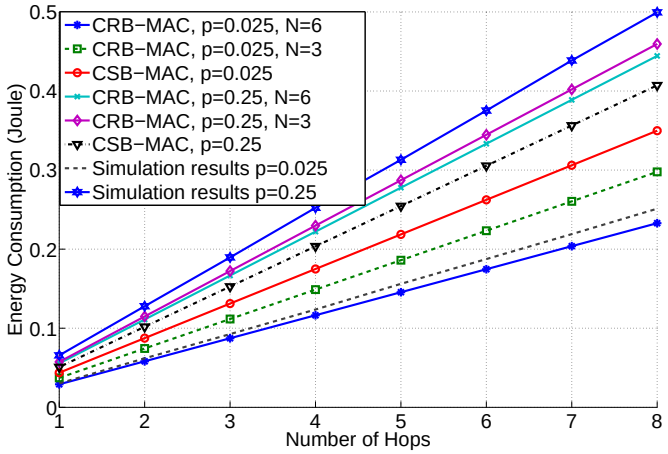

(a)

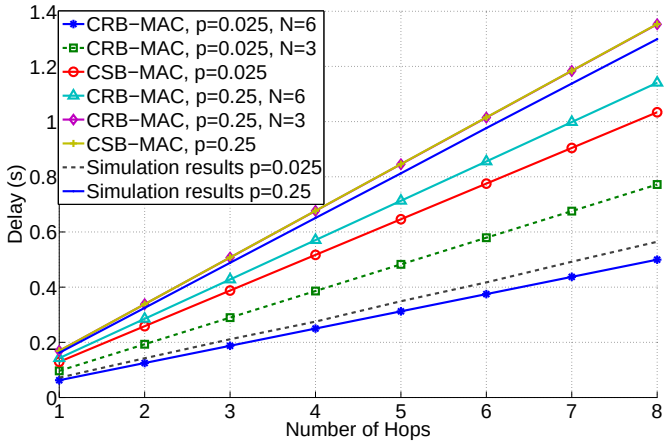

(b)

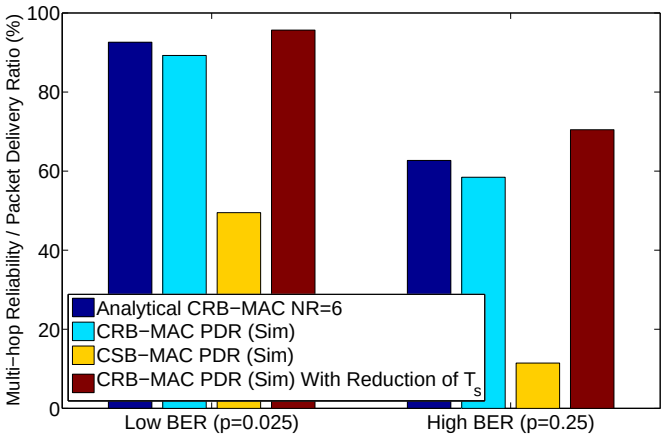

(c)

Figure 4.4: Multi-hop performance of CRB-MAC, (a) energy consumption, (b) delay, (c) reliability; N = no. of receivers, p = bit error probability. Where the energy consumption, delay and reliability can be obtained by (4.17), (4.18) and (4.19), respectively.

channels with rather low BER, CRB-MAC outperforms the CSB-MAC in terms of energy consumption. This is because, the number of retransmissions in CRB-MAC is less than CSB-MAC owing to multiple receivers involved in the forwarding process. That is why CRB-MAC is more resilient to variations in channel quality than CSB-MAC. In very poor channel conditions, CRB-MAC consumes more energy than CSB-MAC and the energy consumption increases with the number of receivers. The energy consumption reaches a saturation point when the maximum number of retransmissions (7 in our case) is reached. Therefore, the high energy consumption of CRB-MAC in poor channel conditions is primarily due to more receivers involved in the forwarding process. Hence, more energy is spent in reception process that increases the overall energy consumption. From Fig. 4.3a, it is also noted that CSB-MAC reaches the saturation point quickly as soon as the BER starts to degrade. However, CRB-MAC shows more resiliency and stays operational, even when CSB-MAC has failed. Next, we discuss the delay performance. Since delay is dependent on the number of retransmissions, CRB-MAC outperforms CSB-MAC in terms of delay performance owing to fewer retransmissions. The delay reduces as the number of receivers increase because of higher probability of successful transmission. Moreover, the delay performance reaches a saturation point as the maximum number of retransmissions is reached. Note that a high PU activity ($P_b^j = 0.7$ in this case), with same number of receivers, further increases the delay due to more spectrum sensing events to find a vacant channel. Last, but not the least, we discuss the reliability performance. As expected, CSB-MAC (which relies on only one receiver) provides the lowest reliability. Whereas, CRB-MAC not only shows resiliency to channel quality variations but also provides much higher levels of reliability due to more receivers involved in the forwarding process. Note that the energy, delay, and reliability performance has a trade-off depending on the size of the preamble [100].

Next, we evaluate the multi-hop performance of CRB-MAC in both good (low BER with $p = 0.025$) and poor channel (high BER with $p = 0.25$) conditions. Figure 4.4a, 4.4b, and 4.4c respectively evaluate the multi-hop energy consumption, delay, and reliability of CRB-MAC. Simulation results for CRB-MAC are also

given. In simulations, we generate $10,000$ packets from different nodes and average the results for different performance metrics. Firstly, we discuss the energy performance. We note that the energy consumption increases with the number of hops, with CRB-MAC outperforming CSB-MAC in low BER conditions. In high BER conditions, the energy consumption of CRB-MAC increases due to higher energy consumption in the reception process as mentioned earlier. The simulation results follow the analytical results and hence validate the analytical modelling. Slight difference from analytical results is due to the fact that in simulations, nodes are randomly distributed and therefore, the number of receivers at each hop is not fixed (some nodes have fewer neighbors than others within the transmission range). Next, we see the delay performance. We note that CRB-MAC (with $N = 6$, and $N = 3$) outperforms CSB-MAC in terms of end-to-end delay (in both high and low BER scenarios) due to fewer retransmissions. Lastly, we discuss the reliability performance. We note that CRB-MAC provides better PDR (obtained through simulations) compared to CSB-MAC under both good and poor channel conditions. Moreover, the multi-hop reliability obtained analytically (using (4.19)) is very close to the PDR which is obtained through simulations. We also note that a higher PDR is achieved by incorporating the performance enhancement technique for mitigating the degradation due to periodic spectrum sensing. The improvement in PDR results due to the reduction of sensing time by tracking the PU activity in the form of a moving window. Hence fewer packets are dropped due to periodic spectrum sensing state of different nodes.

Lastly, we see the performance of deadline-aware CRB-MAC. The performance is compared in terms of deadline violation probability (DVP) which is calculated as the ratio of the number of packets dropped due to violation of deadline at intermediate hops to the total number of packets generated. The results in Fig. 4.5 show the simulation results for DVP against the link success probability. The DVP decreases as link success probability increases due to lesser retransmissions that increase the remaining lifetime of a packet at intermediate nodes. We note that the deadline-aware CRB-MAC achieves the best performance for any given

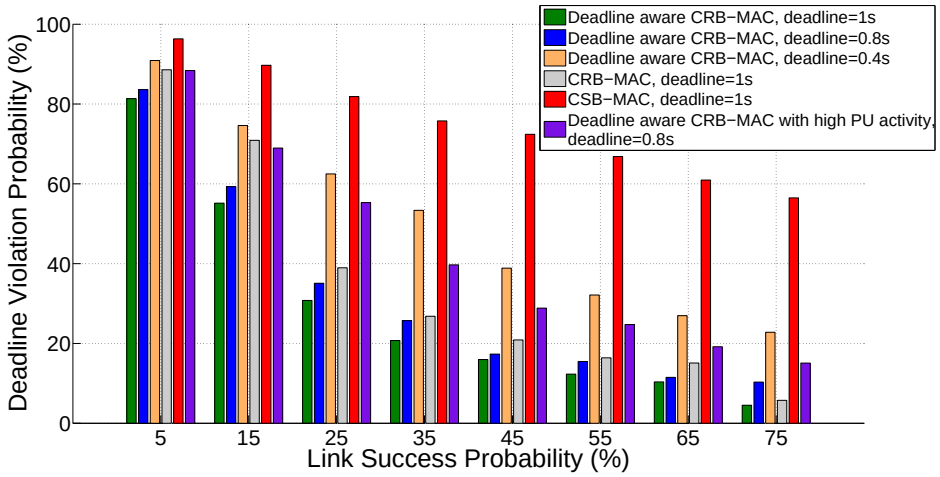

Figure 4.5: Simulation results for deadline violation probability against link success probability.

deadline due to deadline-aware forwarding process. The CSB-MAC shows the worst performance as the forwarding process relies on a single receiver only which leads to higher number of retransmissions and consequently reducing the lifetime of a packet at intermediate nodes. We also note that a high PU activity ($P_b^j = 0.7$ in this case) results increases the DVP as the delay in finding a vacant channel increases.

4.5 Summary and Concluding Remarks

CSNs play an important role in the operation and management of smart grid. Due to challenging cognitive environment, reliability, energy efficiency and delay requirements for sensor devices become critically important. In this chapter, we propose CRB-MAC, which is a receiver-based MAC protocol for CSNs. CRB-MAC employs preamble sampling and opportunistic forwarding techniques to cater for high energy efficiency and reliability requirements of CSNs. CRB-MAC is also enhanced for mitigating the performance degradation due to periodic spectrum sensing state of nodes in the network. Apart from this, a delay-budget based election process for packet forwarding is proposed in order to effectively handle delay sensitive traffic. Especially, reliability improvement of up to 50% can be achieved

compared to CSB-MAC protocol in lossy environments. Analytical and simulation results demonstrate that in lossy wireless environments CRB-MAC generates less retransmissions and therefore, enhances the overall energy and delay performance. Moreover, high reliability can be provided by increasing the number of receivers. Hence, CRB-MAC provides a viable solution for CSNs in realizing the vision of smart grid.

Chapter 5

Routing Protocol Design for Cognitive Radio Enabled Smart Grid AMI Networks

5.1 Introduction

The smart grid is expected to overcome the problems of the legacy power grid [22, 101, 102] through upgrade of power distribution and management by incorporating advanced bi-directional communications, automated control, and distributed computing capabilities. It allows providers, distributors, and consumers of electricity to have a real-time awareness of operating requirements and capabilities. For successful operation of smart grid, an integrated high performance, reliable, scalable, robust, and secure communication network is critical [23, 103].

One of the key elements of the smart grid is the AMI, wherein multiple smart meters (located at customer premises) communicate with a Meter Data Management System (MDMS), which acts as a control center for storage, processing and management of meter data in order to be used by different applications [23]. It provides a two-way communication through which utilities can keep track of consumers' electricity usage, monitor power quality, and inform consumers the latest electricity prices on a real-time basis. However, due to the spectrum scarcity and spectrum inefficiency issues, traditional AMI applications suffer a bottleneck in the development of the future AMI networks. On the other cognitive Machine-to-Machine (M2M) communications paradigm is inherently equipped to address the challenges of spectrum scarcity, interference management, and device heterogeneity [89]. In this regard, CR-AMI networks have attracted a lot of attention recently [104]. In CR-AMI networks, AMI users (secondary users) dynamically access the frequency band/channel whenever the licensed user (primary user) is

absent but have to vacate the band/channel whenever the primary user is detected. Recently, several studies involving *cognitive radio* (CR) technologies for smart grid communications have been considered (e.g., [90–94, 105]).

A practical solution to enable CR-AMI networks is to deploy a static multi-hop wireless mesh network that in turn connects thousands of smart meters to a gateway. The CR users (smart meters) apply spectrum sensing and dynamic Spectrum access (DSA) techniques to access the licensed band/channel and transmit data (e.g., electric bills) to the gateway. In such networks, efficient routing protocols are necessary to ensure low-latency and highly reliable delivery of data. Recently, a specially designed protocol known as Routing Protocol for Low Power and Lossy Netwoks (RPL) [106] has been standardized by the Internet Engineering Task Force (IETF) in order to support a variety of smart grid applications, including AMI networks. While RPL is attractive for conventional AMI networks, it suffers from a number of limitations in CR-AMI networks [107]. Recently, an RPL-based routing protocol, termed as Cognitive and Opportunistic RPL (CORPL), has been proposed for CR-AMI networks [53]. CORPL enhances RPL with novel modifications, especially tailored for operation in CR environments. The key aspect of CORPL is an opportunistic forwarding approach to meet the utility requirements of secondary network (cognitive AMI network) along with protecting the primary users (PUs). Besides, CORPL proposes two different classes of routing protocols and utilizes a cost function approach to prioritize potential forwarding nodes. However, as discussed later, CORPL has certain limitations which necessitate further investigation for optimized routing in CR-AMI networks.

Against this background, the key objective of this chapter is to optimize RPL-based routing in CR-AMI networks such that the routing efficiency increases without increasing the complexity for the AMI network. The key contributions are stated as follows.

- CORPL uses two different classes of routing protocols: one for protection to primary receivers and the other for delay-sensitive traffic. However, this increases the complexity of routing process. It is desirable to achieve the same

objectives with a single routing class. We address this issue by developing a unique routing metric for rank computation that inherently captures the protection to primary receivers within the objective function. Further, the routing process is optimized for delay-sensitive traffic, as discussed later.

- In CORPL, each node has to calculate and maintain the path for routing even when it has no information to send which is potentially a waste of limited computing capabilities of AMI network. The issue is particularly challenging when the scale of AMI network is large. We propose a novel mechanism which allows a source node to chose the complete routing path to the destination, which is global optimal. The intermediate nodes on the path determined by the source node can use the existing path for their own transmission which not only improves the routing efficiency but also saves the computational resources.

- We develop an artificial intelligence approach and use a Directional Mutation Ant Colony Optimization (DMACO) algorithm for improving the routing efficiency as well as for meeting the utility requirements of the secondary network. The DMACO algorithm converges quickly compared to other optimization algorithms.

- The proposed protocol is termed as DMACO-RPL (Directional Mutation Ant Colony Optimization based Cognitive RPL). We conduct a system level performance evaluation of DMACO-RPL and compare with other routing protocols in terms of key performance metrics.

The rest of the chapter is organized as follows. Section 5.2 presents an overview of CORPL. The optimizing RPL-based routing framework is presented in Section 5.3, followed by the performance evaluation in Section 5.4. Finally the chapter is concluded in Section 5.5.

5.2 Overview of CORPL

RPL [106] is a distance-vector and a source routing protocol, which has been standardized by IETF to support a variety of smart grid applications. It is using one or more Directed Acyclic Graphs (DAGs) to maintain the network state information. A DAG is a directed graph wherein all edges are oriented without any cycles. Each DAG includes a root node which acts as a gateway in RPL. Each node (client node) in the DAG is assigned a rank that is computed on the basis of an objective function. The rank monotonically increases in the downward direction (DAG root has the lowest rank) and represents a node's virtual position to other nodes with respect to the DAG root. A node in DAG can only be associated with other nodes having same or smaller rank compared to its own rank in order to avoid cycles.

CORPL is an RPL-based routing protocol for CR-AMI networks, which inherits some common features from RPL. A key aspect of CORPL is using spectrum sensing which is an important technique in the CR environment [108, 109]. Nodes periodically monitor the current channel for primary user (PU) activity before using it for transmission. The transmissions of CR network must ensure protection for both PU transmitters and PU receivers (temporal and spatial protection) [38, 110–112]. An opportunistic forwarding approach is adopted in CORPL, that consists of two key steps: selection of a forwarder set where each node in the network selects multiple next hop neighbors, and unique forwarder selection to ensure that only the best receiver forwards the data.

In CORPL, each node maintains a forwarder set such that the forwarding node is opportunistically selected. CORPL uses a cost function approach to dynamically prioritize the nodes in the forwarder set. Two routing classes have been proposed in CORPL. *Class A* assigns a greater importance to PU receiver protection whereas in *Class B*, the end-to-end latency is the key consideration for supporting the high priority delay sensitive alarms. The difference between the two classes is expressed in the cost function for forwarding node selection. For more information on CORPL, the interested reader is referred to [53].

5.3 DMACO-RPL Framework

In this section, we describe the framework of our proposed routing protocol for CR-AMI networks i.e., Directional Mutation Ant Colony Optimization Based Cognitive RPL (DMACO-RPL). The objective of DMACO-RPL is to retain the DAG based approach of RPL and at the same time introduce a global optimization-based approach to improve the routing performance in CR environment. Before describing the proposed protocol, it is important to discuss the underlying system model.

5.3.1 System Model

A static multi-hop wireless AMI network is considered, which consists of different smart meters (nodes) and a meter concentrator (gateway node). It is assumed that the smart meters are CR-enabled. A single radio transceiver is equipped in each smart meter, which can be tuned to any channel in the licensed spectrum. We assume N stationary PU transmitters with known locations and maximum coverage ranges. The PU (transmitter) activity model for the i^{th} channel is given by a two state independent and identically distributed random process such that the duration of busy and idle periods is exponentially distributed with a mean of $\frac{1}{\mu^i_{ON}}$ and $\frac{1}{\mu^i_{OFF}}$, respectively. Let S^i_{busy} denote the state that the i^{th} channel is busy (PU is active) with probability $P^i_{busy} = \frac{\mu^i_{OFF}}{\mu^i_{ON}+\mu^i_{OFF}}$, and S^i_{idle} the state that the i^{th} channel is idle with probability P^j_{idle}, such that $P^i_{idle} + P^i_{busy} = 1$. We assume that a node employs energy detection technique [108] for primary signal detection wherein it compares the received energy (E) with a predefined threshold (σ) to decide whether the i^{th} channel is occupied or not i.e.,

$$Sensing\ Decision = \begin{cases} S^i_{busy} & \text{if} \quad E \geq \sigma \\ S^i_{idle} & \text{if} \quad E < \sigma \end{cases} . \tag{5.1}$$

The two principle metrics in spectrum sensing are the detection probability (P_d), and the false alarm probability (P_f). A higher detection probability ensures

better protection to incumbents, whereas a lower false alarm probability ensures efficient utilization of the channel. False alarm and detection probabilities for the i^{th} channel can be expressed as follows.

$$P_f^i = \Pr\{E \geq \sigma | S_{idle}^i\} = Q\left(\frac{\sigma - 2n_i}{\sqrt{4n_i}}\right), \tag{5.2}$$

$$P_d^i = \Pr\{E \geq \sigma | S_{busy}^i\} = Q\left(\frac{\sigma - 2n_i\left(\gamma_i + 1\right)}{\sqrt{4n_i\left(2\gamma_i + 1\right)}}\right), \tag{5.3}$$

where $Q(\cdot)$ denotes Q function, which is the complementary error function, and γ_i and n_i denote the signal-to-noise ratio (SNR) of the primary signal and the bandwidth-time product for the i^{th} channel respectively.

5.3.2 Protocol Description

Initially, each node in the CR-AMI periodically performs the spectrum sensing operation to detect channel availability. We consider an imperfect spectrum sensing scenario under realistic conditions. Therefore, there is a possibility of causing harmful interference to PUs.

In DMACO-RPL, the construction process of DAG follows a similar procedure as CORPL. After detecting a vacant channel, the gateway node transmits a DAG Information Object (DIO) message to identify client nodes and update node ranks. We propose Cognitive Radio Transmission Factor (CRTF) as the default metric for rank computation in DMACO-RPL, which considers the trade-off between QoS of the link and the PU receiver protection. Therefore, CRTF includes two key factors, wherein ρ_{ab} as the link quality indicator, is the probability of node b receiving a transmission from node a, and $\varepsilon_a = \sum_{j=1}^{N} c_{aj}$ denotes the fractional coverage overlapping area of node a with all PU transmitters. In order to reduce interference to PU receivers (which can be present anywhere in the coverage area of PU transmitters), the routes for the CR network should be selected such that they pass through regions of minimum coverage overlap with the PU transmission

$$c_{aj} = \frac{1}{\pi}\cos^{-1}\left(\frac{1}{2d_{aj}r_a}\right) + \frac{R_j^2}{\pi r_a^2}\cdot\cos^{-1}\left(\frac{d_{aj}^2 + R_j^2 - r_a^2}{2d_{aj}R_j}\right) - \frac{1}{2\pi r_a^2}\sqrt{\left\{(R_j + r_a)^2 - d_{aj}^2\right\}(d_{aj} + r_a - R_j)(d_{aj} - r_k + R_j)}. \tag{5.4}$$

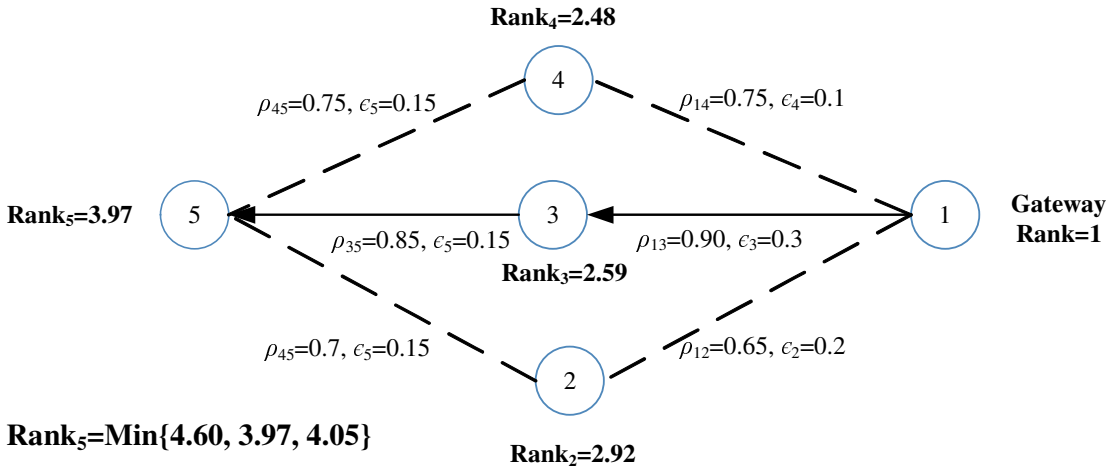

Figure 5.1: Rank computation based on CRTF. The rank of a node is dependent on link quality and fractional overlapping area between client nodes and PU transmitters. Node with the lowest rank is adopted as the default parent.

coverage. The fractional area c_{aj} of node a transmission coverage under the coverage of j^{th} PU transmitter is given by (5.4), where R_j and r_a denote the coverage radii of the j^{th} PU transmitter and the node a respectively, and d_{aj} is the distance between the two. Hence, the CRTF of a link from node a to node b is given by

$$C_a = \frac{1}{\rho_{ab}\cdot(1-\varepsilon_a)}. \tag{5.5}$$

The CRTF of a node will be measured and updated in advance, when the link starts to carry data traffic. The rank of node a can be expressed as follows.

$$rank_a = \min\{rank_p + k\cdot C_a\}, \tag{5.6}$$

where k is a constant, and $p \in \mathbf{P}_a$, where $\mathbf{P}_a$ denotes the parent node set of node a. The rank computation method for a node joining the DAG is illustrated in Fig. 5.1.

Next, the procedure of constructing the forwarder set for nodes will be introduced. It should be noted that each node in DMACO-RPL has a forwarder set (like CORPL) which has been selected based on rank.

The forwarder set is constructed in the back propagation way. The forwarding nodes must be located within the transmission range of the tagged node. During the DIO transmission, each node also reports some additional information using the option field of the DIO message, e.g., whether this node is available for forwarding or not. If the node is not available, it will be deleted from the forwarder lists of all other nodes. Each node updates the information about its neighbors through the DIO message transmission. Based upon the neighborhood information, each node construct the forwarder list based on the rank of its neighbors. It should be noted that only the nodes with lower rank can be included in the forwarder set. Furthermore, when a node does not hear from its neighbor for a pre-defined time interval, its corresponding entry in the forwarder list is deleted. Similarly, the forwarder set is updated when receiving a new DIO message.

In CORPL, the delay for the whole transmission is unknown before the gateway receives the packet. If the deadline has elapsed during the transmission, the packet will be dropped without feedback. Hence, in DMACO-RPL, we propose that the source node determines the whole path to gateway based on a cost function, which is given by

$$\delta = \sum_{i=2}^{M} C_i, \tag{5.7}$$

where M is the number of nodes along the packet forwarding path.

The delay estimation (DE) for the transmission from the source node to the gateway can be expressed as follows.

$$DE = \sum_{i=2}^{M} \left(t_s + t_p\right), \tag{5.8}$$

where t_s is the delay until a idle channel is found, which is estimated by the mean of spectrum sensing events, and t_p is the transmission time per hop, which is estimated

by the packet delivery ratio. Based on the DE, a feedback will be given to the node (source node) if the DE is larger than the deadline. The node receiving the feedback will re-allocate a new path based on the same operation.

DMACO-RPL improves the routing efficiency by utilizing the selected transmission path. As mentioned earlier, once the source node selects the transmission path to the gateway, it includes the relevant information in the header of the packet. During transmission, each node along the forwarding path gets the information after receiving the packet. Therefore, it can use the selected path for its own transmission. However, such transmission path will be emptied when nodes receive a new DIO message. The details of transmission path selection is shown in Algorithm 3.

Algorithm 3: FORWARD NODES SELECTION

```
R_a → Selected (existing) transmission path set of node a
τ → the deadline of packet
check the forward set, R_a.
if R_a = empty then
    calculate the optimal transmission path by using DMACO, according to
    (5.7)
    evaluate DE of the transmission
    if DE ≤ τ then
        use the path for transmission
    end
    else
        give the feedback information
    end
end
else
    use the selected transmission path
end
```

In order to ensure a unique forwarder selection, DMACO-RPL adopts a coordination scheme based on the acknowledgement (ACK) frames. For example, each selected node forwarding the data generates an ACK. The ACK is captured by the nodes in the forwarder set. If the selected node fails to forward the frame within a timeout period (no ACK is received), it will be banned and a new transmission path will be allocated based on the DMACO scheme. In practice, there is an associated

probability of erroneous forwarding of the same frame by multiple nodes. Hence, we consider the *coordination overhead*, which is the probability of a node in the forwarder set retransmitting a frame when any other node has already forwarded it, and is given by

$$\mathbb{O}_a = \rho_{ad} \cdot (1 - \rho_{ad}) + \sum_{p=2}^{|\mathbf{P}|} \prod_{b=1}^{p-1} (1 - \rho_{ab}) \cdot \rho_{ap}, \tag{5.9}$$

where ρ_{ad} and ρ_{ap} denote the probability of successful transmission between node a and the selected next hop d, and the probability of successful transmission between node a and the p^{th} next hop in the forwarder list, respectively.

5.3.3 Directional Mutation Ant Colony Optimization

Mutated Ant Colony Optimization (MACO) provides an effective way to optimize routing protocols in various network environments [113–117]. In this section, we propose a novel MACO, namely, directional mutation ant colony optimization (DMACO) to optimize the routing performance in CR-AMI network. The algorithm of DMACO is introduced as follows.

The main characteristics of DMACO are that, after each iteration, the pheromone values will be updated by all the M ants, and the comparison between the local solution and mutated solution takes place. The whole process of DMACO is given by Fig. 5.2.

The pheromone ρ_{ij}, associated with the edge joining cities i and j, is updated as follows.

$$\tau_{ij}(t+1) = (1 - \theta) \cdot \tau_{ij}(t) + \Delta\tau_{ij}, \tag{5.10}$$

where $\theta \in [0, 1]$ and $\Delta\tau_{ij}$ denote the evaporation rate of pheromone t and the quantity of pheromone laid on edge (i, j) by ant m, respectively.

$$\Delta\tau_{ij}^{m} = \begin{cases} Q/L_m & \text{if ant } m \text{ travels on edge}(i,j) \\ 0 & \text{otherwise} \end{cases}, \tag{5.11}$$

where Q is a constant, and L_m is the length of the tour constructed by ant m.

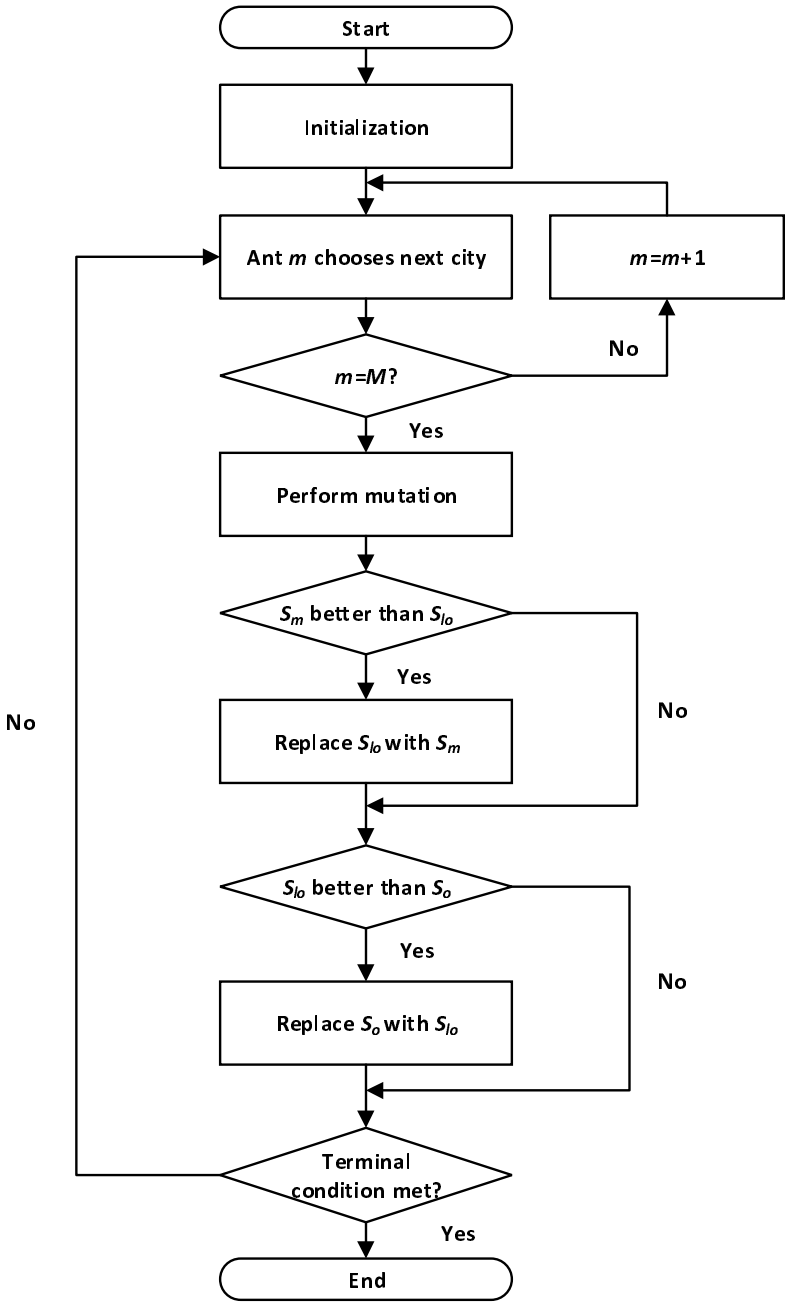

Figure 5.2: The flowchart of DMACO. In the algorithm, the global optimization is obtained by imitating ant foraging.

In the construction of the solution, stochastic mechanism is adopted to select the following city that the ant will visit. Specifically, when ant m is in the city i with the partial solution s^p, the probability of ant m going to the city j is given by:

$$p_{ij}^m = \begin{cases} \frac{[\tau_{ij}]^\alpha [\eta_{ij}]^\beta}{\sum_{e_{il} \in N(s^p)} [\tau_{il}]^\alpha [\eta_{il}]^\beta} & \text{if } e_{ij} \in N(s^p) \\ 0 & \text{otherwise} \end{cases}, \tag{5.12}$$

where $N(s^p)$ is the set of feasible components, that is, edges (i, l), where l is a city that can be visited by ant m. The parameters α and β control the relative importance between pheromone and heuristic information. The heuristic information value is given by:

$$\eta_{ij} = \frac{1}{d_{ij}}, \tag{5.13}$$

where d_{ij} is the distance between city i and j.

In MACO, after each iteration, the local best solution $S^{lb} = (s_1^{lb}, ..., s_K^{lb})$ is obtained, and a mutation operation takes place. One or more elements of the S^{lb} are selected randomly and will be changed in a certain manner. Through the mutation operation, a mutated solution S^m can be obtained. The comparison between S^{lb} and S^m takes place. If S^m is better than S^{lb}, it will be selected as the best solution. Otherwise, the local best solution remains. By using the mutated solution, MACO can overcome the restriction of location solution.

However, as the selection of elements of S^{lb} in MACO is random, the direction of the mutation is uncertain and its efficiency is low. In this regard, we propose a directional mutation mechanism (DMM) to improve the MACO. The proposed algorithm, in terms of DMACO is represented in Algorithm 4. The local optimization problems are addressed by controlling the direction of mutations. More concretely, the common elements between local optimal solution and local second-optimal solution can be found by comparing each element of S^{lb} to S^{ls}. We improve the local optimization overcoming by varying the common elements between S^{lb} and local second-optimal solution (S^{ls}), and promote the algorithm convergence by varying the different elements between S^{lb} and S^{ls}. Therefore, the direction of

mutation is determined and the algorithm capacity of global searching is improved.

Algorithm 4: DIRECTIONAL MUTATION MECHANISM

$S^{lb} = \{s_1, s_2, \cdots, s_K\} \rightarrow$ the local optimal solution
$S^{ls} = \{s'_1, s'_2, \cdots, s'_K\} \rightarrow$ the local second-optimal solution
$S^{m} = \{\grave{s}_1, \grave{s}_2, \cdots, \grave{s}_K\} \rightarrow$ the mutated solution
$S^{e} = \{\acute{s}_1, \acute{s}_2, \cdots, \acute{s}_K\} \rightarrow$ the evolved solution
$S^{a} = \{\tilde{s}_1, \tilde{s}_2, \cdots, \tilde{s}_L\} \rightarrow$ the same element set between S^{lb} and S^{ls}
$S^{d} = \{\breve{s}_1, \breve{s}_2, \cdots, \breve{s}_P\} \rightarrow$ the different element set between S^{lb} and S^{ls}
for $i = 1 : K$ **do**
  Compare s_i to s'_i.
  if $s_i = s'_i$ **then**
    $s_i \in S^a$
  end
  else
    $s_i \in S^d$
  end
end
Randomly select elements from S^a, change the values of according elements in S^{lb} and get the mutated solution S^m.
Randomly select elements from S^d, change the values of according elements in S^{lb} and get the evolved solution S^e.
According to cost function, select the solution with best performance as the new local best solution from S^{lb}, S^e and S^m.

5.3.4 DMACO-based Routing

In our proposed routing protocol, the node employs DMACO to find a new route. As mentioned above, each node has a rank in DAG to show the priority of transmission, which is given by (5.6). It is noted that each node can only transmit to the node which has lower rank. Therefore, the route selection is transformed to select the nodes which can provide the best path cost.

The selection of available nodes can be transformed to an optimization problem,

which is given by

$$\begin{aligned} P_1: \quad & \min \sum_{i=1}^{K} C_{\chi_i} \\ s.t. \quad & (a) \quad K \leq E \\ & (b) \quad \chi_i \in \mathbf{X}, \\ & (c) \quad DE \leqslant \tau - t \quad , \end{aligned} \tag{5.14}$$

where K is the number of selected nodes along the forwarding path, E is the total number of the nodes, t represents the current time (note that the initial current time is 0, it is the moment when the source node starts transmission), and $\mathbf{X}$ and τ denote the set of the nodes in transmission and the deadline associated with the packet, respectively.

In order to solve the optimization problem, DMACO needs modifications to satisfy (5.14). More specifically, l_m, the length of the tour constructed by ant m, is according to the hop distance. Therefore, the quantity of pheromone laid on edge (i, j) by ant m is given by

$$\Delta\tau_{ij}^{m} = \begin{cases} Q/C_{ij} & \text{if ant } m \text{ travels on edge } (i,j) \\ 0 & \text{otherwise} \end{cases}. \tag{5.15}$$

The heuristic information value on the edge between node i and j is updated by

$$\eta_{ij} = \frac{1}{C_{ij}}. \tag{5.16}$$

Therefore, the probability of ant m going to node j is given by

$$p_{ij}^{m} = \begin{cases} \frac{[c_{ij}]^{\varepsilon}}{\sum_{e_{il} \in N(s^P)} [c_{il}]^{\varepsilon}} & \text{if } e_{ij} \in N(s^P) \\ 0 & \text{otherwise} \end{cases}. \tag{5.17}$$

After that, the optimization problem of forwarding node list selection can be solved by using the Algorithm 4 and the flowchart as shown in Fig. 5.2. By iteration,

the optimal solution can be obtained and the transmission path is selected. It is noted that the delay estimation of the selected path must meet the delay constraint.

5.4 Performance Evaluation

In this section, we evaluate the performance of DMACO-RPL under different scenarios. We implement DMACO-RPL with the topology as shown in Fig. 5.3. Other simulation parameters are given in TABLE 5.1. We consider a square region of sides 1200 meters that is occupied by 16 PU transmitters. The secondary users are assumed to be Poisson distributed in the whole region with a mean density. We consider a frequency selective Rayleigh fading channel between any two nodes, where the channel gain accounts for small scale Rayleigh fading, large scale path loss and shadowing. We also compare our proposed DMACO-RPL with RPL and CORPL in the same simulation configuration.

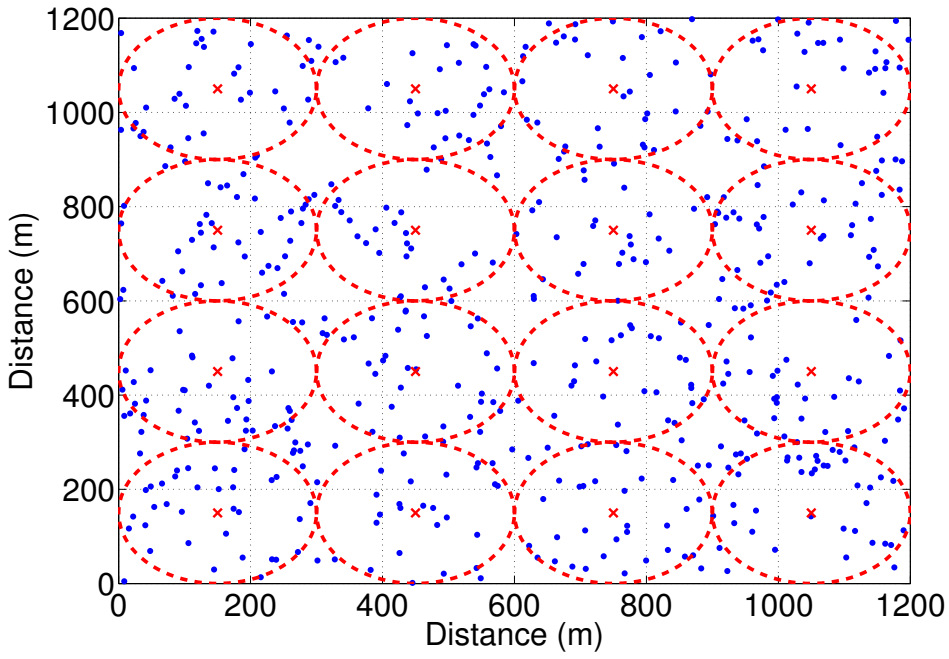

Figure 5.3: Simulated network topology. The circles represent the coverage area of PU transmitters. The density is 4×10^{-4}.

Firstly, we evaluate the impact of the link success probability on the DAG

Table 5.1: Simulation Configuration Parameters.

Parameter	**Value**
Path loss model	$128.1 + 37.6\log_{10}(r)$, r in km
Standard deviation of shadowing	8 dB
Detection probability threshold(P_d)	0.9
Probability of false alarm (P_f)	0.1
Channel bandwidth	200kHz
PU received SNR(γ)	-15dB
Busy state parameter of PU(μ_{ON})	2
Idle state parameter of PU (μ_{OFF})	3
Maximum interference ratio (IR_{max})	0.25
Size of forwarder set (M)	5
Size of DIO message including options	28 bytes

convergence time (defined as the time taken by the set of nodes to obtain topological information and become part of the DAG). As shown in Fig. 5.4, the DAG convergence time decreases as the link success probability (LSP) increases due to lower link layer retransmissions. The DAG convergence time decreases as the node density increases. This is because a higher density results in a faster dissemination of network information as more nodes are located in the coverage range. Compared with both CORPL and RPL, DMACO-RPL requires the shortest DAG convergence time.

Fig. 5.5 depicts the average number of hops against the CR network density. The number of hops is an important factor of delay increasing and associates with the node density in the network. It is shown that the number of hops decreases as the node density increases. Compared with CORPL and RPL, DMACO-RPL has least number hops for the same network density. This is due to global optimization for routing in DMACO-RPL. Through global optimization, the cost function of routing gets minimum. As a result, the number of hops is reduced.

Next, we evaluate the network reliability in terms of *Packet Delivery Ratio* (PDR), which is defined as the ratio of number of packets received to the total

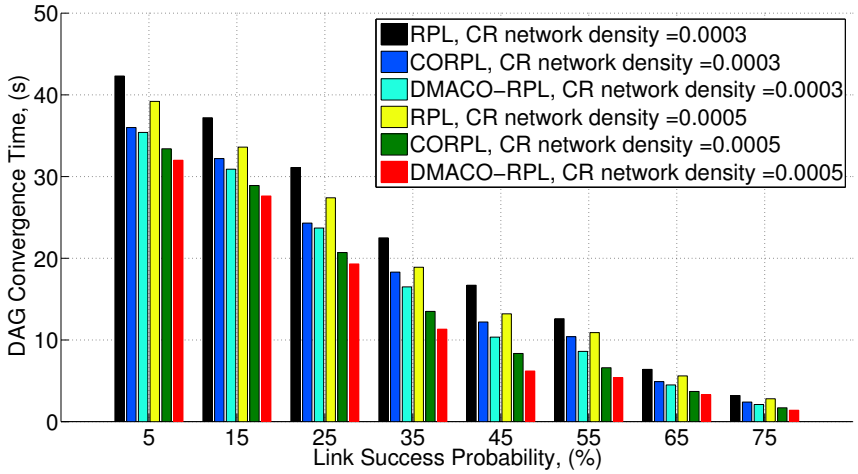

Figure 5.4: DAG convergence time against LSP.

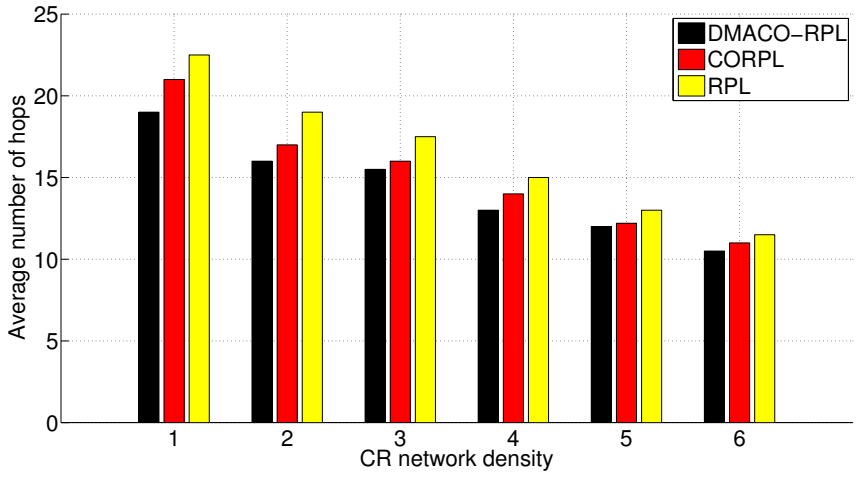

Figure 5.5: Average number of Hops against CR network density.

number of packets sent. We generate 10,000 packets (packet size = 100 bytes) from different nodes and calculate the average PDR for different scenarios. As the results shown in Fig. 5.6, the DMACO-RPL outperforms RPL and CORPL. Especially, the performance gain is significant under poor channel conditions (low LSP). This is because DMACO-RPL provides a global optimization solution for routing protocol in AMI networks, which selects the path with the minimum cost (in this case, the path with the minimum cost has the highest probability of the successful transmission) for data transmission. As a result, the PDR of the route is improved.

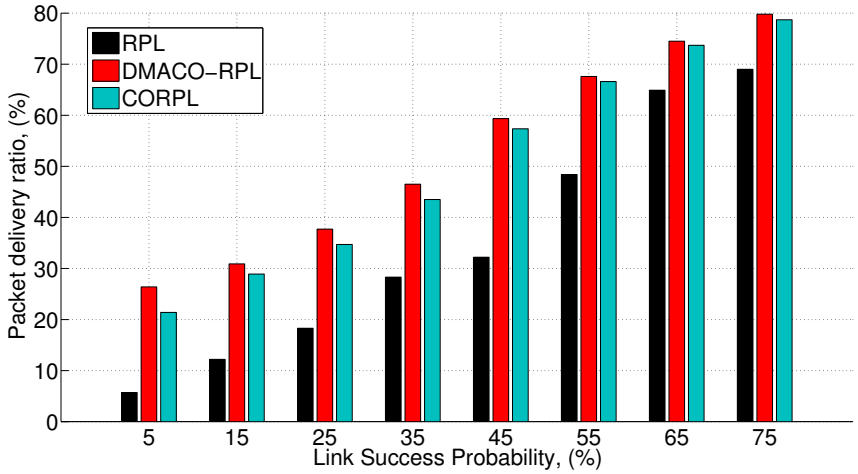

Figure 5.6: PDR performance comparison for different protocols.

We evaluate the end-to-end delay performance against LSP. Fig. 5.7 indicates that the average end-to-end delay decreases as LSP increases, and the average end-to-end delay of DMACO-RPL is within 1.5s, which satisfies the real-time requirements of general AMI applications in smart grid. In this comparison, the performance of DMACO-RPL is better than that of *Class B* of CORPL, which is designed specially for delay sensitive packets. Therefore, we conclude that DMACO-RPL is more robust to LSP in CR environments.

We also evaluate the *Deadline Violation Probability* (DVP) performance of the proposed protocol, which is calculated as the ratio of the number of packets dropped due to violation of deadline at intermediate hops to the total number of packets transmitted. We generate 10,000 packets from different nodes and calculate the

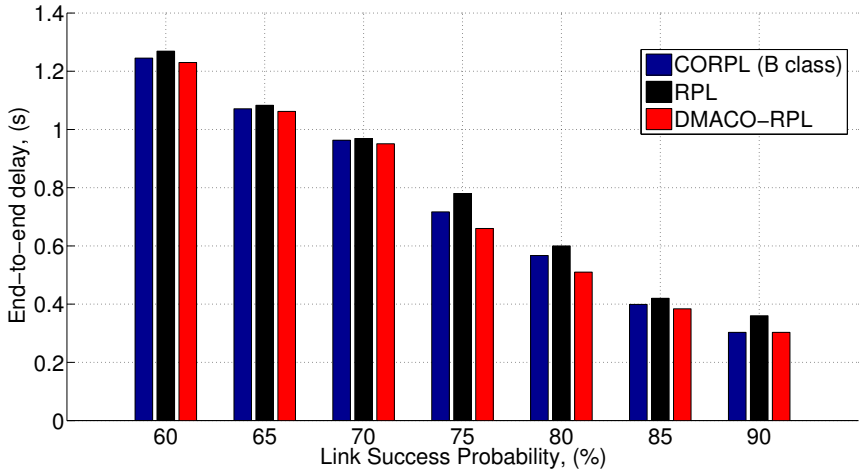

Figure 5.7: Delay performance against different link success probabilities.

average DVP for different scenarios. As shown in Fig. 5.8, the DVP decreases as the LSP increases due to less retransmissions which increase the remaining lifetime of a packet at the intermediate node. DMACO-RPL has the best DVP performance compared with those of CORPL and RPL. This is DMACO-RPL evaluates the DE of the route (given by (5.8)) and selects the route with the minimum delay.

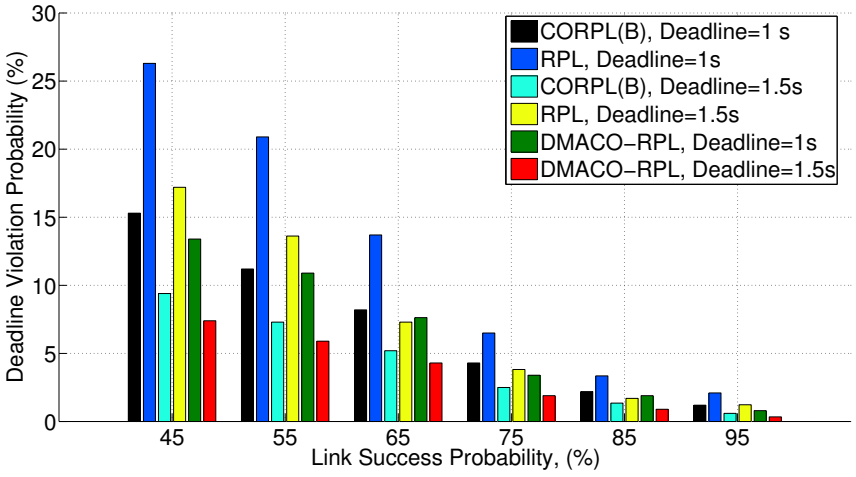

Figure 5.8: Deadline Violation Probability for different scenarios.

In Fig. 5.9, we evaluate the Coordination Overhead (CO) of the DMACO-RPL, which is estimated as the ratio of the number of duplicate packets to the total

number of packets received at the gateway. We notice that the CO increases as the LSP decreases due to the fact that the probability of nodes not capturing ACKs increases, which will result in duplicate packet forwarding. Compared with CORPL and RPL, DMACO-RPL achieves the lowest CO due to global optimized routing approach.

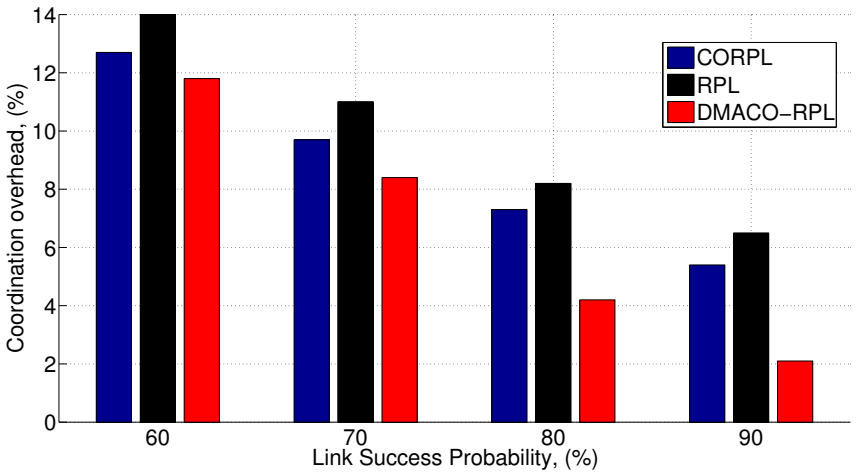

Figure 5.9: Coordination overhead for DMACO-RPL against link success probability (10, 000 packets are transmitted, node density = 4×10^{-4} nodes per unit).

Finally, we evaluate the protection for PU receivers in terms of Collision Risk Factor (CRF), which is defined as the ratio of colliding transmissions to the total number of secondary node transmissions at the PU receivers. Hence, CRF depends on PU transmitter activity and coverage overlap between secondary users and PU transmitters. As shown in Fig. 5.10, DMACO-RPL reduces the chances of collision to PU receivers compared with CORPL and RPL under both low and high PU transmitter activity. This is because DMACO-RPL always selects the route with the minimum coverage overlap between secondary users and PU transmitters (through CRTF routing metric), which significantly reduce the probability of collision with PU receivers. Note that the CRF increases as transmission range of nodes in the CR-AMI network and PU activities increase, because of higher probability of collision with PU receivers.

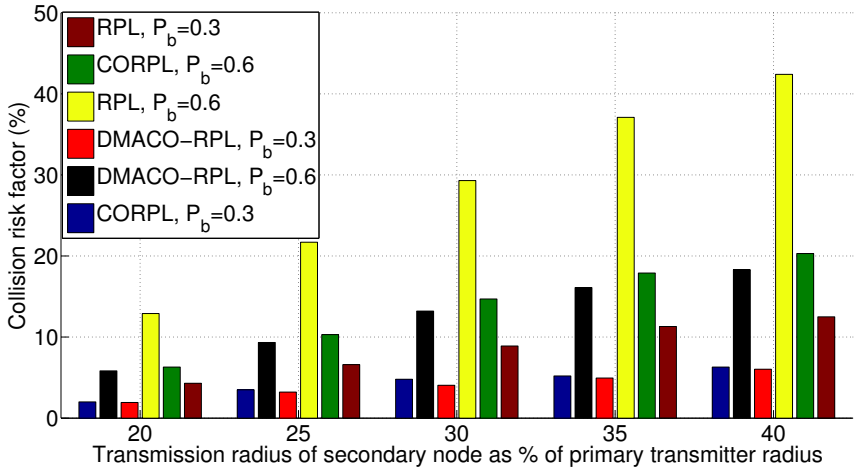

Figure 5.10: Collision risk factor against secondary nodes transmission radii, 10, 000 packet are transmitted, node density $= 4 \times 10^{-4}$ nodes per unit.

5.5 Conclusions

In this chapter, a new RPL-based routing protocol, termed as DMACO-RPL, has been proposed for CR-AMI networks in smart grid. DMACO-RPL is a global optimization-based routing protocol, which employs a novel artificial intelligence optimization algorithm to select the best route from source to gateway. Therefore, DMACO-RPL enhances the reliability and routing efficiency compared to CORPL. It not only fulfills the QoS requirements (in terms of delay and reliability) of the CR-AMI network, but also ensures protection to PUs. Performance evaluation shows that DMACO-RPL generates incurs less end-to-end delay and provides better PDR and DVP, compared to RPL and CORPL, in CR-AMI networks. Besides, DMACO-RPL reduces harmful interference to PU receiver by up to 50% and 10% compared to RPL and CORPL, respectively. Hence, DMACO-RPL provides a viable solution for practical AMI networks.

The performance analysis of CR technique in smart grid is finished in this chapter. In the next chapter, we move to the final stage: analysing and modelling the rate coverage probability in CR enabled HetNet, before concluding the whole thesis.

Chapter 6

Rate Coverage Analysis for Two-Tier Heterogeneous Networks with Cognitive Femtocells

6.1 Introduction

In a HetNet, different network tiers, varying in terms of supported date rates, channel access protocols, transmission power and coverage range, etc. coexist and operate simultaneously [56]. The aggressive frequency reuse in the co-exiting network tiers increases the spatial spectrum efficiency and network capacity, but introduces interference which severely deteriorates the performance of HetNets [55]. In two-tier HetNets consisting of MBSs and FBSs, the users connected to MBSs/FBSs may suffer interference from other MBSs or FBSs in the vicinity.

Cognitive femtocells [54] have recently become an important research area in HetNets, due to their low-power, low-cost, short-range and interference mitigating nature that enhances the network performance (e.g., capacity and coverage) and improves the spectrum efficiency. It involves spectrum sensing and *dynamic spectrum access* (DSA) techniques to avoid using the same frequency bands/channels that are used simultaneously by the major interference sources (either MBSs or other FBSs). Stochastic geometry provides an elegant tool to model HetNets with random topology, where BSs/users are modeled according to a *Poisson Point Process* (PPP) due to its simplicity and tractability. Recently, a number of studies have appeared in literature on investigating various aspects of HetNets using stochastic geometry. The authors in [56, 118] analyzed the outage probability of the two-tier HetNets with cognitive femtocells in multichannel environments over Rayleigh fading and Nakagami-m fading, respectively. In [119], the authors proposed an approximation to the coverage probability of cognitive femtocells. The authors in [57] investigate

Table 6.1: Frequently Used Notations and Symbols

Notation	Description
R_x	The rate achieved by a user associated with the tagged BS in the x^{th}-tier
Θ	The rate coverage
$\mathbb{P}(R > \rho \vert \mathcal{X}_f)$	The rate coverage conditioned on the association with the FBS
$\mathbb{P}(R > \rho \vert \mathcal{X}_m)$	The rate coverage conditioned on the association with the MBS
$\mathcal{A}_f$, $\mathcal{A}_m$	The association probability for the FBS and the MBS, respectively
$\mathcal{L}_I$	The Laplace transform of PDF of the interference
r_{sf}, r_{sm}	The spectrum sensing region (guard-zone) of the FBS or the MBS
λ_f, λ_m, λ_u	The density of FBSs, MBSs and the users
r	The distance between the user and its serving BS
P_f, P_m	The transmit power of FBSs and MBSs, respectively
h_f, h_m	The fading coefficient between the typical user and a FBS or a MBS.

two extremal channel assignment techniques, the random channel assignment and sequential channel assignment techniques in the macro tires to accommodate the overlaid cognitive FBSs with an acceptable opportunistic spectrum access performance. Despite the *rate coverage*[1] analysis for HetNets [35,36], to the best of authors' knowledge, the *rate coverage* for HetNets with cognitive femtocells has not been investigated before, and hence the main focus of this chapter.

We consider a two-tier HetNets with cognitive femtocells. We exploit the concept of "guard-zone" into the analysis of cognitive femtocells, and derive closed-form expressions for rate coverage of each network tier based on the conditional association probability. Our analysis is particularly focused on the *open-access* mode where both femto users and macro users are licensed users, and there is no notion of priority. We also investigate the impact of frequency reuse on the rate coverage in HetNets.

[1]Rate coverage signifies the fraction of user population able to meet their rate thresholds, captures the in-elasticity of traffic such as video services, whereas traditional utility based metrics are more suitable for elastic traffic with no hard rate thresholds [35].

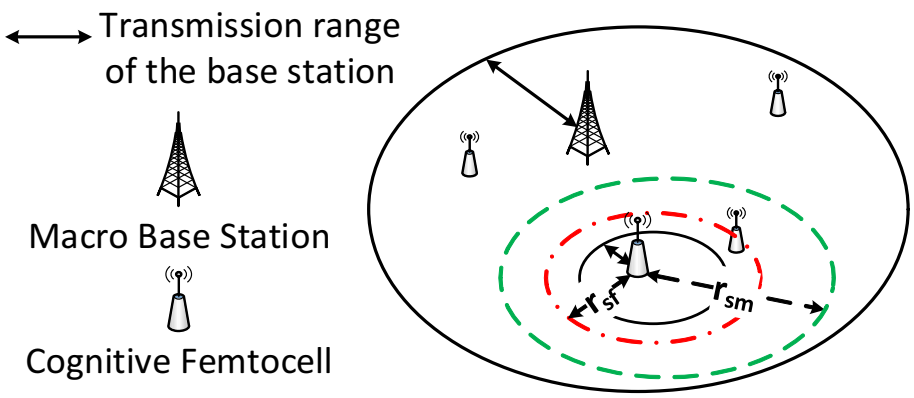

Figure 6.1: An illustration of the two-tier HetNet with cognitive femtocells.

6.2 System Model

We consider a two-tier HetNet consisting of MBSs and cognitive FBSs. The locations of MBSs and FBSs are modeled by two independent and homogeneous PPPs in the $\mathbb{R}^2$ plane. The MBSs are distributed as a PPP $\Phi_m \in \mathbb{R}^2$ with density λ_m, and FBSs are distributed as another PPP $\Phi_f \in \mathbb{R}^2$ with density λ_f. The users are also distributed in the network as an independent PPP with density λ_u. The transmit power of the MBSs and the FBSs is denoted by P_m and P_f, respectively. Integrated with cognitive technology, the FBSs use spectrum sensing to choose the appropriate frequency band for transmission to avoid interference with nearby MBSs and FBSs. Each FBS consists of a sensing slot (T_s) and a transmission slot (T). In T_s stage, the FBS periodically senses the frequency band to identify whether it is occupied or not. We assume that the FBSs employ energy detection technique for spectrum sensing wherein it compares the received energy with a predefined threshold (ϕ) to decide whether the frequency band is occupied or not. For FBSs, the spectrum sensing threshold ϕ defines the spectrum sensing region (SSR) or the guard-zone around each FBS [56]. Therefore, the frequency band is available for a FBS if it is not used by either MBSs or other FBSs within the SSR of this FBS. Due to different transmission power between MBS and FBS, the SSR of a FBS with respect to the MBSs (r_{sm}) is different between the one with respect to other FBSs (r_{sf}), as shown in Fig. 6.1.

For analysis, the standard power loss propagation model is used with path loss exponent α, and only Rayleigh fading environment is considered due to its simplicity and tractability. Thus, the fading coefficient between a MBS m and the typical user is denoted by $h_m \sim \exp(\mu_m)$, which follows an Exponential distribution with mean $1/\mu_m$. Similarly, the fading coefficient between a FBS f and the typical user is denoted by h_f, which is exponentially distributed with mean $1/\mu_f$. Note that both the network tiers share the same set of frequency bands which have the same bandwidth, and each base station can only use one frequency band for transmission.

In *open-access* mode, a user can either associate with a MBS or a FBS by comparing the average received power from the potential serving BSs. The user always associates with the BS which provides better received power. We assume that the users associated with a BS would equally share its frequency band. The rate achieved by a user associated with the tagged BS in the x^{th}-tier is given by

$$R_x = \frac{W}{\mathcal{N}_x} \log_2 \left(1 + SINR_x\right), \tag{6.1}$$

where W is the bandwidth of the frequency band, $\mathcal{N}_x$ is a random variable which denotes the average number of users associated with the tagged BS in the x^{th}-tier [31], $\mathcal{A}_x$ denotes the association probability of the x^{th}-tier, and $SINR_x$ is the received signal-to-interference-plus-noise-ratio from the serving BS for a user, which is given by

$$SINR_x = \frac{P_x h_x r^{-\alpha}}{\sum_{m \in \Phi_m^{\sim}} P_m h_m r_m^{-\alpha} + \sum_{f \in \Phi_f^{\sim}} P_f h_f r_f^{-\alpha} + \sigma^2}, \tag{6.2}$$

where r is the distance between the user and its serving BS, $\Phi_m^{\sim}$ denotes the set of MBSs interfering with the user, $\Phi_f^{\sim}$ denotes the set of FBSs interfering with the user, and σ^2 is the noise power.

6.3 Rate Coverage Analysis

In this section, we analyze the rate coverage of two-tier HetNets with cognitive femtocells. The rate coverage is defined in [35] as: the probability that a randomly chosen user can achieve a target rate ρ, which is given by

$$\Theta \triangleq \mathbb{P}\left(R > \rho\right). \tag{6.3}$$

Since the users can associate with either MBSs or FBSs in *open-access* mode, the overall rate coverage for the chosen user in two-tier HetNets is given by

$$\Theta_o = \mathcal{A}_f \mathbb{P}\left(R > \rho | \mathcal{X}_f\right) + \mathcal{A}_m \mathbb{P}\left(R > \rho | \mathcal{X}_m\right), \tag{6.4}$$

where $\mathcal{A}_f$ and $\mathcal{A}_m$ denote the probability that a user is associated with the FBS and the MBS, and $\mathbb{P}\left(R > \rho | \mathcal{X}_f\right)$ and $\mathbb{P}\left(R > \rho | \mathcal{X}_m\right)$ denote the rate coverage conditioned on the association with the FBS and the MBS, respectively.

In this case, the association probability for the FBS can be expressed as [31]

$$\mathcal{A}_f = \mathbb{P}\left(P_f^r > P_m^r\right) = \left(1 + \frac{\lambda_m}{\lambda_f}\left(\frac{P_m h_m}{P_f h_f}\right)^{2/\alpha}\right)^{-1}, \tag{6.5}$$

and the association probability for the MBS is given by

$$\mathcal{A}_m = 1 - \mathcal{A}_f = 1 - \left(1 + \frac{\lambda_m}{\lambda_f}\left(\frac{P_m h_m}{P_f h_f}\right)^{2/\alpha}\right)^{-1}. \tag{6.6}$$

Next, we derive the rate coverage for different network tiers.

6.3.1 Rate Coverage for Femtocell users

In Rayleigh fading environments, the rate coverage for femtocell users is given by

$$\begin{aligned}\mathbb{P}\left(R>\rho|\mathcal{X}_f\right)&=\mathbb{E}_{\mathcal{N}_f}\left[\mathbb{P}\left(SINR_f>2^{\frac{\rho\mathcal{N}_f}{W}}-1|\mathcal{X}_f\right)\right]\\&=\sum_{n\geq 0}\mathbb{P}\left(\frac{P_f h_f r_f^{-\alpha}}{I+\sigma^2}>\tau|\mathcal{X}_f\right)\mathbb{P}\left(\mathcal{N}_f=n+1\right),\end{aligned}\tag{6.7}$$

where $I=\sum_{m\in\Phi_m^{\sim}}P_m h_m r_m^{-\alpha}+\sum_{f\in\Phi_f^{\sim}}P_f h_f r_f^{-\alpha}$ is the cumulative interference from all other BSs (e.g., MBS, FBS), and $\tau=2^{\frac{\rho\mathcal{N}_f}{W}}-1$.

According to [35], the distribution of the load associated with the x^{th}-tier is given by

$$\begin{aligned}&\mathbb{P}\left(\mathcal{N}_x=n+1\right)=\\&\frac{3.5^{3.5}}{n!}\frac{\Gamma\left(n+4.5\right)}{\Gamma\left(3.5\right)}\left(\frac{\lambda_u\mathcal{A}_x}{\lambda_x}\right)^n\left(3.5+\frac{\lambda_u\mathcal{A}_x}{\lambda_x}\right)^{-n-4.5},\end{aligned}\tag{6.8}$$

with the mean load $\mathbb{E}\left[\mathcal{N}_x\right]=1+1.28\frac{\lambda_u\mathcal{A}_x}{\lambda_x}$, where $\Gamma\left(x\right)=\int_0^\infty t^{x-1}e^{-t}dt$ is the Gamma function. Hence,

$$\begin{aligned}&\mathbb{P}\left(\frac{P_f h_f r_f^{-\alpha}}{I+\sigma^2}>\tau|\mathcal{X}_f\right)=\int_0^\infty\mathbb{P}\left(\frac{P_f h_f r^{-\alpha}}{I+\sigma^2}>\tau\right)f_{X_f}(r)\mathrm{d}r\\&=\frac{2\pi\lambda_f}{\mathcal{A}_f}\int_0^\infty\mathbb{P}\left(\frac{P_f h_f r^{-\alpha}}{I+\sigma^2}>\tau\right)e^{-\pi r^2\left(\lambda_m\left(\frac{P_m h_m}{P_f h_f}\right)^{\frac{2}{\alpha}}+\lambda_f\right)}r\mathrm{d}r\\&=\int_0^\infty\exp\left\{-\frac{\mu_f\tau\sigma^2}{P_f r^{-\alpha}}-\pi r^2\left(\lambda_m\left(\frac{P_m h_m}{P_f h_f}\right)^{\frac{2}{\alpha}}+\lambda_f\right)\right\}\frac{2\pi\lambda_f}{\mathcal{A}_f}\mathbb{E}_I\left[\frac{\mu_f\tau r^\alpha}{P_f}\right]r\mathrm{d}r,\end{aligned}\tag{6.9}$$

where $\mathbb{E}_I\left[s\right]$ is the expected value of the interference to the user, $f_{X_f}(r)$ is given by Lemma 2 of [31], and the proof of (6.9) can be obtained from Theorem 1 in [31].

Following [32] and [56], we have

$$\mathbb{E}_I\left[\frac{\mu_f\tau r^\alpha}{P_f}\right]=\mathcal{L}_{I_{MF}}\left[\frac{\mu_f\tau r^\alpha}{P_f}\right]\mathcal{L}_{I_{FF}}\left[\frac{\mu_f\tau r^\alpha}{P_f}\right],$$

$$\mathcal{L}_{I_{MF}}(s) = \exp\left\{-\frac{\lambda_m \pi}{\kappa}\left((P_m s)^{\frac{2}{\alpha}}\,\mathbb{E}_{h_m}\left[h_m^{\frac{2}{\alpha}}\Gamma_L\left(1-\frac{2}{\alpha}, sP_m h_m\left(r_{sm}-r\right)^{-\alpha}\right)\right] - \frac{P_m s\left(r_{sm}-r\right)^2}{P_m s+\mu_m\left(r_{sm}-r\right)^{\alpha}}\right)\right\}, \tag{6.11}$$

$$\mathcal{L}_{I_{FF}}(s) = \exp\left\{-\frac{\delta\lambda_f \pi}{\kappa}\left((P_f s)^{\frac{2}{\alpha}}\,\mathbb{E}_{h_f}\left[h_f^{\frac{2}{\alpha}}\Gamma_L\left(1-\frac{2}{\alpha}, sP_f h_f\left(r_{sf}-r\right)^{-\alpha}\right)\right] - \frac{P_f s\left(r_{sf}-r\right)^2}{P_f s+\mu_f\left(r_{sf}-r\right)^{\alpha}}\right)\right\}, \tag{6.12}$$

where $\mathcal{L}_{I_{MF}}\left[\frac{\mu_f \tau r^{\alpha}}{P_f}\right]$ is the Laplace transform of the probability density function (PDF) of the interference from the MBSs to the femtocell user, and $\mathcal{L}_{I_{FF}}\left[\frac{\mu_f \tau r^{\alpha}}{P_f}\right]$ is the Laplace transform of the PDF of the interference from other FBSs to the femtocell user.

In cognitive femtocell networks, the interfering MBSs and FBSs must be outside of the Macro or femto SSR of the tagged FBS. Thus, the distance between a user and the nearest interfering MBS or FBS is $r_{sm}-r$ or $r_{sf}-r$. Note that the Laplace transform of the PDF of the aggregate interference measured at the origin from a PPP with intensity λ and existing outside $\mathcal{R}$ is given by [120]

$$\mathcal{L}_I(s) = \exp\left\{-\lambda\pi\left((Ps)^{\frac{2}{\alpha}}\,\mathbb{E}_h\left[h^{\frac{2}{\alpha}}\Gamma_L\left(1-\frac{2}{\alpha}, sPh\mathcal{R}^{-\alpha}\right)\right] - \frac{Ps\mathcal{R}^2}{Ps+\mu\mathcal{R}^{\alpha}}\right)\right\}, \tag{6.10}$$

where $\Gamma_L(x,y) = \int_0^y t^{x-1}e^{-t}dt$ is the lower incomplete Gamma function.

Considering the frequency reuse in HetNets, the Laplace transform of the PDF of the interference from the MBSs to the femtocell user is given by (6.11), where κ is the reuse factor which determines the number of different frequency bands used by the network, and $r_{sm} = \left(\frac{P_m \mu_m}{\phi}\right)^{1/\alpha}$ [56].

Similarly, the Laplace transform of the PDF of the interference from the FBSs to the femtocell user is given by (6.12), where δ denotes the probability that the FBSs cause interference to the user, and $r_{sf} = \left(\frac{P_f \mu_f}{\phi}\right)^{1/\alpha}$ [56]. Without considering frequency resue, the SSR defines the minimum distance between the tagged FBS

$$\mathbb{P}\left(R>\rho|\mathcal{X}_f\right)=\sum_{n\geq 0}\frac{2\pi\lambda_f}{\mathcal{A}_f}\int_0^\infty\frac{3.5^{3.5}}{n!}\frac{\Gamma\left(n+4.5\right)}{\Gamma\left(3.5\right)}\left(\frac{\lambda_u\mathcal{A}_f}{\lambda_f}\right)^n\left(3.5+\frac{\lambda_u\mathcal{A}_f}{\lambda_f}\right)^{-n-4.5}$$
$$\exp\left\{-\pi r^2\left(\lambda_m\sqrt{\frac{P_m h_m}{P_f h_f}}+\lambda_f+\frac{\sqrt{\tau}}{\kappa}\left(\lambda_m\sqrt{\frac{P_m\mu_f}{P_f\mu_m}}\arctan g\sqrt{\frac{P_m\mu_f}{P_f\mu_m}}+\lambda_f\delta\arctan v\right)\right)\right\}r\mathrm{d}r, \tag{6.14}$$

and the MBSs or other FBSs to tolerate the interference. In other words, it defines inactive regions for each MBS and FBS, ouside of which the active FBSs are distributed as two independent Poisson hole processes [121]. Therefore, we have

$$\delta=\delta_f\delta_m=e^{-\left(\lambda_f r_{sf}^2+\lambda_m r_{sm}^2\right)\pi}. \tag{6.13}$$

For $\alpha=4$, $\sigma^2\to 0$, and plugging in $s=\frac{\mu_f\tau r^\alpha}{P_f}$, the rate coverage for femtocell users is given by (6.14), where $g=\frac{r^2\sqrt{\tau}}{\left(r_{sm}-r\right)^2}$, $v=\frac{r^2\sqrt{\tau}}{\left(r_{sf}-r\right)^2}$, $\tau=2^{\frac{\rho\mathcal{N}_f}{W}}-1$, $\mathcal{A}_f$ is given by (6.5) and δ is given by (6.13).

6.3.2 Rate Coverage for Macrocell users

We obtain the rate coverage for macrocell users in a similar way as we described above. The rate coverage for the macrocell users in Rayleigh fading environment is given by

$$\begin{aligned}&\mathbb{P}\left(R>\rho|\mathcal{X}_m\right)\\&=\sum_{n\geq 0}\mathbb{P}\left(SINR_m>\tau|\mathcal{X}_m\right)\mathbb{P}\left(\mathcal{N}_m=n+1\right),\end{aligned} \tag{6.15}$$

where $\tau=2^{\frac{\rho\mathcal{N}_m}{W}}-1$, $\mathbb{P}\left(\mathcal{N}_m=n+1\right)$ can be obtained from (6.8), and

$$\mathbb{P}\left(SINR_m>\tau|\mathcal{X}_m\right)=\int_0^\infty\frac{2\pi\lambda_m}{\mathcal{A}_m}\mathbb{E}_I\left[\frac{\mu_m\tau r^\alpha}{P_m}\right]r$$
$$\cdot\exp\left\{-\frac{\mu_m\tau\sigma^2}{P_m r^{-\alpha}}-\pi r^2\left(\lambda_m+\lambda_f\left(\frac{P_f h_f}{P_m h_m}\right)^{\frac{2}{\alpha}}\right)\right\}\mathrm{d}r,$$

$$\mathcal{L}_{I_{FM}}(s) = \exp\left\{-\frac{\delta\lambda_f\pi}{\kappa}\left((P_f s)^{\frac{2}{\alpha}}\,\mathbb{E}_{h_f}\left[h_f^{\frac{2}{\alpha}}\Gamma_L\left(1-\frac{2}{\alpha}, sP_f h_f\left(r_{sm}-r\right)^{-\alpha}\right)\right] - \frac{P_f s\left(r_{sm}-r\right)^2}{P_f s+\mu_f\left(r_{sm}-r\right)^{\alpha}}\right)\right\}, \tag{6.17}$$

$$\mathbb{P}\left(R>\rho|\mathcal{X}_m\right) = \sum_{n\geq 0}\frac{2\pi\lambda_m}{\mathcal{A}_m}\int_0^{\infty}\frac{3.5^{3.5}}{n!}\frac{\Gamma\left(n+4.5\right)}{\Gamma\left(3.5\right)}\left(\frac{\lambda_u\mathcal{A}_m}{\lambda_m}\right)^n\left(3.5+\frac{\lambda_u\mathcal{A}_m}{\lambda_m}\right)^{-n-4.5} \cdot \exp\left\{-\pi r^2\left(\lambda_m+\lambda_f\sqrt{\frac{P_f h_f}{P_m h_m}}+\frac{\sqrt{\tau}}{\kappa}\left(\lambda_f\delta\sqrt{\frac{P_f\mu_m}{P_m\mu_f}}\arctan g\sqrt{\frac{P_f\mu_m}{P_m\mu_f}}+\lambda_m\arctan\sqrt{\tau}\right)\right)\right\} \cdot r\mathrm{d}r. \tag{6.18}$$

with

$$\mathbb{E}_I\left[\frac{\mu_m\tau r^{\alpha}}{P_m}\right] = \mathcal{L}_{I_{MM}}\left[\frac{\mu_m\tau r^{\alpha}}{P_m}\right]\mathcal{L}_{I_{FM}}\left[\frac{\mu_m\tau r^{\alpha}}{P_m}\right],$$

where $\mathcal{L}_{I_{MM}}\left[\frac{\mu_m\tau r^{\alpha}}{P_m}\right]$ is the Laplace transform of the PDF of the interference from the MBSs to the macrocell user, and $\mathcal{L}_{I_{FM}}\left[\frac{\mu_m\tau r^{\alpha}}{P_m}\right]$ is the Laplace transform of the PDF of the interference from the other FBSs to the macrocell user.

From [32] and [56], $\mathcal{L}_{I_{MM}}(s)$ and $\mathcal{L}_{I_{FM}}(s)$ are respectively given by (6.16) and (6.17).

$$\mathcal{L}_{I_{MM}}(s) = \exp\left(\frac{-2\pi\lambda_m}{\kappa}\int_r^{\infty}\left(1-\frac{\mu_m}{\mu_m+sv^{-\alpha}}\right)v\mathrm{d}v\right). \tag{6.16}$$

For $\alpha = 4$, $\sigma^2 \to 0$, and plugging in $s = \frac{\mu_m\tau r^{\alpha}}{P_m}$, the rate coverage for macrocell users is given by (6.18), where $\mathcal{A}_m$ is given by (6.6). Hence, the overall rate coverage for two-tier HetNets can be obtained from (6.4).

6.4 Numerical Results

In this section, we evaluate the performance of rate coverage in two-tier HetNets with cognitive femtocells. For numerical evaluation, we set $P_m = 45$ dBm, $P_f = 20$ dBm, $\phi = -45$ dBm, $W = 10$ MHz, $\alpha = 4$, $\mu_m = \mu_f = 1$ $\lambda_m = 1$ BS/km^2, and

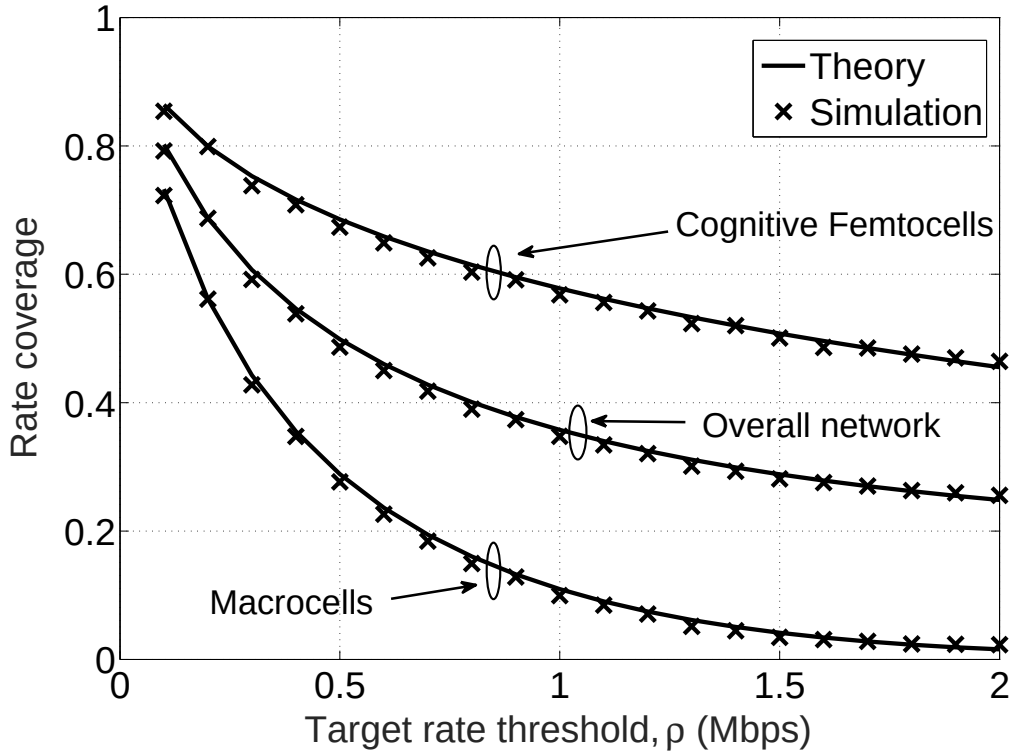

Figure 6.2: The rate coverage against the target rate threshold, $\lambda_f = 20$ BSs/km^2 and $\kappa = 1$.

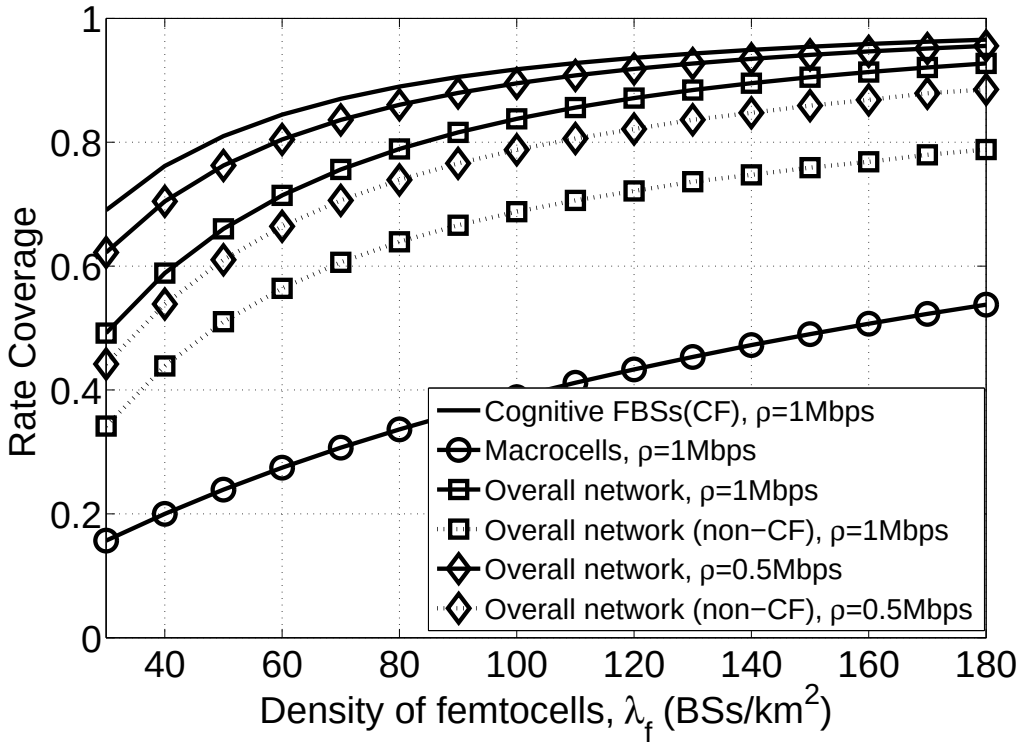

Figure 6.3: The rate coverage against the density of femtocells λ_f, $\kappa = 1$.

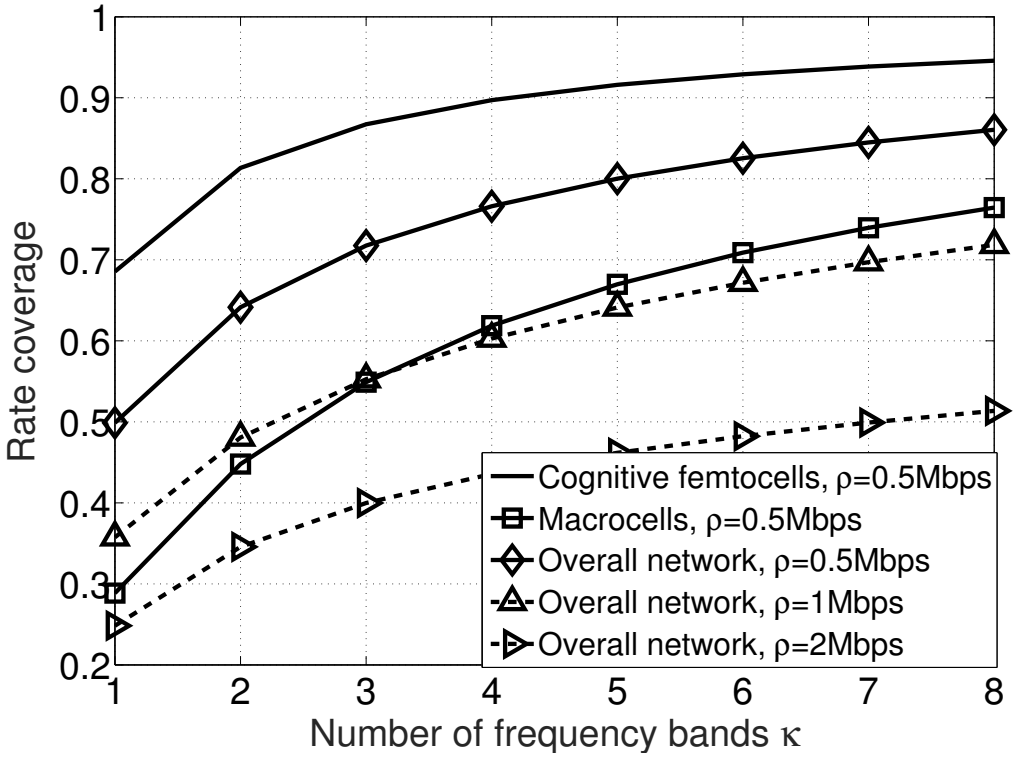

Figure 6.4: The rate coverage against the number of frequency bands (reuse factor) κ, $\lambda_f = 20$ BSs/km^2.

$\lambda_u = 200$ km^{-2}. We assume that the density of cognitive femtocells λ_f, the target rate threshold ρ, and the reuse factor (the number of freqency bands) κ are varying.

Fig.6.2 shows the rate coverage against the target rate threshold. As shown, the rate coverage decreases with the target rate threshold. The rate coverage of the cognitive femtocells is much higher than that of the macrocells. Moreover, femtocells increase the overall rate coverage by improving the network capacity through efficiency sharing the frequency band with macrocells. The cognitive aspect mitigates the interferences between MBSs/FBSs and FBSs, which also enhances the network performance significantly. We also conduct a simulation study and note that the analytical results closely follow the simulation results.

Fig.6.3 depicts the rate coverage against the density of femtocells. The rate coverage increases with the density of the femtocells. This is because more users will associate with the femtocells when the density of femtocells increases. The femtocells increase the network capacity and improve the spectrum efficiency, which provides higher rate coverage for the associated users. The rest of users associated with the macrocells also achieve higher rate coverage as each user can utilize more spectrum resources from the macrocells. Moreover, as mentioned above, the cognitive aspect reduces the interference and enhances the network performance. In Fig. 6.3, we also compare the rate coverage of HetNet with cognitive femtocells to that of the one without cognition. The result shows that the HetNet with cognitive femtocells outperform the one without cognition.

Last, but not least, we evaluate the impact of the frequency reuse on the rate coverage in HetNets. Fig.6.4 shows the rate coverage against the number of frequency bands (reuse factor). It is clear that the rate coverage increases with the number of frequency bands. This is because the interferences between MBSs/FBSs and FBSs/MBSs decreases with the number of frequency bands.

6.5 Summary and Conclusion

Cognitive femtocells have recently become an important research area in HetNets, due to their low-power, low-cost and interference mitigating nature that enhances the network performance and improves the spectrum efficiency. As an important metric, rate coverage signifies the fraction of user population able to meet their rate thresholds, captures the in-elasticity of traffic, whereas is more suitable for elastic traffic compared to the traditional utility based metrics. Furthermore, stochastic geometry modeling for HetNets provides a tractable and accurate expression for the performance metrics in terms of the design parameters. In this chapter, we have investigated an analytical approach to investigate the rate coverage of two-tier HetNets with cognitive femtocells. We consider the association probability for both tiers and derive closed-form expressions for rate coverage of both MBSs and FBSs. We also analyze the impact of the frequency reuse on rate coverage in HetNets. Results show that cognitive femtocells can significantly enhance the overall rate coverage of the two-tier HetNets by improving the network capacity through efficient spectrum utilization and mitigation of the interference.

Chapter 7

Conclusions and Future Work

7.1 Conclusions

CR technology plays an important role in realizing the vision of future wireless communications. It is envisaged to solve the issues of spectrum scarcity and spectrum inefficiency through DSA technique, wherein unlicensed (CR) users opportunistically use licensed bands when not occupied. In order to achieve the goal of truly ubiquitous spectrum aware communications, CR devices need to incorporate the functionalities such as spectrum sensing, spectrum decision, spectrum sharing and spectrum mobility. Therefore, CR aware protocols are required at different layers of the protocol stack that not only fulfil the requirements of CR devices but also provide a low cost DSA solution.

This thesis focuses on the performance analysis of CR networks. The main objective of this research is to investigate different challenges related to CR networks, which not only focuses on developing novel solutions, algorithms, and protocol enhancements for different layers of the protocol stack (e.g., PHY, MAC, and Network layers), but also emphasises on applications of CR technology in different wireless environments (e.g., CRAHN, smart grid, and HetNet). In addition, the thesis not only made original contributions to the research community but also opened up interesting areas for future research. Since each chapter of the thesis addressed an independent research issue, the main contributions of the thesis are summarized as follows which provide a overall picture of the research conducted.

7.1.1 Summary of Chapter 3

In Chapter 3, a spectrum aggregation-based cooperative routing protocol, termed as SACRP is proposed for CRAHNs, which includes two classes of cooperative routing protocols: *Class A* for power minimization or throughput maximization, and *Class B* for reducing the end-to-end delay. A stochastic geometry approach has been used to develop the analytical model for the proposed protocol. Performance evaluation demonstrate that *Class A* aggregates multiple channels and selects suitable relay nodes, and therefore achieves higher power efficiency and throughput. *Class B* reduces the number of re-transmissions by selecting the relay nodes with better channel conditions, and therefore reduces the end-to-end delay. In addition, a performance comparison of SACRP with other relevant protocols in literature is also conducted. Results shows that SACRP *Class A* reduces the transmit power by up to 70% compared to MSA in cooperative as well well as non-cooperative scenarios. Apart from this it enhances the overall throughput by up to 50% and 20% compared to MSA in non-cooperative and cooperative scenarios, respectively. Besides, SACRP *Class B* reduces the end-to-end delay by up to 38% and 55% compared to MSA in non-cooperative and cooperative scenarios respectively.

7.1.2 Summary of Chapter 4

CSNs play an important role in the operation and management of smart grid. In Chapter 4, CRB-MAC, which is a receiver-based MAC protocol for CSNs, is proposed with special emphasis on energy efficiency, reliability and end-to-end delay. CRB-MAC employs preamble sampling and opportunistic forwarding techniques to cater for high energy efficiency and reliability requirements of CSNs. CRB-MAC is also enhanced for mitigating the performance degradation due to periodic spectrum sensing state of nodes in the network. On the other hand, a delay-budget based election process for packet forwarding is proposed in order to effectively handle delay sensitive traffic. Especially, reliability improvement of up to 50% can be achieved

compared to CSB-MAC protocol in lossy environments. Analytical and simulation results demonstrate that in lossy wireless environments CRB-MAC generates less retransmissions and therefore, enhances the overall energy and delay performance. Moreover, high reliability can be provided by increasing the number of receivers. Hence, CRB-MAC provides a viable solution for CSNs in realizing the vision of smart grid.

7.1.3 Summary of Chapter 5

RPL as a routing protocol for Low Power and Lossy Networks, has been recently standardized by IETF and intends to support a variety of applications in smart grid. In Chapter 5, a new RPL-based routing protocol, termed as DMACO-RPL, has been proposed for CR-AMI networks in smart grid. DMACO-RPL is a global optimization-based routing protocol, which employs a novel artificial intelligence optimization algorithm to select the best route from source to gateway. Therefore, DMACO-RPL enhances the reliability and routing efficiency compared to CORPL. It not only fulfills the QoS requirements in terms of delay and reliability of the CR-AMI network, but also ensures protection to PUs. Performance evaluation demonstrates that DMACO-RPL generates incurs less end-to-end delay and provides better PDR and DVP, compared to RPL and CORPL, in CR-AMI networks. Besides, DMACO-RPL reduces harmful interference to PU receiver by up to 50% and 10% compared to RPL and CORPL, respectively. Hence, it provides a viable solution for practical AMI networks.

7.1.4 Summary of Chapter 6

Cognitive femtocells have recently become an important research area in HetNets, due to their low-power, low-cost and interference mitigating nature. As an important metric, rate coverage signifies the fraction of user population able to meet their rate thresholds, captures the in-elasticity of traffic, whereas is more suitable for elastic traffic compared to the traditional utility based metrics. In addition,

stochastic geometry as an elegant tool, provides a tractable and accurate approach to the modelling, analysis and design of HetNets. Therefore, Chapter 6 proposed an analytical approach to investigate the rate coverage of two-tier HetNets with cognitive femtocells. The association probability for both tiers is considered in order to obtain closed-form expressions for rate coverage of both MBSs and FBSs. Besides, the impact of the frequency reuse on rate coverage in HetNets is also investigated. Results show that cognitive femtocells can significantly enhance the overall rate coverage of the two-tier HetNets by improving the network capacity through efficient spectrum utilization and mitigation of the interference.

7.2 Future Work

It is easily noticed that the research on CR technology is far from complete. The thesis covers some of the key issues in CR networks and provides the foundations for future research. A number of challenges remain that need to be addressed. Therefore, this section highlights some research directions for future researchers.

7.2.1 Network Reliability and PU receiver Protection for Cognitive Radio Ad-Hoc Networks

It would be interesting to investigate the applicability of SACRP for the network reliability and PU receiver protection in CRAHNs. Although the combination of spectrum aggregation and cooperation provides an opportunity of enhancing the performance in terms of different metrics such as energy efficiency and throughput, it also creates challenges and complexities for network reliability. For instance, as aforementioned in Chapter 3.3, spectrum aggregation needs to exchange control information of multiple spectrum bands/channels before transmission. A collision for control packets may occur owing to simultaneous transmission from multiple users in multi-user scenario. In this research, a random back-off solution is only given to schedule retransmissions after collisions. There is no consideration about how to reduce or avoid this kind of collision. Therefore, a collision mitigation or

avoidance solution requires further investigation. Moreover, cooperative spectrum sensing techniques [122] for multiple channels can be employed to improve the channel detection performance, which also improves the network reliability.

PU receiver protection for CRAHNs has been discussed in literature [38, 74]. Minimizing the overlapped transmission area between the PU transmitter and CR users becomes an efficient way to protect PU receivers. However, this scenario has not been investigated under spectrum aggregation scheme. Apart from this, power allocation provides an efficient transmit power control for CR users, which allows the transmission of CR users under a tolerant level. It should be noted that PU protection also improves the reliability of the network due to reducing harmful interference to the primary network.

7.2.2 Protocols Design for Smart Grid with a Cognitive Approach

Since CR technology plays an important role in smart grid, it would be interesting to investigate other protocols from the perspective of cognitive approach in smart grid. For example, cross-layer protocol design can improve the performance of the network through joint optimization of parameters at different layers. Neither CRB-MAC protocol (presented in Chapter 4) nor DMACO-RPL protocol (presented in Chapter 5) has considered the cross-layer design. In addition, the research related to the cross-layer design in either CSNs or CR-AMI networks is still infancy. Therefore, It is important to consider the CRB-MAC and DMACO-RPL protocols from the cross-layer perspective.

Moreover, as smart grid comprises of both power and communication layers [22], it is important to investigate the cognitive-based protocols with power systems perspective for smart grid. Therefore, a new MAC or routing protocol is required, which is specially designed under the dynamics of power systems, in either CSNs or CR-AMI networks.

7.2.3 Resource Allocation for Heterogeneous Networks with Cognitive Small Cells

In HetNets, Cognitive small cells provide a fast, flexible and cost-efficient solution to satisfy the increasing demand for network capacity [123]. Current research is mainly focused on the modeling and analysis of HetNets with Cognitive small cells. Therefore, it is important to investigate the resource allocation for HetNets with cognitive small cells. For example, in Chapter 6, the rate coverage for two-tier HetNets with cognitive femtocells is analysed. This analysis can be extended to the K-tier cognitive small cells, and the resource allocation scheme can be applied to maximize the network performance (in terms of throughput and reliability). Reinforcement Learning (Q-Learning) [124] as an elegant tool, provides an efficient approach for resource allocation due to its simplicity. So far, Q-Learning has been used for Radio Access Technology (RAT) in Heterogeneous Cellular Networks [125]. It would be interesting to investigate the application of Q-Learning for resource allocation in HetNets with cognitive small cells.

Appendices

Appendix A

Proof of Equation (3.39)

Based on Shannon's Theorem, the total transmission power for aggregating N_A channels is given by

$$P_{x,y}^{min} \triangleq \mathbb{E}\left[\sum_{k=1}^{N_A} \frac{\left(2^{\frac{R_d^k}{\mathbb{P}_{acc}^k B_k}} - 1\right)\delta^2}{|h_{x,y}^k|^2}\right], \tag{A.1}$$

where $|h_{x,y}^k|^2 = |F_{x,y}^k|^2/L_{x,y}$. Note that all aggregated channels are independent and identically distributed (i.i.d). In Rayleigh fading environments, $|F_{x,y}^k|^2 \sim \text{Exp}(\mu)$. Note that for a random variable X taking non-negative values, the expected value can be calculated using the complementary Cumulative Distribution Function

(CDF) i.e., $\mathbb{E}[X] = \int_{t>0} \mathbb{P}(X > t)\ dt$. Therefore,

$$
\begin{aligned}
P_{x,y}^{min} &\triangleq \mathbb{E}\left[\sum_{k=1}^{N_A} \frac{\left(2^{\frac{R_d^k}{\mathbb{P}_{acc}^k B_k}} - 1\right)\delta^2 L_{x,y}}{|F_{x,y}^k|^2}\right] \\
&= \sum_{k=1}^{N_A} \mathbb{E}\left[\frac{\left(2^{\frac{R_d^k}{\mathbb{P}_{acc}^k B_k}} - 1\right)\delta^2 L_{x,y}}{|F_{x,y}^k|^2}\right] \\
&= \sum_{k=1}^{N_A} \int_{t>0} \mathbb{P}\left(\frac{\left(2^{\frac{R_d^k}{\mathbb{P}_{acc}^k B_k}} - 1\right)\delta^2 L_{x,y}}{|F_{x,y}^k|^2} > t\right) dt \qquad \text{(A.2)} \\
&= \sum_{k=1}^{N_A} \int_{t>0} \mathbb{P}\left(|F_{x,y}^k|^2 < \frac{\left(2^{\frac{R_d^k}{\mathbb{P}_{acc}^k B_k}} - 1\right)\delta^2 L_{x,y}}{t}\right) dt \\
&= \sum_{k=1}^{N_A} \int_0^{\infty} 1 - \exp\left[-\mu \frac{\left(2^{\frac{R_d^k}{\mathbb{P}_{acc}^k B_k}} - 1\right)\delta^2 L_{x,y}}{t}\right] dt,
\end{aligned}
$$

which completes the proof.

Appendix B

Proof of Equation (3.49)

According to (3.25), we have $\rho = \mathbb{P}\left[\mathcal{E}_{x,r} + \mathcal{E}_{r,y} < \mathcal{E}_{x,y}\right]$. From (3.48), we have $\mathcal{E}_{x,y} = \exp\left[\alpha L_{x,y}\right]$, where $\alpha = \mu\gamma\delta^2/P_{x,y}$. In this case, μ, γ, and δ^2 are constant for all CR nodes. Under the assumption of fixed transmission power $P_{x,y}$, ETX ($\mathcal{E}$) is a log-normal distributed with mean $\mu_{etx} = 0$ and variance $\sigma^2 = \alpha^2$. Using the substitution $X \to \mathcal{E}_{x,r}$ and $Y \to \mathcal{E}_{r,y}$, we have $\rho = \mathbb{P}\left[X + Y < \mathcal{E}_{x,y}\right]$.

The probability of finding the relay node for *Class B* requires the pdf of a sum of two log-normal random variables. As X and Y have the same mean and variance, the pdf can be found using the Fenton-Wilkinson (FW) approximation [126], according to which the random variable $X+Y$ is also log-normally distributed with mean $\mu'_{etx} = \ln 2 + \frac{1}{2}\left(\sigma^2 - \sigma'^2\right)$, where σ'^2 is the variance and is given by $\sigma'^2 = \ln\left(\frac{\exp(\sigma^2)-1}{2} + 1\right)$.

The CDF for the log-normal distributed random variable g having mean μ_g and variance σ_g^2 is given by

$$\frac{1}{2} + \frac{1}{2}\mathrm{erf}\left[\frac{\ln g - \mu_g}{\sqrt{2}\sigma_g}\right]. \tag{B.1}$$

Changing $g \to \mathcal{E}_{s,d}$, $\mu_g \to \mu'_{etx}$ and $\sigma_g^2 \to \sigma'^2$, we have the probability ρ_B in (3.49). This completes the proof.

Appendix C

Proof of Equation (3.50)

Note that the delay for a single hop for a single transmission can be expressed by $\Phi = N_{ss}T_s + T_t + T_b$, where N_{ss} is the number of spectrum sensing events, T_s is the spectrum sensing duration, T_t is the total time for transmitting data packets, and T_b is the average back-off time for control packets until successful transmission.

Let $\mathbb{P}_n$ denote the probability that a CR node will successfully transmit data after n spectrum sensing times. Thus, $\mathbb{P}_n$ is given by

$$\mathbb{P}_n = (1 - \mathbb{P}_{acc})^n \mathbb{P}_{acc}. \tag{C.1}$$

Let n_s be the random variable that represents the total number of spectrum sensing events until success. Since $\mathbb{P}_n$ represents the Probability Mass Function (PMF) of n_s, the average number of spectrum sensing events until success is given by

$$N_s = \mathbb{E}(n_s) = \sum_{n=0}^{\infty} n\mathbb{P}_n = \frac{1 - \mathbb{P}_{acc}}{\mathbb{P}_{acc}}, \tag{C.2}$$

where $\mathbb{P}_{acc} = \min(\mathbb{P}_{acc}^j)$ due to the data packets are split and transmitted simutaneously over the aggregated channels.

Note that if $T_t > T$, the CR node cannot transmit all data packets within the duration of one transmission time T. Hence, the total number of spectrum sensing events N_{ss} can be calculated by

$$N_{ss} = N_s + \left\lceil \frac{N_{data}L_{data}}{TR_d} \right\rceil - 1, \tag{C.3}$$

where N_{data} is the number of data packets, R_d is the rate demand, and L_{data} is the

data packet size.

Next, using a similar methodology as employed for calculating the average number of spectrum sensing events, the average number of collisions for control packets until successful transmission N_c is given by

$$N_c = \frac{\mathbb{P}_c}{1-\mathbb{P}_c} = \frac{1-(1-\mathbb{P}_{RTS})(1-\mathbb{P}_{CTS})(1-\mathbb{P}_{RES})}{(1-\mathbb{P}_{RTS})(1-\mathbb{P}_{CTS})(1-\mathbb{P}_{RES})}, \tag{C.4}$$

where $\mathbb{P}_c$ is the probability that a collision for control packets occurs owing to simultaneous transmission from multiple nodes. It should be noted that Geometric distribution has been employed to compute N_c, similar to the analysis in [127].

Thus, the expected backoff time T_b (which can be calculated according to (27) in [127])is given by

$$T_b = N_e T_{slot} = \left(\frac{N_c+1}{\mathbb{P}_t} - 1\right) T_{slot}, \tag{C.5}$$

where N_e is the expected number of back-off time slots, T_{slot} is the duration of back-off time slot, and $\mathbb{P}_t = 1-(1-\mathbb{P}_c)^{1/\left(\lambda\pi\mathcal{R}^2-1\right)}$ denotes the probability that a given node will transmit in an arbitrary time slot which is also given by [127] . Therefore, Φ is given by (3.50). This completes the proof.

Appendix D

Analytical Modeling for CSB-MAC

The expressions for CSB-MAC protocol can be obtained using a similar framework as described for CRB-MAC in Section III.

The single hop energy consumption for CSB-MAC is given by

$$\mathcal{E}^j_{CSB\_total} = \chi_{CSB}(\mathcal{E}\_T^j_{fail} + \mathcal{E}\_R^j_{fail}) + \mathcal{E}\_T^j_{succ} + \mathcal{E}\_R^j_{succ} + \chi^j_{ss}\mathcal{E}^j_{ss}, \quad \text{(D.1)}$$

where χ_{CSB} denotes the number of retransmissions which can be obtained in a similar way as described in (4.15) with $P_a = (P^j_{fail})^a(1 - P^j_{fail})$.

The single hop delay for CSB-MAC is given by

$$\mathcal{D}^j_{CSB} = \chi_{CSB} \cdot (T_{pr} + T_d + T_{CW}) + \chi^j_{ss} \cdot T_s + T_{CI} \cdot (\chi^j_{ss} - 1). \quad \text{(D.2)}$$

Finally, the single-hop reliability of CSB-MAC is given by

$$\mathcal{R}^j_{CSB} = 100 \times \left(1 - (P^j_{fail})^{(\chi_{CSB}+1)}\right). \quad \text{(D.3)}$$

References

[1] H. Rahul, F. Edalat, D. Katabi, and C. Sodini, "Frequency-aware rate adaptation and MAC protocols," in *Proc. ACM MobiCom*, 2009, pp. 193–204.

[2] I. F. Akyildiz, W.-Y. Lee, M. C. Vuran, and S. Mohanty, "NeXt Generation/Dynamic Spectrum Access/Cognitive Radio Wireless Networks: A Survey," *Comput. New*, vol. 50, no. 13, Sept 2006.

[3] I. F. Akyildiz, W.-Y. Lee, and K. R. Chowdhury, "CRAHNs: Cognitive radio ad hoc networks," *Ad Hoc Networks*, vol. 7, no. 5, pp. 810–836, 2009.

[4] S. Haykin, "Cognitive radio: brain-empowered wireless communications," *IEEE J. Sel. Areas Commun.*, vol. 23, no. 2, pp. 201–220, Feb 2005.

[5] R. W. Thomas, L. A. DaSilva, and A. B. MacKenzie, "Cognitive networks," in *DySPAN 2005.*, Nov 2005, pp. 352–360.

[6] "FCC Rules and Regulations Pt2."

[7] Ofcom, in *TV White-spaces, http://stakeholders.ofcom.org.uk/spectrum/tv-white-spaces/.*

[8] S. J. Shellhammer, A. K. Sadek, and W. Zhang, "Technical challenges for cognitive radio in the tv white space spectrum," in *Information Theory and Applications Workshop, 2009*, Feb 2009, pp. 323–333.

[9] Ofcom, "Implementing TV White Spaces," in *statement, February 2015,accessible at http://stakeholders.ofcom.org.uk/consultations/white-space-coexistence/statement, accessed May 2015.*

[10] C. Cordeiro, K. Challapali, D. Birru, and S. Shankar, "Ieee 802.22: the first worldwide wireless standard based on cognitive radios," in *IEEE DySPAN 2005*, Nov 2005, pp. 328–337.

[11] J. Wang, M. Ghosh, and K. Challapali, "Emerging cognitive radio applications: A survey," *IEEE Comm. Mag.*, vol. 49, no. 3, pp. 74–81, March 2011.

[12] S. Amin and B. Wollenberg, "Toward a Smart Grid: Power Delivery for the 21st Century," *IEEE Power and Energy Mag.*, vol. 3, no. 5, pp. 34–41, 2005.

[13] K. Pelechrinis, P. Krishnamurthy, M. Weiss, and T. Znati, "Cognitive radio networks: Realistic or not?" *SIGCOMM Comput. Commun. Rev.*, vol. 43, no. 2, pp. 44–51, 2013.

[14] K.-L. Yau, F.-A. Tan, P. Komisarczuk, and P. Teal, "Exploring new and emerging applications of cognitive radio systems: Preliminary insights and framework," in *2011 IEEE Colloquium on Humanities, Science and Engineering (CHUSER)*, Dec 2011, pp. 153–157.

[15] A. El-Hoiydi, "Aloha with Preamble Sampling for Sporadic Traffic in Ad-hoc Wireless Sensor Networks," in *IEEE International Conference on Communications (ICC)*, vol. 5, 2002, pp. 3418–3423 vol.5.

[16] "FCC, Notice of proposed rule making and order,," in *ET Docket*, Dec 2003, pp. No.03–222.

[17] J. Palicot, "Cognitive radio: an enabling technology for the green radio communications concept," in *Proceedings of the 2009 International Conference on Wireless Communications and Mobile Computing: Connecting the World Wirelessly*. ACM, 2009, pp. 489–494.

[18] Y. C. Liang, K. C. Chen, G. Y. Li, and P. Mahonen, "Cognitive radio networking and communications: an overview," *IEEE Transactions on Vehicular Technology*, vol. 60, no. 7, pp. 3386–3407, Sept 2011.

[19] D. Cabric, S. M. Mishra, and R. W. Brodersen, "Implementation issues in spectrum sensing for cognitive radios," in *Conference Record of the Thirty-Eighth Asilomar Conference on Signals, Systems and Computers, 2004.*, vol. 1, Nov 2004, pp. 772–776 Vol.1.

[20] J. Zhao, H. Zheng, and G.-H. Yang, "Distributed coordination in dynamic spectrum allocation networks," in *IEEE DySPAN 2005*, Nov 2005, pp. 259–268.

[21] G. Ganesan and Y. Li, "Cooperative spectrum sensing in cognitive radio networks," in *IEEE DySPAN 2005*, Nov 2005, pp. 137–143.

[22] C.-H. Lo and N. Ansari, "The Progressive Smart Grid System from Both Power and Communications Aspects," *IEEE Commun. Surveys & Tut.*, vol. 14, no. 3, pp. 799–821, 2012.

[23] K. C. Budka, J. G. Deshpande, T. L. Doumi, M. Madden, and T. Mew, "Communication Network Architecture and Design Principles for Smart Grids," *Bell Labs Technical Journal*, vol. 15, no. 2, pp. 205–227, 2010.

[24] H. Farhangi, "The path of the smart grid," *IEEE Power and Energy Magazine*, vol. 8, no. 1, pp. 18–28, January 2010.

[25] V. C. Gungor and D. Sahin, "Cognitive radio networks for smart grid applications: A promising technology to overcome spectrum inefficiency," *IEEE Vehicular Technology Magazine*, vol. 7, no. 2, pp. 41–46, June 2012.

[26] D. Wang, Z. Tao, J. Zhang, and A. A. Abouzeid, "Rpl based routing for advanced metering infrastructure in smart grid," in *2010 IEEE International Conference on Communications Workshops*, May 2010, pp. 1–6.

[27] J. Huang, H. Wang, Y. Qian, and C. Wang, "Priority-based traffic scheduling and utility optimization for cognitive radio communication infrastructure-based smart grid," *IEEE Trans. Smart Grid*, vol. 4, no. 1, pp. 78–86, March 2013.

[28] C. H. Lo and N. Ansari, "The progressive smart grid system from both power and communications aspects," *IEEE Communications Surveys Tutorials*, vol. 14, no. 3, pp. 799–821, Third 2012.

[29] M. E. Helou, M. Ibrahim, S. Lahoud, K. Khawam, D. Mezher, and B. Cousin, "A network-assisted approach for rat selection in heterogeneous cellular networks," *IEEE Journal on Selected Areas in Communications*, vol. 33, no. 6, pp. 1055–1067, June 2015.

[30] C.Cicconetti, "5g radio network architecture," in *Radio Access and Spectrum.*

[31] H.-S. Jo, Y. J. Sang, P. Xia, and J. Andrews, "Heterogeneous cellular networks with flexible cell association: A comprehensive downlink sinr analysis," *IEEE Trans. Wireless Commun*, vol. 11, no. 10, Oct 2012.

[32] J. Andrews, F. Baccelli, and R. Ganti, "A tractable approach to coverage and rate in cellular networks," *IEEE Trans. Commun*, vol. 59, no. 11, pp. 3122–3134, November 2011.

[33] H. S. Jo, Y. J. Sang, P. Xia, and J. G. Andrews, "Heterogeneous cellular networks with flexible cell association: A comprehensive downlink sinr analysis," *IEEE Transactions on Wireless Communications*, vol. 11, no. 10, pp. 3484–3495, October 2012.

[34] R. B. F. A. J. G. Dhillon, Harpreet S.; Krishna Ganti, "Modeling and analysis of k-tier downlink heterogeneous cellular networks," *IEEE Journal on Selected Areas in Communications*, vol. 30, no. 3, pp. 550–560, April 2012.

[35] S. Singh, H. Dhillon, and J. Andrews, "Offloading in heterogeneous networks: Modeling, analysis, and design insights," *IEEE Trans. Wireless Commun*, vol. 12, no. 5, pp. 2484–2497, May 2013.

[36] H. Dhillon and J. Andrews, "Downlink rate distribution in heterogeneous cellular networks under generalized cell selection," *IEEE Wireless Commun. Letters*, vol. 3, no. 1, pp. 42–45, February 2014.

[37] M. Cesana, F. Cuomo, and E. Ekici, "Routing in cognitive radio networks: Challenges and solutions," *Ad Hoc Netw.*, vol. 9, no. 3, pp. 228–248, May 2011.

[38] K. Chowdhury and I. Akyildiz, "CRP: A routing protocol for cognitive radio ad hoc networks," *J. Sel. Areas Commun.*, vol. 29, no. 4, pp. 794–804, 2011.

[39] M. Caleffi, I. F. Akyildiz, and L. Paura, "Opera: Optimal routing metric for cognitive radio ad hoc networks," *IEEE Transactions on Wireless Communications*, vol. 11, no. 8, pp. 2884–2894, August 2012.

[40] G. Cheng, W. Liu, Y. Li, and W. Cheng, "Spectrum aware on-demand routing in cognitive radio networks," in *2007 2nd IEEE International Symposium on New Frontiers in Dynamic Spectrum Access Networks*, April 2007, pp. 571–574.

[41] Y. Liu, L.Cai, and X. Shen, "Spectrum-aware opportunistic routing in multi-hop cognitive radio networks," *IEEE J. Sel. Areas Commun.*, vol. 30, no. 10, pp. 1958–1968, 2012.

[42] J. Jia and S. Zhang, "Cooperative transmission in cognitive radio ad hoc networks," *International J. Distributed Sensor Networks*, p. 10, 2012.

[43] M. Xie, W. Zhang, and K.-K. Wong, "A geometric approach to improve spectrum efficiency for cognitive relay networks," *Wireless Communications, IEEE Transactions on*, vol. 9, no. 1, pp. 268–281, January 2010.

[44] J.-P. Sheu and I.-L. Lao, "Cooperative routing protocol in cognitive radio ad-hoc networks," in *Proc. IEEE WCNC*, 2012, pp. 2916–2921.

[45] S. Y. N. Joshi, Gyanendra Prasad and S. W. Kim., "Cognitive radio wireless sensor networks: Applications, challenges and research trends," *Sensors (Basel, Switzerland)*, pp. 11 196–11 228, April 2013.

[46] O. B. Akan, O. B. Karli, and O. Ergul, "Cognitive radio sensor networks," *IEEE Network*, vol. 23, no. 4, pp. 34–40, July 2009.

[47] Z. A. Khan and Y. Faheem, "Cognitive radio sensor networks: Smart communication for smart gridsa case study of pakistan," *Renewable and Sustainable Energy Reviews*, vol. 40, pp. 463 – 474, 2014.

[48] A. Jamal, C. K. Tham, and W. C. Wong, "Cr-wsn mac: An energy efficient and spectrum aware mac protocol for cognitive radio sensor network," in *2014 9th International Conference on Cognitive Radio Oriented Wireless Networks and Communications (CROWNCOM)*, June 2014, pp. 67–72.

[49] S. A. Gyanendra Prasad Joshi and S. W. Kim, "A mac protocol for cr-wsn without a dedicated common control channel," *International Journal of Distributed Sensor Networks*, 2015.

[50] M. A. R. M. M. H. M. A. H. Mir Mehedi Ahsan Pritom, Sujan Sarker and A. Alelaiwi, "A multiconstrained qos aware mac protocol for cluster-based cognitive radio sensor networks," *International Journal of Distributed Sensor Networks*, 2015.

[51] A. A. Khan, M. H. Rehmani, and M. Reisslein, "Cognitive radio for smart grids: Survey of architectures, spectrum sensing mechanisms, and networking protocols," *IEEE Communications Surveys Tutorials*, vol. 18, no. 1, pp. 860–898, Firstquarter 2016.

[52] A. Aijaz and A. H. Aghvami, "Prma-based cognitive machine-to-machine communications in smart grid networks," *IEEE Transactions on Vehicular Technology*, vol. 64, no. 8, pp. 3608–3623, Aug 2015.

[53] A. Aijaz, H. Su, and A.-H. Aghvami, "CORPL: A Routing Protocol for Cognitive Radio Enabled AMI Networks," *IEEE Trans. Smart Grid*, vol. PP, no. 99, pp. 1–9, July 2014.

[54] L. Huang, G. Zhu, and X. Du, "Cognitive femtocell networks: an opportunistic spectrum access for future indoor wireless coverage," *IEEE Wireless Commun.*, vol. 20, no. 2, pp. 44–51, April 2013.

[55] H. ElSawy, E. Hossain, and M. Haenggi, "Stochastic geometry for modeling, analysis, and design of multi-tier and cognitive cellular wireless networks: A survey," *IEEE Commun. Surveys Tutorials*, vol. 15, no. 3, pp. 996–1019, Third 2013.

[56] H. ElSawy and E. Hossain, "Two-tier hetnets with cognitive femtocells: Downlink performance modeling and analysis in a multichannel environment," *IEEE Trans. Mobile Computing*, vol. 13, no. 3, March 2014.

[57] H. Elsawy and E. Hossain, "Channel assignment and opportunistic spectrum access in two-tier cellular networks with cognitive small cells," in *IEEE GLOBECOM*, Dec 2013, pp. 4477–4482.

[58] S.-M. Cheng, W. C. Ao, and K. C. Chen, "Downlink capacity of two-tier cognitive femto networks," in *21st IEEE International Symposium on Personal, Indoor and Mobile Radio Communications*, Sept 2010, pp. 1303–1308.

[59] M. Wildemeersch, T. Q. S. Quek, C. H. Slump, and A. Rabbachin, "Cognitive small cell networks: Energy efficiency and trade-offs," *IEEE Transactions on Communications*, vol. 61, no. 9, pp. 4016–4029, September 2013.

[60] C. Li, W. Liu, J. Li, Q. Liu, and C. Li, "Aggregation based spectrum allocation in cognitive radio networks," in *Proc. IEEE/CIC ICCC Workshops*, 2013, pp. 50–54.

[61] M. Nekovee, "Quantifying the Availability of TV White Spaces for Cognitive Radio Operation in the UK," in *IEEE International Conference on Communications (ICC) Workshops*, 2009, pp. 1–5.

[62] P. Ren, Y. Wang, Q. Du, and J. Xu, "A survey on dynamic spectrum access protocols for distributed cognitive wireless networks," *EURASIP J. Wireless Comm. and Netw.*, vol. 2012, p. 60, 2012.

[63] W. Wang, Z. Zhang, and A. Huang, "Spectrum aggregation: Overview and challenges," *Network Protocols and Algorithms*, vol. 2, 2010.

[64] B. Gao, Y. Yang, and J. Park, "Channel aggregation in cognitive radio networks with practical considerations," in *Proc. IEEE ICC*, 2011, pp. 1–5.

[65] F. Huang, W. Wang, H. Luo, G. Yu, and Z. Zhang, "Prediction-based spectrum aggregation with hardware limitation in cognitive radio networks," in *Proc. IEEE VTC*, 2010, pp. 1–5.

[66] H. Salameh, M. Krunz, and D. Manzi, "Spectrum bonding and aggregation with guard-band awareness in cognitive radio networks," *IEEE Trans. Wireless Commun.*, vol. 13, no. 3, pp. 569–581, 2014.

[67] D. Chen, Q. Zhang, and W. Jia, "Aggregation aware spectrum assignment in Cognitive Ad-hoc Networks," in *Proc. CROWNCOM*, 2008, pp. 1–6.

[68] J. Lin, L.Shen, N. Bao, B. Su, Z. Deng, and D. Wang, "Channel characteristic aware spectrum aggregation algorithm in cognitive radio networks," in *Proc.IEEE LCN*, 2011, pp. 634–639.

[69] J. Poston and W. Horne, "Discontiguous OFDM considerations for dynamic spectrum access in idle TV channels," in *Proc. IEEE DySPAN*, 2005, pp. 607–610.

[70] S. Salim and S. Moh, "On-demand routing protocols for cognitive radio ad hoc networks," *EURASIP J. Wireless Comm. and Netw*, vol. 2013, p. 102, 2013.

[71] D. Lei, T. Melodia, S. Batalama, and J. Matyjas, "Distributed routing, relay selection, and spectrum allocation in cognitive and cooperative ad hoc networks," in *Proc. IEEE SECON*, 2010, pp. 1–9.

[72] J. Jia, J. Zhang, and Q. Zhang, "Cooperative relay for cognitive radio networks," in *Proc. IEEE INFOCOM*, 2009, pp. 2304–2312.

[73] S. You, S. Misra, T. Lang, and E.Anthony, "Cooperative routing for distributed detection in large sensor networks," *IEEE J. Sel. Areas Commun.*, vol. 25, no. 2, pp. 471–483, 2007.

[74] S. Ping, A. Aijaz, O. Holland, and A. Aghvami, "Energy and interference aware cooperative routing in cognitive radio ad-hoc networks," in *IEEE Wireless Communications and Networking Conference (WCNC)*, April 2014, pp. 87–92.

[75] P. aramvir Bahl, R. Chandra, T. Moscibroda, R. Murty, and M. Welsh, "White space networking with wi-fi like connectivity," in *Proc. ACM SIGCOMM*, August 2009.

[76] P. Ren, Y. Wang, and Q. Du, "CAD-MAC: A channel-aggregation diversity based mac protocol for spectrum and energy efficient cognitive ad hoc networks," *IEEE J. Sel. Areas Commun.*, vol. 32, no. 2, pp. 237–250, 2014.

[77] H. Urkowitz, "Energy Detection of Unknown Deterministic Signals," *Proceedings of the IEEE*, vol. 55, no. 4, pp. 523–531, 1967.

[78] A. Ghasemi and E. Sousa, "Optimization of Spectrum Sensing for Opportunistic Spectrum Access in Cognitive Radio Networks," in *IEEE Consumer Communications and Networking Conference (CCNC)*, 2007, pp. 1022–1026.

[79] W.-Y. Lee and I. Akyildiz, "Optimal Spectrum Sensing Framework for Cognitive Radio Networks," *IEEE Trans. Wireless Commun.*, vol. 7, no. 10, pp. 3845–3857, 2008.

[80] D. S. J. De Couto, D. Aguayo, J. Bicket, and R. Morris, "A High-Throughput Path Metric for Multi-hop Wireless Routing," in *ACM International Conference on Mobile Computing and Networking (MOBICOM)*, 2003, pp. 134–146.

[81] M. Haenggi, "On distances in uniformly random networks," *Information Theory, IEEE Transactions on*, vol. 51, no. 10, pp. 3584–3586, Oct 2005.

[82] ——, "On routing in random rayleigh fading networks," *Wireless Communications, IEEE Transactions on*, vol. 4, no. 4, pp. 1553–1562, July 2005.

[83] D. Moltchanov, "Survey paper: Distance distributions in random networks," *Ad Hoc Netw.*, vol. 10, no. 6, pp. 1146–1166, Aug. 2012.

[84] J. S. Seybold, "Introduction to RF propagation," in *Wiley*, 2005.

[85] I. Akyildiz, W. Su, Y. Sankarasubramaniam, and E. Cayirci, "Wireless Sensor Networks: A Survey," *J. Comput. Networks*, vol. 38, no. 4, pp. 393 – 422, 2002.

[86] V. Gungor, B. Lu, and G. Hancke, "Opportunities and Challenges of Wireless Sensor Networks in Smart Grid," *IEEE Trans. Indust. Electronics*, vol. 57, no. 10, pp. 3557–3564, Oct 2010.

[87] Y. Yang, F. Lambert, and D. Divan, "A Survey on Technologies for Implementing Sensor Networks for Power Delivery Systems," in *IEEE Power Engineering Society General Meeting*, June 2007, pp. 1–8.

[88] M. Erol-Kantarci and H. T. Mouftah, "Wireless Multimedia Sensor and Actor Networks for the Next Generation Power Grid," *J. Ad-Hoc Networks*, vol. 9, no. 4, pp. 542 – 551, 2011.

[89] A. Aijaz and A. Aghvami, "Cognitive machine-to-machine communications for internet-of-things: A protocol stack perspective," *IEEE Internet of Things Journal*, vol. 2, no. 2, pp. 103–112, 2015.

[90] R. Qiu, Z. Hu, Z. Chen, N. Guo, R. Ranganathan, S. Hou, and G. Zheng, "Cognitive Radio Network for the Smart Grid: Experimental System Architecture, Control Algorithms, Security, and Microgrid Testbed," *IEEE Trans. Smart Grid*, vol. 2, no. 4, pp. 724–740, 2011.

[91] A. Ghassemi, S. Bavarian, and L. Lampe, "Cognitive Radio for Smart Grid Communications," in *IEEE International Conference on Smart Grid Communications (SmartGridComm)*, 2010, pp. 297–302.

[92] R. Deng, J. Chen, X. Cao, Y. Zhang, S. Maharjan, and S. Gjessing, "Sensing-performance tradeoff in cognitive radio enabled smart grid," *IEEE Trans. Smart Grid*, vol. 4, no. 1, pp. 302–310, 2013.

[93] M. Brew, F. Darbari, L. Crockett, M. B. Waddell, M. Fitch, S. Weiss, and R. Stewart, "UHF white space network for rural smart grid communications," in *IEEE International Conference on Smart Grid Communications (SmartGridComm)*, 2011, pp. 138–142.

[94] J. Huang, H. Wang, Y. Qian, and C. Wang, "Priority-based traffic scheduling and utility optimization for cognitive radio communication infrastructure-based smart grid," *IEEE Trans. Smart Grid*, vol. 4, no. 1, pp. 78–86, 2013.

[95] A. Bicen, O. Akan, and V. Gungor, "Spectrum-Aware and Cognitive Sensor Networks for Smart Grid Applications," *IEEE Commun. Mag.*, vol. 50, no. 5, pp. 158–165, 2012.

[96] O. Akan, O. Karli, and O. Ergul, "Cognitive Radio Sensor Networks," *IEEE Network*, vol. 23, no. 4, pp. 34–40, July 2009.

[97] T. Watteyne, A. Bachir, M. Dohler, D. Barthel, and I. Auge-Blum, "1-hopMAC: An Energy-Efficient MAC Protocol for Avoiding 1-hop Neighborhood Knowledge," in *IEEE International Conference on Sensor and Ad Hoc Communications and Networks (SECON)*, Sept 2006, pp. 639–644.

[98] T. Winter, "IPv6 Routing Protocol for Low Power and Lossy Networks," Internet Engineering Task Force, RFC 6550, Mar. 2012. [Online]. Available: http://www.rfc-editor.org/rfc/rfc6550.txt

[99] K. Chowdhury, M. Di Felice, and I. Akyildiz, "TP-CRAHN: A Transport Protocol for Cognitive Radio Ad-Hoc Networks," in *IEEE International Conference on Computer Communications (INFOCOM)*, 2009, pp. 2482–2490.

[100] M. R. Akhavan, S. Choobkar, A. Aijaz, and A.-H. Aghvami, "Adaptive Preamble Sampling Techniques for Receiver Based MAC Protocols in Lossy Wireless Sensor Networks," *IET Wireless Sensor Systems*, vol. PP, no. 99, pp. 1–11, 2014, (accepted for publication).

[101] H. Sun, A. Nallanathan, B. Tan, J. S. Thompson, J. Jiang, and H. V. Poor, "Relaying technologies for smart grid communications," *Wireless Communications, IEEE*, vol. 19, no. 6, pp. 52–59, 2012.

[102] E. Hossain, Z. Han, and H. V. Poor, *Smart grid communications and networking*. Cambridge University Press, 2012.

[103] H. Sun, A. Nallanathan, N. Zhao, and C.-X. Wang, "Green data transmission in power line communications," in *Global Communications Conference (GLOBECOM), 2012 IEEE*. IEEE, 2012, pp. 3702–3706.

[104] Y. Zhang, R. Yu, M. Nekovee, Y. Liu, S. Xie, and S. Gjessing, "Cognitive machine-to-machine communications: visions and potentials for the smart grid," *Network, IEEE*, vol. 26, no. 3, pp. 6–13, 2012.

[105] A. Aijaz, S. Ping, M. Akhavan, and A.-H. Aghvami, "CRB-MAC: A Receiver-Based MAC Protocol for Cognitive Radio Equipped Smart Grid Sensor Networks," *Sensors Journal, IEEE*, vol. 14, no. 12, pp. 4325–4333, 2014.

[106] T. Tsvetkov, "Rpl: Ipv6 routing protocol for low power and lossy networks," *Sensor Nodes–Operation, Network and Application (SN)*, vol. 59, p. 2, 2011.

[107] A. Aijaz, H. Su, and A. Aghvami, "Enhancing rpl for cognitive radio enabled machine-to-machine networks," in *IEEE Wireless Communications and Networking Conference (WCNC)*, 2014, pp. 2090–2095.

[108] H. Sun, W.-Y. Chiu, J. Jiang, A. Nallanathan, and H. V. Poor, "Wideband spectrum sensing with sub-nyquist sampling in cognitive radios," *arXiv preprint arXiv:1302.1847*, 2013.

[109] N. Zhao, "A novel two-stage entropy-based robust cooperative spectrum sensing scheme with two-bit decision in cognitive radio," *Wireless personal communications*, vol. 69, no. 4, pp. 1551–1565, 2013.

[110] H. Sun, W.-Y. Chiu, and A. Nallanathan, "Adaptive compressive spectrum sensing for wideband cognitive radios," *Communications Letters, IEEE*, vol. 16, no. 11, pp. 1812–1815, 2012.

[111] N. Zhao and H. Sun, "Robust power control for cognitive radio in spectrum underlay networks," *KSII Transactions on Internet and Information Systems (TIIS)*, vol. 5, no. 7, pp. 1214–1229, 2011.

[112] N. Zhao, F. R. Yu, H. Sun, and A. Nallanathan, "An energy-efficient cooperative spectrum sensing scheme for cognitive radio networks," in *Global Communications Conference (GLOBECOM), 2012 IEEE*. IEEE, 2012, pp. 3600–3604.

[113] P.-Y. Yin, R.-I. Chang, C.-C. Chao, and Y.-T. Chu, "Niched ant colony optimization with colony guides for qos multicast routing," *Journal of Network and Computer Applications*, vol. 40, pp. 61–72, 2014.

[114] M. Mavrovouniotis and S. Yang, "Ant colony optimization with immigrants schemes for the dynamic travelling salesman problem with traffic factors," *Applied Soft Computing*, vol. 13, no. 10, pp. 4023–4037, 2013.

[115] Z. Wu, N. Zhao, G. Ren, and T. Quan, "Population declining ant colony optimization algorithm and its applications," *Expert Systems with Applications*, vol. 36, no. 3, pp. 6276–6281, 2009.

[116] N. Zhao, X. Lv, and Z. Wu, "A hybrid ant colony optimization algorithm for optimal multiuser detection in ds-uwb system," *Expert Systems with Applications*, vol. 39, no. 5, pp. 5279–5285, 2012.

[117] N. Zhao, Z. Wu, Y. Zhao, and T. Quan, "Ant colony optimization algorithm with mutation mechanism and its applications," *Expert Systems with Applications*, vol. 37, no. 7, pp. 4805–4810, 2010.

[118] H. Elsawy and E. Hossain, "On cognitive small cells in two-tier heterogeneous networks," in *Modeling Optimization in Mobile, Ad Hoc Wireless Networks (WiOpt),*, May 2013, pp. 75–82.

[119] C.-H. Lee and C.-Y. Shih, "Coverage analysis of cognitive femtocell networks," *IEEE Wireless Commun. Letters*, vol. 3, no. 2, April 2014.

[120] M. Haenggi and R. K. Ganti, "Interference in large wireless networks," *Foundations and Trends in Networking*, vol. 3, no. 2, pp. 127–248, 2008.

[121] C. han Lee and M. Haenggi, "Interference and outage in poisson cognitive networks," *IEEE Trans. Wireless Commun*, vol. 11, no. 4, pp. 1392–1401, April 2012.

[122] I. F. Akyildiz, B. F. Lo, and R. Balakrishnan, "Cooperative spectrum sensing in cognitive radio networks: A survey," *Phys. Commun.*, vol. 4, no. 1, pp. 40–62, Mar. 2011.

[123] H. ElSawy, E. Hossain, and D. I. Kim, "Hetnets with cognitive small cells: user offloading and distributed channel access techniques," *IEEE Comm. Mag.*, vol. 51, no. 6, pp. 28–36, June 2013.

[124] C. Watkins and P. Dayan, "Technical note: Q-learning," *Machine Learning*, vol. 8, no. 3-4, pp. 279–292, 1992.

[125] M. El Helou, M. Ibrahim, S. Lahoud, K. Khawam, D. Mezher, and B. Cousin, "A network-assisted approach for rat selection in heterogeneous cellular networks," *IEEE J. Sel. Areas Commun.*, vol. 33, no. 6, pp. 1055–1067, June 2015.

[126] L. Fenton, "The sum of log-normal probability distributions in scatter transmission systems," *Communications Systems, IRE Transactions on*, vol. 8, no. 1, pp. 57–67, March 1960.

[127] B.-J. Kwak, N.-O. Song, and M. Miller, "Performance analysis of exponential backoff," *Networking, IEEE/ACM Transactions on*, vol. 13, no. 2, pp. 343–355, April 2005.